5-10-2010

An Algorithm and Methodology for Static Response Based Damage Detection in Structural Systems

Augusto Terlaje
Washington University in St. Louis

WASHINGTON UNIVERSITY IN ST. LOUIS

Department of Mechanical, Aerospace, and Structural Engineering

Dissertation Examination Committee:
Kevin Truman, Co-chair
Phillip Gould, Co-chair
Shirley Dyke
Thomas Harmon
Kenneth Jerina
Hiroaki Mukai

AN ALGORITHM AND METHODOLOGY FOR STATIC RESPONSE BASED DAMAGE
DETECTION IN STRUCTURAL SYSTEMS

By

Augusto S. Terlaje III

A dissertation presented to the Graduate School of Arts and Sciences of Washington University in
St. Louis in partial fulfillment of the requirements for the degree of Doctor of Philosophy

May 2010

Saint Louis, Missouri

ABSTRACT

An Algorithm and Methodology for Static Response Based Damage Detection in Structural Systems

By

Augusto S. Terlaje III

Doctor of Philosophy in Structural Engineering

Washington University in St. Louis, 2010

Research Advisor: Dr. Kevin Z. Truman

A damage detection algorithm and procedure is presented in this dissertation that utilizes static response data and Optimality Criterion optimization. Static displacement measurements are used as constraints in the damage detection algorithm that identifies potential areas of damage in structural systems. The research aims to improve upon the master's level research performed by the author. First, the robustness of the algorithm is improved by use of a least squares approximation for determining the Lagrange multipliers that are necessary for optimization. Second, an active parameter selection subroutine is used to improve the accuracy of damage detection in the presence of experimental error. Third, an optimal load case algorithm is presented to eliminate procedural ambiguity and help engineers determine the best load case locations for damage detection. Last, modeling was improved with the creation of a new finite element that better models reduced moment resistance in connections. The new element is derived from elementary principles and is very well suited for optimization. The research attempts to utilize experimental test data whenever possible. When test data is not available, efforts are made to simulate real test conditions for damage detection. To illustrate the robustness of the algorithm, damage is detected in three different structural types. Reduced flexural stiffness is detected in a steel moment frame, reduced cross sectional area is detected in a three dimensional truss, and lastly a combination of reduced flexural stiffness and reduced moment capacity of connections is detected in a three dimensional structural grid.

Acknowledgements

Thank you to Dr. Kevin Truman for your guidance during the research process. The input you have provided has been invaluable and is certainly appreciated. Thank you goes to the members of the dissertation committee for taking the time to review this document and provide valuable comments that adds to the legitimacy of this research.

Thank you to Dr. Bill Spencer and graduate student Shinae Jang at the Smart Structures Technology Laboratory at the University of Illinois at Urbana-Champaign for aiding in the set-up and use of their experimental truss structure.

Lastly, thank you to Gus and Sue Terlaje, my parents, and Tim Terlaje, my brother, for your unwavering love and support. It has been a long, arduous process and I hope that I have made you proud.

Table of Contents

List of Tables

List of Figures

1   Introduction

Recent catastrophic failures within the nation's civil infrastructure, including the collapse of the Interstate 35W bridge in Minneapolis in 2007, the New York City crane collapses in March and May of 2008, and the multitude of broadcasting towers that have collapsed over the last decade, has put a renewed emphasis on damage detection of large scale structural systems. Further, a 2008 study by the Federal Highway Administration reports that 5.2%, or more than 1 in every 20, National Highway System bridges is structurally deficient. Rhode Island topped the list with 21% of NHS bridges deemed structurally deficient. The increasing age of the nation's civil infrastructure and the rise in vehicle traffic makes these bridges highly susceptible to structural damage.

Even well designed structures can experience damage when construction is faulty or unexpected loads are experienced. Older structures are especially susceptible to damage as their construction may not meet current design standards. Additionally, local damage that is present prior to an extreme loading event, such as fatigue or corrosion, can lead to unexpected behavior both during and following such an event. If damage goes undetected for an extensive amount of time it can ultimately lead to large repair costs or catastrophic failure of the structural system. Prompt detection of damage is essential in order to ensure the safety of these structures.

The most popular method of detecting structural damage is visual inspection. As the name implies, visual inspection requires personnel to physically observe damage and document its location and severity. One glaring drawback of visual inspection is that unless damage is so severe that its effects can be easily seen (i.e. large floor deflections, increased vibrations, etc.) damage cannot be located a priori. Take the San Francisco-Oakland Bay Bridge as a recent example. One of the links in the truss structure was severely cracked, yet the effects of this damage went unnoticed. The damaged link was finally discovered by construction workers during a seismic retrofit project. Another drawback of visual inspection is that often nonstructural elements must be removed or destroyed in order to

uncover potentially damaged areas. Exploring these areas can also be hazardous for inspection personnel.

Structural health monitoring (SHM) attempts to avoid the drawbacks of visual inspection by using a noninvasive, computational method to detect structural damage. SHM comes in many forms, typically categorized by the characteristics of the structural response data utilized for monitoring. In the broadest sense, SHM methodologies are classified as structural response based or local inspection based. Local inspection often utilizes methods in tomography to generate images of member cross sections to inspect for cracks or corrosion. The direct imaging of damage is a powerful tool, however due to the cost of imaging technology and the highly localized nature of the method, global damage detection often becomes infeasible. As a result, local inspection methods are often used as a secondary step once suspected areas of damage have been identified. Structural response based methods, on the other hand, monitor changes in the response behavior of structural systems without damaging any of the nonstructural elements. From these changes, researchers attempt to locate and quantify areas of damage before it threatens the structural integrity of the entire system.

Extensive work has been done using dynamic response data to locate damage. By observing changes in the dynamic behavior of structures, for example shifts in natural frequencies or mode shapes, damaged locations can be identified. Static based procedures, on the other hand, have not been researched as extensively. The exact reason for this lack of research is difficult to determine, but one contributing factor is the difficulty once faced in obtaining accurate static measurements. The precision of accelerometers has made dynamic response data readily available, but technological advances have also made static data much easier to obtain than in recent history. Thus, the intention of this research is to show the usefulness of a static based procedure and shed light on some of the advantages it has over other methods.

By creating an easily executed damage detection methodology able to locate and quantify damage without unnecessary destruction of nonstructural elements, many of the costs associated with visual inspection can be avoided. A new damage detection algorithm is presented that utilizes static response data to accurately detect areas of stiffness reduction. Using Optimality Criterion optimization, areas of stiffness reduction can be detected using minimal computing effort. Displacement measurements are compared both pre and post damage to accurately identify elements that have sustained damage. Previous work by the author has shown that the algorithm can accurately detect stiffness reductions in the absence of modeling error. The work presented here helps to establish the effect modeling error has on the damage detection algorithm. Through presented examples the efficiency of the algorithm will also be illustrated.

1.1 Static Response Based Damage Detection

Even though implementation of static methods has been slow to develop, some research has been done in this area. The majority of static based procedures follow a common framework. A mathematical model is first created that can accurately mimic the static behavior of the test structure. Next, static loads are applied to the structure before damage occurs and response measurements are taken (displacements, strains, etc.). The structural properties of the model are then adjusted to match the experimental response behavior. After damage occurs, the loads are reapplied to the structure and the same response measurements are taken. Next, utilizing a correlation technique, the structural parameters of the model are adjusted to match the change in response measurements between the healthy and damaged response data.

Damage detection is often formulated as an inverse problem where the input excitation is known and certain output data, the structural response, is also known. It is then the responsibility of the engineer to extract the properties of the system. The main difference in the various static based methods is the correlation algorithm to solve the inverse problem. The majority of research uses optimization to match calculated response behavior with observed response data.

Bakhtiari-Nejad [2] used sequential quadratic programming to find areas of stiffness reduction by using constraints to match the change in measured displacements while minimizing the error between the calculated load vector of the damaged structure with that of the healthy structure. The method requires an initial approximation for the healthy stiffness parameters to begin the optimization problem. To obtain these initial parameters a least squares approximation is performed on a first order approximation of the change in displacements as a function of the change in stiffness parameters. Due to the inaccuracy of the first order approximation, the least squares approximation can only be used as an initial value and not the final change in stiffness. Damage was able to be detected in a 25 member truss using simulated data. Monte Carlo simulations showed that the algorithm was able to detect damage even in the presence of simulated 1% uniform proportional error.

The algorithm was then tested using experimental data from a scale model of a one bay one story steel moment frame. For the experimental test, the displacement constraints were used, however the cost function attempts to minimize the error between the model's natural frequencies and damaged experimental natural frequencies. Damage was induced using a saw cut, that reduced the cross

sectional area of one section of the frame by 62%. The algorithm was able to locate damage; however error in the measurements did create several false positive damage locations.

Sanayei et al. [54] compared the algorithms developed in Sanayei and Onipede [50], Badu [8], and Sanayei and Saletnik ([51],[52]) using both displacement data as well as static strain measurements. Using experimental tests of a one bay, two story steel moment frame, the stiffness parameters of each element were successfully updated. It was shown that the use of strain measurements produced more accurate results due to the high precision and low noise of strain data.

Genetic algorithms have gained in popularity for damage detection problems as their formulation eliminates the need for calculating system gradients, which can be computationally expensive. Chou et al. [15] used a genetic algorithm and the output error formula of Sanayei and Onipede [50] as the fitness function. The genetic algorithm approach used a novel redundant representation of the genetic strings and the results showed a marked improvement in handling measurement noise in simulated examples.

Hu [31] also used a genetic algorithm for damage detection; however this work differed from the majority of static based research because the damage detection procedure relied on the redistribution of dead load stresses. Similar to dynamic methods that use ambient vibration to excite the structure, Hu proposed using the inherent dead load as the excitation. Detection of damage was good for severe damage but was sensitive to measurement error as well as areas of low stress.

Bernal [5] developed a technique that avoids optimization all together. Even though dynamic data is used to estimate the flexibility matrix of the structure in the predamaged and damaged state, the damage locating vectors (DLV) are identified simply from the flexibility matrices themselves and have the property of inducing stress fields with zero magnitude in the damaged elements. Although dynamic data is used to identify the flexibility matrices, the DLV theory remains valid even if static response data is used to identify the flexibility matrices.

1.1.1 Challenges of Static Based Methods

Although research has yielded promising results for both simulated and experimental data, several challenges remain that prevent the widespread use of static based methods. The first and most important challenge is the means of measuring static response data. Deflection measurements can be easily obtained on scale models by means of displacement dial gauges. However, the same

4

measurement devices cannot be used on full scale structures. A different means of measuring must be used for larger structures. Advances in global positioning systems (GPS) make it possible to quickly, and precisely identify position in a predetermined coordinate system. Observing relative positioning allows for accurate deflection measurements to be calculated. The main advantage of GPS measurements is that they provide a global deflection measurement from a stationary frame. Alternatively, relative displacements can be obtained using electro-optical measuring systems, where an array of optical sensors are mounted along a span, and each sensor is able to record its relative displacement from each of its neighboring sensors. A multitude of relative measurements are possible including deflection and rotation of a structural member.

Static strain measurements are often easier to obtain and are less susceptible to noise. As such, many devices are available to measure strain data. Traditional strain gauges can be mounted at several points on a structure to monitor the structural response. Fiber optic strain gauges have gained in popularity in recent years due to their long term reliability and high resolution. The main drawback with strain data is the large cost due to the high level of technical knowledge required when mounting each device. Several considerations must be taken, such as the optimal member surface on which to mount, the number of devices to mount, and the location of each device. Faulty installation during construction can render a device or group of devices inoperable and repair or replacement can be costly.

The second challenge facing static based SHM is the issue of measurement error. As evidenced by the results of the previous research, measurement noise can have a large effect on the accuracy of many algorithms. It is obvious that damage detection is highly dependent on the quality of the measurement data obtained; however a properly designed algorithm must be able to withstand a certain level of measurement noise and still effectively locate damage. Real data will inevitably contain error and structural models, no matter how detailed and sophisticated, will never fully mimic real structures. Therefore damage detection algorithms must be able to detect damage even in the presence of these errors.

Third, computing effort can hinder the wide spread use of both static and dynamic based damage detection methodologies alike. To facilitate the universal acceptance of these methods, any damage detection algorithm must not overburden the user with high computation demand. Minimizing the computation effort will help promote the privatization of the damage detection practice, by giving even small, private firms the ability to solve large damage detection problems. It is the hope that privatization of the practice will lead to market competition and spur innovation.

1.2 Summary of MS Thesis work

The current research is a continuation of previous work performed by the author which laid the groundwork for a static response based damage detection methodology.

The damage detection algorithm uses Optimality Criterion optimization to calculate areas of stiffness reduction based on changes in the static response of a structure. In the absence of measurement error, the Optimality Criterion algorithm has been shown to be an effective tool for damage detection in simulated 2-dimensional steel truss and moment frame models. The algorithm accurately detects areas of reduced stiffness based on measured static displacements resulting from known load cases. The results were calculated with minimal computing effort.

The damage detection procedure is created with practicality in mind. To provide a basis from which to convert theory to practice, each step attempts to simulate the sequence of steps in the order it would be performed in the field. The damage detection procedure is as follows:

1) Apply static point loads to the structure

2) Measure displacements resulting from the applied point loads

3) Create a mathematical model of the structure

4) Simulate the applied loads from step 1

5) Adjust the stiffness parameters of the mathematical model to match the response data of the structure

6) Repeat steps 1 and 2 periodically, using the same load cases and measurement locations to monitor changes in the static response

7) Use optimization to adjust the stiffness parameters of the mathematical model to match the change in static response of the model with the measured change in response of the test structure

Fundamental to solving the damage detection problem is the force-displacement relation given in Eqn 1.1.

$$P = Ku \tag{1.1}$$

where **P** is an applied load vector, **K** is the structural stiffness matrix of the model, and **u** is a vector of nodal displacements.

The goal of the 7 step procedure is to define, as best as possible, the terms of Eqn 1.1 to aid the optimization algorithm of step 7.

Apply Static Point Loads (Step 1)

Excitation of the structure is necessary in order to observe its response behavior. Static point loads are used to induce the static displacements needed to pinpoint damage. The load cases are fully defined by the damage detection procedure. Therefore the load vector, **P**, of Eqn 1.1 can be fully defined by the engineer. One caveat is that in order for the procedure to be practical to implement, the static point loads must be easily applied. Therefore, the damage detection procedure will only apply static point loads as gravity loads in the vertical direction. A discussion of the optimal load locations is given in Section 2.8.

Measure Displacements (Step 2)

The displacement vector, **u**, of Eqn 1.1 can be partially defined by measuring strategic displacements resulting from the applied static loads of step 1. It is impractical to measure displacements at every degree of freedom, therefore the damage detection procedure will only partially define the displacement vector. Because not every degree of freedom of the mathematical model can be defined by measuring displacements of the test structure, what results is an under constrained problem where multiple sets of stiffness parameters of the finite element model can mimic the measured displacements of the real structure. Therefore, an alternate criterion is needed to determine the correct stiffness parameters of the mathematical model that gives the best solution for the given measurement data. The criterion will be presented in Section 2.4.1.

Create a Mathematical Model (Step 3)

A mathematical model of the structure must be created that mimics its behavior under the influence of static loads. Using the force-displacement relation of Eqn 1.1, the stiffness matrix is this mathematical model. The stiffness matrix is typically composed of 3 groups of variables, member lengths, material moduli, and cross section properties of each member. The length of each structural member is easily determined based on structural geometry. Further, the elastic modulus is material

specific and can also be defined. Therefore, the algorithm must be able to detect the change in cross sectional properties that comprise the stiffness matrix of the mathematical model. For example, truss structures contain only axial elements and as a result each element contains only one structural parameter that must be detected, area of the cross section. For frame structures, assuming axial and shear deformations are negligible, two dimensional bending elements can be used to recreate the stiffness matrix of the structure. Again, only one structural parameter must be detected, the moment of inertia of each element. A more in depth discussion of the mathematical model is given in Section 2.7.

Simulate Applied Loads (Step 4)

In order to accurately detect the stiffness parameters of the structure, the loads applied to the structure must be simulated on the mathematical model. To do this the mathematical model must contain degrees of freedom at the same location(s) as loads applied to the test structure. To simulate the applied loads, the load vector of Eqn 1.1 is defined according to the known static loads on the structure of step 1.

Adjust Stiffness Parameters (Step 5 and 7)

A method of adjusting the stiffness parameters of the mathematical model must be developed to match the change in measured displacements with the change in calculated displacements of the mathematical model. A systematic way of accomplishing this goal is through the use of constrained optimization. A typical constrained optimization problem contains two parts, an objective function that must be minimized, and a set of constraint equations that must be satisfied. Both the objective function and constraint equations must be a function of the design variables adjusted by the algorithm. The design variables are the parameters comprising the stiffness matrix of the mathematical model. The objective function is necessary because the measured displacements of step 2 do not fully define the displacement vector, **u**, of Eqn 1.1. What results is an incomplete picture of the total response of the structure. Therefore, an alternate criterion is needed to determine the response of the structure at the locations where displacements can't be measured. The objective function provides this alternate criterion. Both the objective function and constraint equations of the damage detection problem are discussed in Section 2.4.

This methodology has shown to have the ability to identify changes in the stiffness parameters for two types of simulated civil structures. The optimization algorithm was able to correctly identify the change in cross sectional area of members in 2 dimensional truss structures and the moments of

inertia of elements in 2 dimensional moment frame structures using a limited number of simulated applied loads and measured displacements.

The procedure has also shown promise as a structural identification tool. The structural identification problem performs steps 1-4 of the damage detection procedure but uses structural optimization to perform step 5. The importance of this discovery is that the same algorithm used for damage detection can also be used to extract the current stiffness parameters of a structure, thus providing the vital baseline model used for comparison to identify areas of damage. The structural identification and damage detection methods showed good results for simulated data. Only static point loads and displacement measurements are used to detect each stiffness parameter, adding to the practicality of the method. Current research slightly modifies this procedure in order to incorporate new research objectives. The updated procedure is presented in Section 0.

1.3 Objectives

Previous research by the author began to uncover the power of optimality criterion optimization applied towards damage detection (See Terlaje [57]). To improve upon previous work, the following research objectives will be accomplished:

- Improve the robustness of the damage detection algorithm in preparation for handling measurements that contain error
- Develop a methodology to determine the optimal load locations for damage detection
- Develop a general strategy for choosing optimal measurement locations
- Improve the accuracy of damage detection by modifying the handling of active variables based on constraint gradients
- Illustrate the efficacy of the algorithm in the presence of both modeling error and measurement error
- Prove the validity of damage detection using experimental tests on scale structures
- Test the extent of damage that can be detected by the algorithm
- Develop a finite element to better detect damage in structural connections

Each of these points will now be further explained:

First, the previous research by the author was hampered by numerical instability of the optimization algorithm due to ill-posed constraints. These problems were particularly prevalent when the number of constraint equations approached the number of design variables. It was also apparent, from preliminary tests, that ill-posed constraints are an issue when experimental errors are introduced. In order for a damage detection algorithm to be viable, it must be able to produce stable, accurate results for data of varying quality.

Next, to aid engineers in damage detection, a general strategy must be put forth to determine both the locations where loads must be applied as well as where static displacements must be measured. By developing a strategy for loading and measurement there will be a reduced dependency of damage detection on preliminary simulations of the test structure. The goal is to develop a fully automated system that will limit the involvement of the engineer and eliminate human error as best as possible.

Through simulated examples, it will be illustrated that the algorithm is able to accurately detect damage in the presence of both modeling and measurement error. Once the reliability of the algorithm is established, experimental tests can be performed to judge the effectiveness of the methodology in the presence of real data and real error. The damage detection methodology will be shown to be able to detect varying degrees and types of structural damage.

Lastly, as evidenced by previous researchers, error is a major hindrance in damage detection. Therefore error, both modeling and measurement, should be minimized if possible. Measurement error is often a result of both the testing procedure and the tolerance limits of measuring devices. A portion of modeling error can be attributed to the environmental conditions when the testing procedure is performed, however another major source of modeling error is attributed to an engineer's ability to accurately model the behavior of the type of damage that can be expected in a structure. Therefore, an additional objective for this research is to develop a finite element that can better model the behavior of damage in structural connections. The validity of this new element type will be proven in an array of damage detection examples to assess its usefulness.

1.4 Scope

The previous work done by the author has illustrated the potential of the algorithm as a tool in structural identification. The identification step is vital in damage detection in order to establish a model that can best recreate baseline data. The importance of this step is recognized, however the current work does not attempt to further the structural identification aspect of the previous research.

This research attempts to develop the optimization algorithm to better detect damage. Next, researchers in the area of static response damage detection often use dynamic data to supplement static data to achieve more accurate damage detection results (see, for example, Bakhtiari-Nejad [2], Hajela et al. [27], and Oh et al. [43]). However, use of combined data clouds the effectiveness of a static based method. Static data must be able to stand on its own before being used in conjunction with other types of data. Therefore, the author remains committed to developing the damage detection methodology utilizing only static response data. Finally, any methodology must, at the very least, detect the presence of damage. However, as large an achievement as detecting the presence of damage is, the goal of this research is to go beyond the detection of the presence of damage and to both locate and quantify damage in a structural system. Assessing the remaining life of the structure is not a goal of the current research.

2   Damage Detection by Optimization

Most damage detection techniques, the current method included, identify damage by creating a mathematical model of the test structure and choosing stiffness parameters that can accurately reproduce a sample of measured structural responses. For small structures with very few members, adjusting these stiffness parameters manually is possible. However, for large scale structures with numerous elements, adjustment of each individual parameter of a mathematical model can be daunting. As such an automated correlation technique must be implemented. This technique, in most cases, is optimization.

Many of the optimization methods used in damage detection are unconstrained or random search methods. The typical approach is to use the measured response data from the test structure and the calculated response from the model to create an error function that must be minimized. In essence the objective function is used to match, as closely as possible, the measured response with the calculated response of the mathematical model. The use of unconstrained methods is a logical choice as constrained methods, which force all error functions to exactly equal zero, can become ill-posed when the number of constraints approaches the number of design variables. This complication is particularly prevalent when measurements contain error. This isn't to say that constrained methods should not be used. In the absence of error, a constrained method would be ideal as it is known that a feasible solution exists and constraints can help aid the optimization process. If the ill-posed equations commonly associated with constrained methods can be mitigated, a constrained optimization algorithm can be a valuable tool for damage detection.

The algorithm that will be presented in this research will achieve this goal. The algorithm will have the advantages of constrained optimization, but apply it toward real measurements that contain error without sacrificing stability. First, however, a comment must be made as to the sources of error that are contained in the experimental measurements.

2.1 Modeling Error

Modeling error is inevitable. Highly sophisticated finite element models can be created and the greatest care can be taken to model every structural component, yet modeling error will persist. Many factors contribute to modeling error. For example, even if the material composition of every structural member is known, often the material behavior is temperature dependent. Changes in temperature during testing can skew results and therefore care must be taken to assure environmental conditions are similar when tests are performed. Further, damage often produces nonlinear response behavior, which if not known before hand can be difficult to accurately model. Also, the simple fact that a continuous structure is modeled by discrete elements is an additional contributor to error. Care must be taken to model a structure using a sufficient number of elements to accurately mimic the test structure. Yet even the most careful modeling and testing procedure will still result in some level of error. Even though error is inevitable, attempting to minimize this error is essential. Model validation is an important step to prevent the compounding of error and to limit the cumulative error at the end of a damage detection problem.

One challenge is that computation power can often limit the level of detail that can be included in a finite element model. Decisions must be made to reduce the sophistication of the model, or truncate the number elements, in order to make calculation of a solution possible in a reasonable amount of time and using a reasonable amount of computing effort. The designer must determine which characteristics are essential to model and which can be omitted but still retain validity of the model. For example a possible question that must be answered is, if structural elements are sufficiently slender can shear deformations be ignored? If the structural response is dominated by bending or axial stiffness and the shear modulus can be omitted then computation effort can be greatly reduced in generating the mathematical model.

2.2 Measurement Error

Measurement error is another source of error in damage detection problems. Measurement error is commonly a result of the limitations of measuring devices and equipment. Often the precision of measuring devices is dependent on the maximum response expected to be measured. Unfortunately this means that responses less than that maximum setting are subject to the precision of the larger measurement.

The reliability of devices can also be an issue. Device failure is an obstacle that may be encountered during testing. If time permits, the faulty device should be replaced in order to obtain reliable data. However if a device cannot be repaired, testing must still continue. A careful examination of the test data should be performed prior to solving the damage detection problem in order to identify any faulty measurements. In these cases it is beneficial to have a damage detection algorithm that is able to determine the vicinity of damage even when crucial data is missing.

2.3 Unconstrained vs. Constrained Optimization

 Due to the error inherent to both modeling of the test structure and in the measured response data, most researchers attempt to formulate damage detection as an unconstrained optimization problem. Typically a function incorporating the difference in the calculated and measured responses is grouped into a single objective and minimized. In essence the objective is to minimize the cumulative difference between all measured and calculated responses.

The unconstrained technique is not adopted for this research, however. Even though the use of unconstrained methods appears logical in terms of maintaining stability of the algorithm, it unfortunately underutilizes the most important tool in optimization, the objective function. The measured data gives a fairly specific set of response characteristics that the final model must exhibit. Thus, the measured data resemble rigid constraints placed upon the mathematical model. The objective function, on the other hand, is best utilized as a tool to choose an optimal solution when multiple feasible solutions exist. By incorporating functions that could be used as constraints in to an objective function, the additional criterion for choosing optimal solutions from multiple feasible solutions no longer exists. These methods tend to necessitate additional response measurements in order to reduce the pool of feasible solutions. Additionally, these unconstrained methods tend to exhibit much slower convergence rates than their constrained counterparts. Again the disadvantage of constrained methods is that problems can become ill-posed. The use of soft constraints, or inequality constraints, can often alleviate these issues as the algorithm is able to set constraints inactive once they have been reduced below a specified value. However the goal here is to match the measured data as closely as possible and therefore the current problem does not lend itself to inequality constraints as all constraints must remain active. The ideal algorithm would combine the advantages of all of these methods. The algorithm would be able to minimize the constraint error and have the stability properties of the unconstrained methods, but at the same time it would have

use of the objective function and the quick convergence properties of the constrained methods. This research attempts to create such an algorithm.

Built from the classic Optimality Criterion (OC) theory, the current algorithm includes additional solution techniques and subroutines to improve accuracy and avoid the problem of ill-posed constraints. Prior to presenting the modified OC algorithm for damage detection, we must first review the classic form of the OC algorithm.

2.4 Optimality Criterion

The Optimality Criterion algorithm is an indirect optimization technique based on the Lagrange multiplier method. Ideally suited for structural optimization problems, the OC algorithm is able to locate points of optimality in very few iterations. The algorithm is also able to solve engineering problems with highly nonlinear constraint and objective functions, yet requires only first order derivatives of both the constraint and objective surfaces. The choice of objective function and constraints is critical for all constrained optimization problems. A brief comment on each of these aspects follows.

2.4.1 Objective Function

The objective function, also commonly known as the cost function, in an optimization problem is a scalar valued function that will be minimized by the algorithm within the bounds of the constraint equations. The objective is a function of the system parameters that will be adjusted by the algorithm. For example, the majority of the problems presented in this research will use the stiffness parameters of the mathematical model as the design parameters. As such, the objective function used for damage detection will be dependent on the stiffness parameters of the mathematical model.

The current damage detection methodology attempts to locate and quantify damage by measuring a limited number of static displacements resulting from applied static loads. Since displacement measurements are not taken at all degrees of freedom of the mathematical model, what results is an incomplete picture of the structural response of the structure. A carefully chosen objective function is needed to provide the algorithm with a means of determining the remaining design variables of the structure.

The objective function for this research is chosen based on the Principle of Minimum Potential Energy, which states:

"The correct displacement of all states which may satisfy the boundary conditions is that which makes the total potential energy a minimum."[24]

This principle lends itself well as an objective function as the optimal design parameters must produce a displacement field that minimizes the potential energy of the system. Therefore, strain energy is the objective function of choice for damage detection.

As stated earlier, the cost function must be a scalar value, but the damage detection procedure allows for the use of multiple load cases. Therefore, the cumulative strain energy from each load case is used as the cost function. The objective function is written as:

$$\min \Phi = \sum_{a=1}^{q} \frac{1}{2} \mathbf{u}_a^T \mathbf{K} \mathbf{u}_a \qquad \textbf{2.1}$$

Where q is the number of load cases, $\mathbf{u}_a$ is the calculated displacement field for load case a, and $\mathbf{K}$ is the global stiffness matrix of the mathematical model. Recognize that both the stiffness matrix and the displacement field are functions of the stiffness parameters of the system.

2.4.2 Constraints

Despite the multiple sources of error, damage detection relies on the measured response data. Care can be taken to minimize the error in these measurements, but in the end the engineer does not know which measurements contain error and which ones do not. Therefore, the engineer must act under the assumption that all data is true but at the same time recognize that error may be present. The key then is to match the change in the calculated response with the change in the measured data. To match the calculated response, the constraints are written as:

$$g_j = \Delta u_j^* - \Delta u_{j,measured}^* = 0 \quad for\ j = 1,2,\dots,p \qquad \textbf{2.2}$$

where

$$\Delta u_j^* = (u_{j,damaged}^A - u_{j,healthy}^A)/u_{j,healthy}^A$$

$$\Delta u_{j,measured}^* = (u_{j,damaged}^m - u_{j,healthy}^m)/u_{j,healthy}^m$$

$$u_j^A = j^{th} \text{ displacement calculated from the analytical model}$$

$$u_j^m = j^{th} \text{ displacement obtained from experimental measurements}$$

These displacement vectors are normalized with respect to the healthy displacements in order to ensure that all constraints are evenly weighted.

Many researchers attempt to incorporate similar functions into the objective of an unconstrained optimization algorithm. That approach is not adopted here because the measured static response is the only data obtained from the structure, and so it is desired to match this data as closely as possible. This is also the reason for using equality constraints as opposed to inequality constraints. All constraints must remain active in order to completely match the measured response data.

The reason constrained optimization is not commonly used in other research is because since error is unavoidable in the measured data, it is possible, especially with problems where the number of constraints approaches the number of design variables, that inconsistent constraints can result, i.e. no solution exists. As will be explained in Section 2.5.1 a modified Optimality Criterion algorithm will be used to alleviate this potential problem. However, first, the classic Optimality Criterion algorithm will be presented.

2.4.3 Classic OC Algorithm

Using the objective function of Eqn 2.1 and the constraints of Eqn 2.2 the damage detection problem takes the form:

$$\min \Phi = \sum_{a=1}^{q} \frac{1}{2} \mathbf{u}_a^T \mathbf{K} \mathbf{u}_a \qquad \text{(a)}$$

2.3

$$s.t. \quad g_j = \Delta u_j^* - \Delta u_{j,measured}^* = 0 \quad for\ j = 1,2,...\,p \qquad \text{(b)}$$

$$x_{i,healthy} \geq x_i \geq 0 \ for\ i = 1,2,...,n \qquad \text{(c)}$$

where x_i is the ith design variable. The side constraint $x_{i,healthy} \geq x_i \geq 0$ places a restriction on each design variable assuring that the stiffness terms remain positive, real and also do not increase beyond the initialized parameters. To solve, the Lagrangian is formed [36]:

$$L = \sum_{a=1}^{q} \frac{1}{2} \mathbf{u}_a^T \mathbf{K} \mathbf{u}_a + \sum_{j=1}^{p} \lambda_j (\Delta u_j^* - \Delta u_{j,measured}^*) \qquad \textbf{2.4}$$

where $\mathbf{p}$ is the total number of constraints and λ_j are unknown Lagrange multipliers corresponding to the jth measured displacement. The Karesh-Kuhn-Tucker condition for optimality is found by taking the derivative of the Lagrangian with respect to each design variable [36]:

$$\frac{\partial L}{\partial x_i} = \frac{d\Phi}{dx_i} + \sum_{j=1}^{p} \lambda_j \frac{\partial g_j}{\partial x_i}$$

$$\qquad \textbf{2.5}$$

$$= \frac{1}{2} \sum_{a=1}^{q} \left(\frac{\partial \mathbf{u}_a}{\partial x_i}^T \mathbf{K} \mathbf{u}_a + \mathbf{u}_a^T \frac{\partial \mathbf{K}}{\partial x_i} \mathbf{u}_a + \mathbf{u}_a \mathbf{K} \frac{\partial \mathbf{u}_a}{\partial x_i} \right) + \sum_{j=1}^{p} \lambda_j \frac{\partial u_j}{\partial x_i} = 0 \quad for\ i = 1,2,...\,n$$

where $\frac{\partial \mathbf{u}}{\partial x_i} = -\mathbf{K}^{-1} \frac{\partial \mathbf{K}}{\partial x_i} \mathbf{u}$

Rearranging Eqn 2.5, the condition for optimality can be written as [14]:

$$T_i = \frac{-\sum_{j=1}^{p} \lambda_j \frac{\partial g_j}{\partial x_i}}{\frac{d\Phi}{dx_i}} = 1 \quad for\ i = 1,2,...,n \qquad \textbf{2.6}$$

The optimal solution must satisfy the optimality criterion of Eqn 2.6.

For any given set of design variables, Eqn 2.6 can be used to check whether optimality has been satisfied. However, in order to determine how the design variables must be changed to better satisfy

optimality, a recursion relation is developed from the optimality criterion itself. Multiplying both sides of Eqn 2.6 by x^r and taking the rth root yields [35]:

$$x_i = x_i T_i^{1/r} \quad for \ i = 1,2, \dots, n \qquad\qquad 2.7$$

A recursion relation based on this equation can be written as [35]:

$$x_i^{k+1} = x_i^k T_i^{1/r} \quad for \ i = 1,2, \dots, n \qquad\qquad 2.8$$

where x_i^k is the ith design variable for the current iteration and x_i^{k+1} is the ith design variable for the next iteration.

Retaining the linear terms of the Taylor Series expansion of Eqn 2.8 about the point x_i^k with T_i as the variable yields [35]:

$$x_i^{k+1} = x_i^k + \frac{1}{r}(1 - T_i)x_i^k \quad for \ i = 1,2, \dots, n \qquad\qquad 2.9$$

The change in each design variable can be found by subtracting the design variable of the current iteration from both sides of Eqn 2.9:

$$\Delta x_i = x_i^{k+1} - x_i^k = \frac{1}{r}(1 - T_i)x_i^k \quad for \ i = 1,2,\dots, n \qquad\qquad 2.10$$

For any given set of design variables, Eqn 2.10 can be used to determine how each variable can be changed to better satisfy optimality.

Eqn 2.10 provides a means of determining the change in each of the n design variables, however embedded in each T_i equation are the p unknown Lagrange multipliers. The gradient of each constraint equation provides the p additional equations required to solve for each Lagrange multiplier.

The change in each constraint equation can be written as:

$$g_j(\mathbf{X} + \Delta\mathbf{X}) - g_j(\mathbf{X}) = \sum_{i=1}^{n} \frac{\partial g_j}{\partial x_i}\Delta x_i \quad for \ j = 1,2,\dots, p \qquad\qquad 2.11$$

where $\mathbf{X} = [x_1,x_2,\dots,x_n]$ and $\Delta\mathbf{X} = [\Delta x_1,\Delta x_2,\dots, \Delta x_n]$

The change in each design variable, $\mathbf{\Delta X}$, is chosen such that each constraint equation is satisfied, thus $g(\mathbf{X} + \mathbf{\Delta X}) = 0$, yielding:

$$-g_j(\mathbf{X}) = \sum_{i=1}^{n} \frac{\partial g_j}{\partial x_i} \Delta x_i \quad for \;\; j = 1,2,..., p \qquad \textbf{2.12}$$

The Lagrange multipliers are related to each constraint equation through the change in each design variable Δx_i, given by Eqn 2.10. Plugging in gives:

$$-g_j(\mathbf{X}) = \sum_{i=1}^{n} \frac{\partial g_j}{\partial x_i} \left\{ \frac{1}{r}(T_i - 1)x_i^k \right\} \quad for \;\; j = 1,2,..., p \qquad \textbf{2.13}$$

Plugging Eqn 2.6 in for T_i and rearranging terms to group all Lagrange multipliers yields:

$$rg_j(x_1, x_2,..., x_n) - \sum_{i=1}^{n} \frac{\partial g_j}{\partial x_i} x_i^k = \sum_{h=1}^{p} \lambda_h \left\{ \sum_{i=1}^{n} \left(\frac{\partial g_j}{\partial x_i} \frac{\partial g_h}{\partial x_i} \middle/ \frac{\partial \Phi}{\partial x_i} \right) x_i^k \right\} \quad for \;\; j = 1,2,..., p \qquad \textbf{2.14}$$

Eqn 2.14 represents a system of p linearly independent equation used to solve for all Lagrange multipliers. For any given set of initial design values, Eqns 2.6, 2.10, and 2.14 are used to iteratively adjust the design variables until optimality has been satisfied.

2.4.4 Side constraints

Upper and lower bounds can be set on the design variables similar to the bounds of Eqn 2.3(c). These bounds, known as side constraints, can be treated as regular constraints, however it is more computationally efficient to treat them in a separate manner. Rather than introduce additional Lagrange multipliers for each side constraint, a sub routine is created within each iteration of the optimization algorithm to check if a side constraint has been violated. If a side constraint has been violated, the algorithm repeats the current iteration, but makes the design variable(s) that will violate the side constraint passive and sets the variable(s) to the maximum or minimum value for the current iteration. However, artificially setting the design variable(s) to the extreme value must be accounted for inside the gradient calculations for the current iteration. Rewriting Eqn 2.13 to include passive design variables gives [14]:

$$- g_j(\mathbf{X}) = \sum_{i=1}^{n_1} \frac{\partial g_j}{\partial x_i} \Delta x_i + \sum_{i=n_1+1}^{n} \frac{\partial g_j}{\partial x_i} \left(\overline{x}_i^{\,p} - x_i^k \right) \quad for \;\; j = 1,2,..., \; m \qquad \textbf{2.15}$$

where $\overline{x}_i^{\,p}$ represents the upper or lower bound of the ith design variable and n_1 is the number of active elements for the kth iteration. The T_i values of Eqn 2.6 are artificially set to unity for all passive elements. Optimality is then only checked for those elements that remain active. Rearranging Eqn 2.15 in the same manner as Eqn 2.14 yields

$$rg_j(x_1,x_2,...,x_n) - \sum_{i=1}^{n_1} \frac{\partial g_j}{\partial x_i} x_i^k + r \sum_{i=n_1+1}^{n} \frac{\partial g_j}{\partial x_i} (\overline{x}_i - x_i^k) = \sum_{h=1}^{p} \lambda_p \left\{ \sum_{i=1}^{n_1} \left(\frac{\partial g_j}{\partial x_i} \frac{\partial g_h}{\partial x_i} \middle/ \frac{\partial \Phi}{\partial x_i} \right) x_i^k \right\} \quad for \; j = 1,2,...,p \qquad \textbf{2.16}$$

When a set of design variables becomes passive, it is possible for another set of variables to become passive once the original group is set to the extreme value. Generally the passive elements are not known prior to calculating the recurrence relation, so an iterative process within the kth iteration must be employed to fully identify all passive design variables.

2.4.5 Linking

A topic that will be important to some of the damage detection problems is the topic of linking variables. A preliminary localization step will be performed in which groups of variables all must be changed by the same amount during the optimization process to pin point areas of damage. This is accomplished by representing several elements by a single design variable. However, even though two or more elements are represented by a single variable, the change in each element still has an effect on how the optimization converges to the constraint equations, thus they must be accounted for in the gradient calculations. To do this Equation 2.14 must be modified so that the gradient of both the constraint equations and objective function with respect to each design variable include the sum of the gradients of each linked element represented by that design variable. Modifying the gradient of the Lagrangian, Eqn 2.5, to include linked variables and using the summation from 1 to s to represent the sum of the set of elements linked to the lth variable gives

$$\frac{\partial L}{\partial x_l} = \sum_{v=1}^{s} \frac{\partial L}{\partial x_v} = \sum_{v=1}^{s} \left(\frac{\partial \Phi}{\partial x_v} + \sum_{j=1}^{m} \lambda_j * \frac{\partial g_j}{\partial x_v} \right) = 0 \rightarrow \frac{\partial L}{\partial x_l} = \sum_{v=1}^{s} \frac{\partial \Phi}{\partial x_v} + \sum_{j=1}^{m} \lambda_j * \sum_{v=1}^{s} \frac{\partial g_j}{\partial x_v} = 0 \quad for \, l = 1,2,...,w \qquad \textbf{2.17}$$

where w is the number of linked and non-linked variables, and s is the number of design variables linked to the lth variable. From this, the optimality criterion of Equation 2.6 becomes

21

$$T_l = -\frac{\sum_{j=1}^{m} \lambda_j * \sum_{v=1}^{s} \frac{\partial g_j}{\partial x_v}}{\sum_{v=1}^{s} \frac{\partial \Phi}{\partial x_v}} = 1 \quad for\ l = 1,2,...,n \qquad \textbf{2.18}$$

Including linking, Equation 2.14 becomes

$$rg_j - \sum_{i=1}^{n} \frac{\partial g_j}{\partial x_i} x_i^k = \sum_{p=1}^{m} \lambda_p \left\{ \sum_{i=1}^{n} \left(\frac{\partial g_j}{\partial x_i} \sum_{v=1}^{s} \frac{\partial g_p}{\partial x_v} \right) \middle/ \sum_{v=1}^{s} \frac{\partial \Phi}{\partial x_v} \right\} x_i^k \quad for\ j = 1,2,3,4 \qquad \textbf{2.19}$$

The general form of Equation 2.14, including possible side constraints and linked variables, becomes

$$rg_j - \sum_{i=1}^{n_1} \frac{\partial g_j}{\partial x_i} x_i^k + r \sum_{i=n_1+1}^{n} \frac{\partial g_j}{\partial x_i} \left(\overline{x_i} - x_i^k \right) = \sum_{p=1}^{m} \lambda_p \left\{ \sum_{i=1}^{n_1} \left(\frac{\partial g_j}{\partial x_i} \sum_{v=1}^{s} \frac{\partial g_p}{\partial x_v} \right) \middle/ \sum_{v=1}^{s} \frac{\partial \Phi}{\partial x_v} \right\} x_i^k \quad for\ j = 1,2,...m \qquad \textbf{2.20}$$

The constrained optimization algorithm has been shown to be fast and efficient for many types of damage detection problems. However, as explained in earlier sections, many researchers do not utilize constrained optimization techniques. This is because of the likelihood, as the number of constraints approaches the number of design variables, that a system of inconsistent equations will result. These inconsistent sets of constraints are a result of the inherent error in the measured displacements. There does not exist a set of design parameters that will satisfy all constraints and therefore the constrained optimization algorithm can become unstable. The possibility of inconsistent constraints is no less likely for the classic optimality algorithm just presented. However a damage detection methodology must be allowed to collect as much pertinent data as possible during the experimental testing phase without being concerned with producing an ill-posed problem. Therefore, it is necessary to develop a constrained method that will not be hindered by a large number of constraints. Some modifications to the algorithm must be made.

2.5 Modifications to the Classic OC Algorithm

The classic OC Algorithm is a proven tool in structural optimization. However software packages typically do not include the OC method because problems tend to require a customized algorithm. Fortunately the basic framework presented in Section 2.4 can be implemented quickly and as problem requirements change, the algorithm can be modified easily to match specific needs. Further,

the convergence rate, even for nonlinear problems, is unmatched among any iterative first order gradient optimization methods. The one main problem with the OC algorithm when used for damage detection is ill-posed constraints. Equality constrained problems can create difficulties if the constraints are inconsistent. To help avoid this complication as well as improve the accuracy of damage detection, modifications have been made to the classic OC algorithm.

2.5.1 Modified Least Squares Algorithm

Ill-posed equations occur when Eqn 2.20 forms a set of inconsistent linear equations where no set of Lagrange multipliers can solve the system of equations. This typically results when the number of constraints approaches or exceeds the number of design variables when error is present in the measurement data. An alternate complication occurs when Eqn 2.20 forms a singular set of equations. This can occur when the number of constraints exceeds the number of design variables and so the number of unknown Lagrange multipliers exceeds the dimension of the problem space.

To resolve these issues, a combined least squares and minimum norm approach is employed to solve for all Lagrange multipliers. This method works well for a system of inconsistent equations as well as a singular set of equations. For the strictly inconsistent case, the traditional least squares approach could be taken. The traditional least squares method attempts to find a point that minimizes the error between inconsistent constraints. In other words, the least squares algorithm solves a system of inconsistent equations of the form

$$Ax = b \qquad \qquad \textbf{2.21}$$

by minimized the objective function

$$\min \ \|b - Ax\| \qquad \qquad \textbf{2.22}$$

Notice that Eqn 2.20 forms a set of linear equations of similar form:

$$A\lambda = b \qquad \qquad \textbf{2.23}$$

In the presence of error, Eqn 2.20 is often an inconsistent set of equations. The least squares approximation of λ is the solution to the equations:

$$A^T A \lambda = A^T b \qquad\qquad \textbf{2.24}$$

Note that the Lagrange multipliers, λ, are still found by solving a system of linear equations and thus do not require any greater computing power than was already required for solving Eqn 2.20.

This traditional least squares approach would be sufficient if the only complications were due to inconsistent equations. However the separate issue of singular equations must also be addressed. To solve singular equations the minimum norm least squares approach is used, where Eqn 2.23 must be satisfied while minimizing the objective function

$$\min \ \|\lambda\| \qquad\qquad \textbf{2.25}$$

Notice, however, that both the inconsistent and singular cases can be solved using a single method by employing the objective function of Eqn 2.25 subject to the constraints of Eqn 2.24. If the system of equations of Eqn 2.23 is inconsistent, then only a single solution exists and is determined from Eqn 2.24, while if the equations are singular then the objective function will help find the optimal solution. Note that the solution to this combined least squares problem can be found using an array of methods. The Lagrange multiplier method is employed here because of the ease of implementation as well as the ability to solve for the Lagrange multipliers by still solving a system of linear equations. The theory can be found in many textbooks, for example [6] and [36]. In total, the method requires solving the system of equations given by

$$\begin{bmatrix} I & A^T A \\ A^T A & 0 \end{bmatrix} \begin{Bmatrix} \lambda \\ \omega^* \end{Bmatrix} = \begin{Bmatrix} 0 \\ A^T b \end{Bmatrix}$$

where I is the p-by-p identity matrix and ω^* are the Lagrange multipliers of the least squares problem.

Recall that the Lagrange multipliers are needed to solve the constraints given by Eqn 2.13, which is attempting to satisfy the condition that $g(X+\Delta X)=0$. The least squares approximation attempts to find a solution to the optimization problem that minimizes this constraint error, much like many of the unconstrained methods discussed previously. Therefore the least squares approximation exhibits much better stability of the algorithm, but still has the benefits of constrained optimization. These benefits again being objective function use and quick convergence.

Using the least squares approach to solve for the Lagrange multipliers greatly improves the robustness of the algorithm and allows the OC method to solve damage detection problems that once had severe stability issues due to ill-posed constraints under the classic algorithm.

2.5.2 Gradient Based Active Parameter Selection Subroutine

Now that algorithm stability has be been addressed, another problem encountered in previous research using the OC method for damage detection is the tendency of the algorithm to smear damage. Often when a limited number of displacement measurements are taken, the OC algorithm will attempt to "smear" damage over many elements in an attempt to satisfy all constraint equations. Widespread damage is often unlikely, especially since the intent of this research is to detect damage as early as possible, before it has had the chance to spread. Therefore, a modification must be made to the algorithm in order to "entice" the algorithm to concentrate damage in few elements rather than spread damage among many. To do this, a subroutine is created that chooses the active design variables based on their gradient participation in the optimization problem.

The first step of the parameter selection subroutine is to determine the active constraints. The constraints are evaluated at the beginning of each iteration. If static measurements are taken over a large area of the structure, only a few of these measurement locations will exhibit significant change in the static response. Therefore, to minimize computing effort it is beneficial to omit the constraints that contribute little to damage detection. As an initial screening method only the constraints that are violated by a prespecified factor of the maximum violated constraint magnitude are reserved as active. Those constraints that are violated by less than this value are considered to have converged and therefore do not need to be active for that current iteration. For most problems a value of 10% of the maximum violated constraint is sufficient to define convergence. All constraints are checked for this criterion at the beginning of each iteration. The active parameter subroutine will then choose the parameters that will participate in the optimization algorithm for the current iteration.

Next, the gradient of each active constraint is calculated. Utilizing only the active constraints, the components of each gradient are ranked according to magnitude. In order to retain only the most important design variables for each iteration, only the variable with the largest derivative for each active constraint is retained as an active design variable. The subroutine is repeated at the beginning of each iteration, thus giving all variables an opportunity to participate for each iteration.

Member Grouping

One complication with the subroutine is that when a structure contains different types of members, for example a building system can be composed of girders, beams, and columns, it is possible that a single member type will hold a much larger influence on the constraints and objective functions than other member types. In other words the component of the gradient, i.e. the derivative of the constraints and objective functions with respect to these elements, is so large that it dominates the optimization process and prevents other elements from participating. To avoid this complication, active parameters are chosen from prespecified member groups. Member groups are defined prior to optimization and attempt to group elements with similar characteristics. For example, in a building system, all of the column elements can be one group, all of the beam elements are another group, and then finally all girders are a third group. Alternatively, groups could also be defined according to specific geometries or lengths. Once the member groups are defined, the active parameter selection subroutine is invoked on each member group. Again, the goal of this member grouping scheme is to give elements that naturally have less influence on the constraint and objective functions the opportunity to remain active during the optimization process.

Why is it necessary to force certain parameters to be inactive? The reason this active parameter selection subroutine is necessary is because when an element has little to no influence on the constraints, the algorithm attempts to eliminate that element even though elimination may not be beneficial for the objective function. The reason this happens can be easily seen. Repeating the optimality criterion of Eqn 2.6

$$T_i = \frac{-\sum_{j=1}^{p} \lambda_j \frac{\partial g_j}{\partial x_i}}{\frac{d\Phi}{dx_i}} = 1 \quad for\ i = 1,2,\dots,n$$

one can see that if the gradient is very small for all constraints with respect to element i, then the numerator of the optimality criterion will be very small (<<1). As a result, the recursion relation of Eqn 2.10 will reduce the stiffness of element i for every iteration that the gradients remain small, thus attempting to eliminate the element.

For most structural optimization problems this scenario goes unnoticed because in an attempt to minimize structural weight an engineer would welcome the elimination of elements that do not have much affect on the constraints. For damage detecton, however, the reduction of stiffness of an element simply because it does not influence the constraints incorrectly infers that there is damage

present in that element when it may not be. The parameter selection subroutine attempts to eliminate this complication by only retaining elements that have a large influence on the constraints as active.

Unconstrained Method for Inactive Variables

The active parameters defined by the subroutine will participate in the OC algorithm just as they have in the classic OC algorithm, but a modification of the algorithm has been created for the inactive variables. As described in the previous section, stiffness parameters are deemed inactive if their constraint gradient components are small. However, setting an element as inactive simply because it fails to influence the constraint equations ignores the fact that the element may still have influence on the objective function. Recall that the optimization problem of Eqn 2.3 not only must satisfy the constraints of Eqn 2.3b, but also must minimize the objective of Eqn 2.3a. Therefore, every inactive parameter will be adjusted so that it reduces the objective function.

Many unconstrained methods have been developed, but since gradient information is already available from the previous steps of the algorithm, the easiest method to employ at this point is the Steepest Descent Method. Utilizing first derivatives of the objective function, each inactive design parameter is adjusted according to Eqn 2.26.

$$x_i^{n+1} = x_i^n - \alpha \frac{d\Phi}{dx_i^n}$$
<div align="right">**2.26**</div>

It is recognized by the author that the Steepest Descent Method is often less efficient than other unconstrained methods, however due to its ease of implementation it was chosen for this portion of the algorithm. Further, it has been observed that the design parameters that are deemed inactive by the parameter selection subroutine are near their optimal values when becoming inactive and so a highly efficient unconstrained method is not imperative at this step.

An example illustrating the used of the theory presented in Sections 2.4 and 2.5 will be given in Chapter 3.

2.6 Damage Localization

For many damage detection problems, especially those with a large number of variables, it is beneficial to reduce the number of active variables for optimization. It is advantageous to eliminate

variables that are known not to contain damage because it reduces the dimension of the search space of the optimization process, thus reducing the computation effort. The process also reduces the chances of false positive damage detection. Two methods of localization will be employed for damage detection. The first will utilize the linking algorithnm of Section 2.4.5 and will be presented in Chapter 6. The second technique will utilize the Damage Location Assurance Criterion (DLAC), developed in Messina [41], to identify parameters that are most likely damaged. The DLAC was originally created for damage detection using dynamic data of structural systems. The DLAC is an adaptation of the Modal Assurance Criterion that identifies damage by comparing the linear correlation between the changes in natural frequencies due to simulated damage of an analytical model and the true change in natural frequencies of the test structure. Even though correlation techniques are common for dynamic based procedures, they are virtually unused for static procedures. However the derived principles are not specific to dynamic data. Adaptation of the DLAC to accommodate static measurments takes the form:

$$DLAC = \frac{|\{\Delta u\}^T\{\Delta u_m\}|^2}{(\{\Delta u\}^T\{\Delta u\})(\{\Delta u_m\}^T\{\Delta u_m\})} \qquad \textbf{2.27}$$

where

$$\Delta u = \frac{u_{damage} - u_{healthy}}{u_{healthy}} \qquad \textbf{2.28}$$

$\Delta u =$ the vector of normalized differences in the calculated displacements

$\Delta u_m =$ the vector of normalized differences in the measured displacements

The DLAC values range from 0, indicating no correlation, to 1 which represents perfect correlation between the test data and simulated data. The measured static response data for the pre and post damage states is assembled into the column vector defined by Eqn 2.28. Next, simulated response data is generated by changing the structural parameter(s) of the analytical model to mimic a possible damage scenario of the structure. A DLAC value is then calculated for this possible damage. Next, the procedure is repeated until all possible damage scenarios have been tested and a DLAC value has been calculated. The damage scenario with the highest DLAC value is chosen as the most likely damage state of the structure. Only the variables with the highest likelihood of damage remain active for the optimization problem. Eqn 2.28 is normalized with respect to the healthy static displacement data to ensure that a single change in static displacement is not unfairly weighted in the correlation calculation.

One advantage of using the DLAC as a localization technique is that it does not require any additional measurements of the test structure. The measured displacements used to assemble $\{\Delta u_m\}$ can be the same measurements used in the optimization problem for damage detection. The reason that the optimization problem is still needed is because the DLAC method is typically only used to locate damage and is not able to quantify damage. One advantage to using static data for this step is that researchers have found it to be much more sensitive to localized damage than modal data (Chou and Ghaboussi [15]). Further, structural symmetry does not pose a problem provided multiple displacements are measured.

2.7 Structural Model

The damage detection algorithm detects damage by adjusting parameters of a structural model until an optimal solution to the set of equations given in Eqn 2.3 is found. Depending on the type of model, several choices exist for adjustable parameters for the optimization algorithm. As explained earlier, this static response based damage detection method concentrates on detecting changes in stiffness of the structure. Using the Finite Element Method, models are assembled using a system of smaller finite elements, each of which can have their own unique set of stiffness parameters.

2.7.1 Two Dimensional Models

In some cases a three dimensional model is not absolutely necessary to detect damage. When the in plane and out of plane response can be decoupled, or nearly decoupled, then the use of a two dimensional finite element model is warranted. The use of two dimensional models can speed up the damage detection process as the size of the elemental stiffness matrices is significantly smaller. Therefore, when possible, two dimensional models will be employed in the damage detection algorithm.

Truss Element

Truss structures will be modeled using truss elements where the adjustable stiffness parameter is the element's cross sectional area, A. The other parameters, which are assumed to remain constant both

pre and post damage, are the element length, L, and Young's modulus, E. A picture of a typical truss element is shown in Figure 2.1.
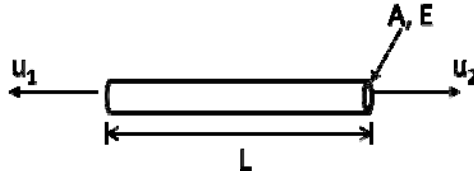
Figure 2.1 Two Dimensional Truss Element Degrees of Freedom

The elemental stiffness matrix is:

$$K = \begin{bmatrix} \dfrac{AE}{L} & -\dfrac{AE}{L} \\ -\dfrac{AE}{L} & \dfrac{AE}{L} \end{bmatrix}$$ **2.29**

Even though the stiffness matrix of Eqn 2.29 appears to be a highly simplified model, it often provides very good response behavior at only a fraction of the computation effort of three dimensional models.

Beam Element

For structures where the structural response is dominated by bending stiffnes, i.e. axial displacement of most elements is negligible, two dimensional beam elements will be employed. For example, two dimensional moment frame structures where, one, loads are applied in the transverse direction to the beams, and two, the column cross sectional areas are sufficient to provide little axial displacement, two dimensional beam elements can be used for the structural model. The adjustable stiffness parameter for these models is the element major axis moment of inertia, I. Again, the element length, L, and Young's modulus, E, remain constant both pre and post damage. A typical beam element is shown in Figure 2.2.
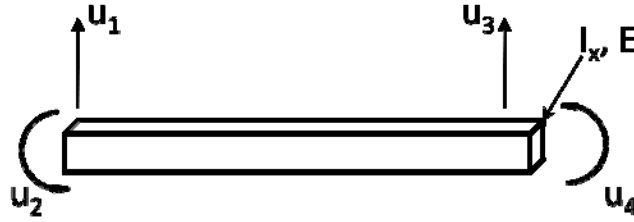
Figure 2.2 Two Dimensional Beam Element Degrees of Freedom

The elemental stiffness matrix is:

$$K = \begin{bmatrix} \dfrac{12EI}{L^3} & \dfrac{6EI}{L^2} & -\dfrac{12EI}{L^3} & \dfrac{6EI}{L^2} \\ \dfrac{6EI}{L^2} & \dfrac{4EI}{L} & -\dfrac{6EI}{L^2} & \dfrac{2EI}{L} \\ -\dfrac{12EI}{L^3} & -\dfrac{6EI}{L^2} & \dfrac{12EI}{L^3} & \dfrac{6EI}{L^2} \\ \dfrac{6EI}{L^2} & \dfrac{2EI}{L} & \dfrac{6EI}{L^2} & \dfrac{4EI}{L} \end{bmatrix} \qquad \textbf{2.30}$$

As a simplifying assumption, you will notice that the shear modulus is absent from Eqn 2.30. This assumption is valid if all beams are loaded in the transverse direction and the lengths of the structural members are sufficiently long such that the shear deformation of the cross section is negligible compared to the deflection due to bending.

2.7.2 Three Dimensional Models

Often the only way to capture the full response behavior of a structure is to assemble a three dimensional model. Whether the test structure is a three dimensional truss, grid, or moment frame, the same elemental stiffness matrix will be used to assemble the model. The various structures can be accomodated by adjusting the moment releases at the element connections. Care must also be taken to assure that the correct parameter is deemed "adjustable" in the optimization algorithm. For example, the cross sectional area must be set active for truss structures, while the moment of inertia must be set active for structures where the response is dominated by bending. A typical element is shown in Figure 2.3 with local degrees of freedom.
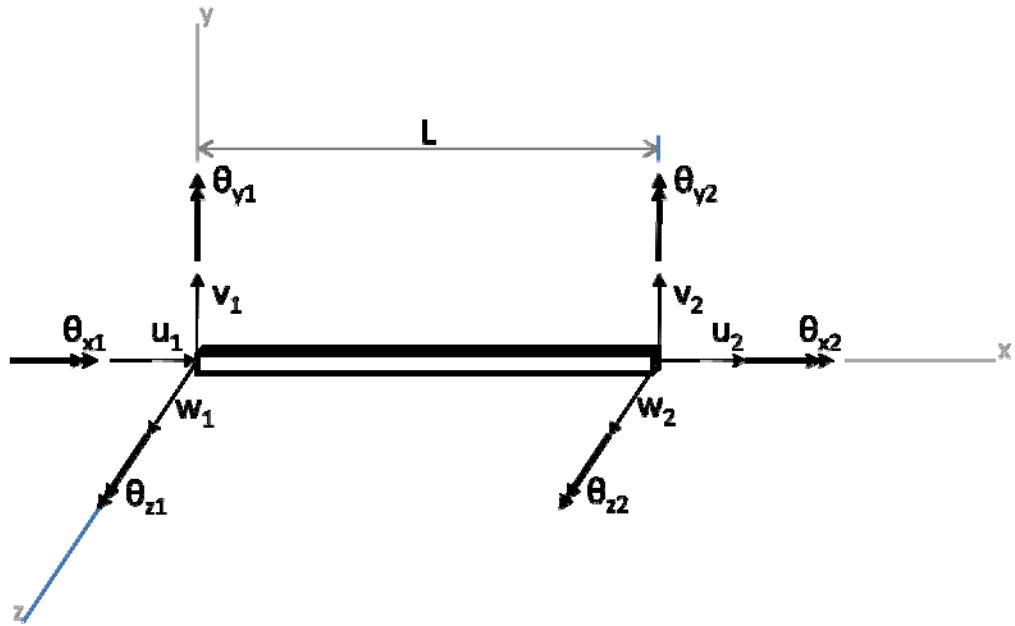
Figure 2.3 Three Dimensional Frame Element Degrees of Freedom

The elemental stiffness matrix is [16]:

$$
\mathbf{K} = \begin{bmatrix}
X & 0 & 0 & 0 & 0 & 0 & -X & 0 & 0 & 0 & 0 & 0 \\
 & Y_1 & 0 & 0 & 0 & Y_2 & 0 & -Y_1 & 0 & 0 & 0 & Y_2 \\
 & & Z_1 & 0 & -Z_2 & 0 & 0 & 0 & -Z_1 & 0 & -Z_2 & 0 \\
 & & & S & 0 & 0 & 0 & 0 & 0 & -S & 0 & 0 \\
 & & & & Z_3 & 0 & 0 & 0 & Z_2 & 0 & Z_4 & 0 \\
 & & & & & Y_3 & 0 & -Y_2 & 0 & 0 & 0 & Y_4 \\
 & & & & & & X & 0 & 0 & 0 & 0 & 0 \\
 & & & & & & & Y_1 & 0 & 0 & 0 & -Y_2 \\
 & & & & & & & & Z_1 & 0 & Z_2 & 0 \\
 & & & & & & & & & S & 0 & 0 \\
 & & & & & & & & & & Z_3 & 0 \\
 & & & & & & & & & & & Y_3
\end{bmatrix}
\qquad \textbf{2.31}
$$

where

$$X = \frac{AE}{L},$$

$$Y_1 = \frac{12EI_z}{(1+\phi_y)L^3}, \; Y_2 = \frac{6EI_z}{(1+\phi_y)L^2}, \; Y_3 = \frac{(4+\phi_y)EI_z}{(1+\phi_y)L}, \; Y_4 = \frac{(2-\phi_y)EI_z}{(1+\phi_y)L},$$

32

$$\phi_y = \frac{12EI_zk_y}{AGL^2},$$

$$Z_1 = \frac{12EI_y}{(1+\phi_z)L^3}, Z_2 = \frac{6EI_y}{(1+\phi_z)L^2}, Z_3 = \frac{(4+\phi_z)EI_y}{(1+\phi_z)L}, Z_4 = \frac{(2-\phi_z)EI_y}{(1+\phi_z)L}$$

$$\phi_z = \frac{12EI_yk_z}{AGL^2},$$

$$S = \frac{GK_T}{L}.$$

Note that k_y and k_z are factors to determine the effective shear area to account for transverse shear deformation and G is the shear modulus. To ignore transverse shear deformation, ϕ_y and ϕ_z are set to zero. The parameter S gives the torsional stiffness of each member where K_T is a property of the cross section. For truss structures the torsional stiffness is ignored, however for three dimensional grid systems the torsional stiffness can have a significant effect on the structural response. Care must be taken in choosing the correct values for K_T. This parameter must be chosen on a case by case basis as will be explained in presented examples.

All of the damage detection examples to be presented utilize doubly symmetric members, where the y and z axis of Figure 2.3 coincide with lines of symmetry, thus validating the use of Eqn 2.31. After damage, it is possible that a portion of a structural member will no longer contain any lines of symmetry, thus requiring recalculation of the principal centroidal axis of the cross section. As a simplifying step, all induced damage will try to ensure that structural elements remain symmetric or nearly symmetric so that use of Eqn 2.31 is warranted.

2.8 Optimal Load Cases

Previous sections have concentrated on changes to the damage detection algorithm. Next, improvements to the damage detection procedure will be discussed. The procedure of Section 1.2 calls for static point loads to be applied to the test structure, but where should these static point loads be applied?

One disadvantage of using static response data for damage detection is that during the loading process, participation of all elements is not guaranteed. Inherently, damage in members that are highly stressed is much easier to detect than damage in members that are lightly stressed or experience rigid body displacements. Therefore, the static method must aim to use load cases that

maximize the participation of each element in the structure. Determining the optimal load cases is a three step process.

1) **List all possible load locations**

Often some loading points are unavailable during a testing procedure. Nonstructural elements may obstruct these loading points hindering their use. It is also possible that access to these points may be too dangerous for testing personnel to make them viable. Also, certain loads may not be possible due to difficulty or cost. For example, loading a building laterally requires large hydraulic actuators as well as a support frame on which to mount these actuators. The cost of applying these loads can make the testing process infeasible. As such, listing all possible load locations is an important step in the damage detection process.

2) **Determine the number of load cases that will be used, n:**

Any damage detection methodology is bound by practical limitations. Some of which may be financial limitations, labor limitations, or physical limitations. As such, under this damage detection methodology, the number of load cases must be determined on a case by case basis. Careful consideration must be taken when determining the number of load cases. Take for example, a bridge structure. Measurement data cannot be polluted by outside interference, therefore the structure must be closed to vehicle traffic. Extended closures may be possible for small bridges on low volume roads but for large, high traffic volume bridges, minimizing the out of service time is paramount for metropolitan areas. Therefore, the number of load cases cannot be overly time consuming, but at the same time cannot compromise accuracy of the method.

The number of load cases is largely dependent on the logistics of the testing procedure. The number of applied loads can be a function of the amount of time available to perform the test. If the test structure is vital to local infrastructure, then the testing procedure must be quick in order to allow the structure to be reopened and resume service to the public.

3) **Determine the best load case combination for damage detection:**

Once logistical decisions have been made regarding the number of load cases and the possible loading points, the next step is to determine the optimal load case locations. The load cases are chosen so that the maximum strain energy is produced in the finite element model. By choosing load cases with the largest strain energy, it encourages participation of the largest number of structural members.

To determine the best load case combinations, we must first generate the strain energy contribution matrix of all possible load cases. Using the analytical model of the test structure, the elemental strain energies are calculated for each load case and assembled in to a matrix using the equation:

$$ESE_{ij} = \frac{1}{2}u_{ij}^T K_i u_{ij}$$

2.32

where u_{ij} is the element displacement vector resulting from the jth load case for the ith element and K_i is the stiffness matrix of the ith element.

Next a binary matrix is created where each column is a unique combination of all possible load cases taken n at a time. For example, say 3 possible load locations exist and 2 loads cases will be used for testing. The binary matrix would be:

$$PLC = \begin{bmatrix} 1 & 1 & 0 \\ 0 & 1 & 1 \\ 1 & 0 & 1 \end{bmatrix}$$

Strain energy contribution matrices (SEC) are created by multiplying ESE by a diagonal matrix created from the columns of PLC

$$SEC_q = ESE * diag(PLC_q) \quad for\ q = 1 \dots number\ of\ columns\ of\ PLC$$

2.33

where SEC_q is the strain energy contributions of each element from the qth load case combination and $diag(PLC_q)$ is a diagonal matrix generated from the qth column of PLC.

Next, a vector of maximum strain energy contributions (MSEC) for each element, from each load case combination, is assembled.

$$MSEC_q = \max\left((SEC_q)^T\right)$$

2.34

where $MSEC_q$ is the qth vector of maximum values from each column of $(SEC_q)^T$.

Finally, generate a row vector of maximum strain energy contribution norms (MSECN) of the maximum element strain energy contributions of each element for a given load case combination.

$$MSECN_q = \|MSEC_q\|$$

2.35

where $MSECN_q$ is the norm of the qth $MSEC$ vector

The best load case combination is that which produces the largest strain energy norm. For example, if the second entry of *MSECN* is the largest value then the load case combination given by the second column of *PLC* is the chosen load case combination for damage detection.

2.9 Optimal Measurement Locations

The same considerations required to determine the optimal loading scheme are required for determining the optimal measurement locations. However, since most of these considerations have already been taken when choosing the optimal load cases, fewer decisions are necessary for measurement locations. Typically if a location is available for loading, it can also be available for measurement. It is desirable to take measurements where the static displacements are the largest. Usually the largest displacements occur at or near an applied static load. Analysis can be used to verify this statement on a case-by-case basis, but for the intent of creating a general rule for the damage detection procedure, displacement measurements will be taken at the point where a load is applied as well as locations near an applied load. One consideration that must be made when determining measurement locations is the possibility of symmetric loading and measurements that give little insight in to the location of damage. As an example, observe the fully constrained beam loaded in the center shown in Figure 2.4.

$$\Delta_P = \frac{PL^3}{192EI}$$
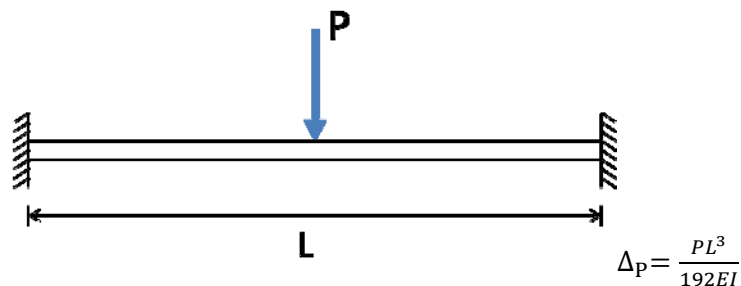
Figure 2.4 Fixed Beam Loaded at the Midspan

where Δ_P is the displacement under the load, P.

The maximum displacement occurs at the midspan of the beam under the applied load. Now assume damage occurs in the form of reduced moment capacity of the left support. As a result, the beam behaves similar to the propped cantilever shown in Figure 2.5.

$$\Delta_P = \frac{7PL^3}{768EI}$$
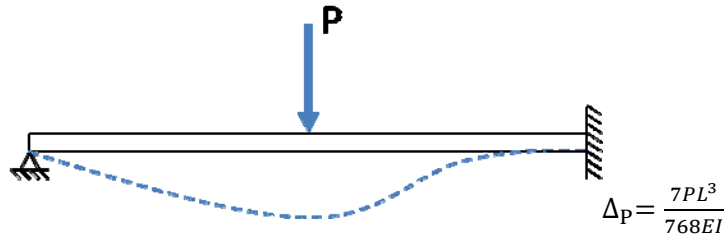
Figure 2.5 Beam Loaded at Midspan with Damaged Left Support

The damage at the left connection creates a larger displacement under the load compared to the healthy case. However the measured displacement of Figure 2.5 is identical to the displacement shown in Figure 2.6 which is also a propped cantilever but the damaged connection at the right support.

$$\Delta_P = \frac{7PL^3}{768EI}$$
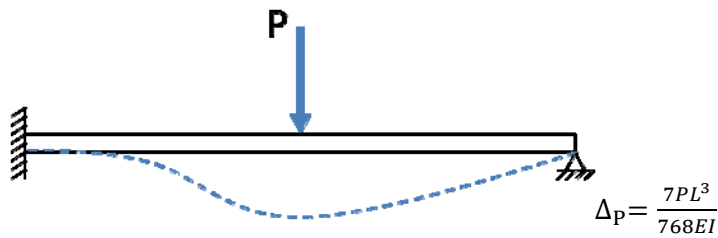
Figure 2.6 Beam Loaded at Midspan with Damaged Right Support

As can be seen, due to the symmetric loading and symmetric displacement measurement, the presence of damage can be detected, but the exact location cannot. These situations should be avoided, if possible. Unfortunately an automated system does not exist to detect these cases and so loading and measurement schemes will need to be manually inspected on a case-by-case basis once a preliminary testing procedure has been created.

2.10 New Damage Detection Procedure

Incorporating the ideas presented in the previous sections and aiming to accomplish the objectives of Section 1.3, a slightly modified procedure from that presented in Section 1.2 can better accomplish these goals. The new procedure is as follows:

1) **Create a preliminary model of the test structure:**
   A preliminary model of the structure is needed to determine the optimal load cases to apply for testing. Using the elements presented in Section 2.7 a structural model is created. Before testing, the stiffness parameters of the structure are unknown. However, using available measurements or structural drawings, a rough topology can be created to aid in the modeling process. The goal is to develop a structural model that can provide a rough idea of the strain energy distribution for various load cases.

2) **Determine the optimal load cases for damage detection:**
   Using the mathematical model of Step 1 and the algorithm of Section 2.8, the optimal load case combinations can be calculated.

3) **Apply static points loads to test structure (Step 1 of Section 1.2)**

4) **Measure displacements resulting from the applied point loads (Step 2 of Section 1.2):**
   Displacement measurements must be taken following the general guidelines of Section 2.9.

5) **Use the measurement data of Step 4 and the simulated loads of Step 2 to update the stiffness parameters of the mathematical model:**
   To reduce modeling error, the stiffness parameters of the model should be adjusted so the static response matches the measured data collected. Depending on the size of the finite element model, adjustment of the stiffness parameters may be done manually or autonomously. Previous work, see [57], offers an autonomous method for adjusting parameters, but for the current work parameters will be adjusted manually.

6) **Repeat steps 3 and 4 periodically using the same load cases and measurement locations to monitor changes in the static response (Step 6 of Section 1.2)**

7) **Use optimization to adjust the stiffness parameters of the mathematical model to match the change in static response of the model with the measured change in response (Step 7 of Section 1.2):**

The damage detection problem of Eqn 2.3 can be formulated and the modified OC algorithm can be used to calculate the location(s) of damaged.

2.11 Algorithm Programming

Matlab is the chosen software and computing language to solve the damage detection algorithm. The heavy use of matrix operations in finite element modeling makes Matlab a natural choice. Further, the ease of algorithm development and the data analysis options adds to the appeal of the software. Even though all finite element coding is done in Matlab, the accuracy of the mathematical models is checked using Risa-3D. It may be asked why Risa-3D, or similar finite element software, is not used as the primary finite element modeling software and the reason for this is that the optimization algorithm requires constraint gradients and derivatives of the stiffness matrix with respect to parameters of each element. In order to utilize third party software, a data purturbation method would need to be employed, which can be time intensive. By creating the finite element assembly algorithm in Matlab, the gradient equations can be written explicity, greatly reducing the computation time of the algorithm.

3   Algorithm Illustration

The damage detection algorithm and procedure contain a multitude of steps. The best way to understand each step is by example. To do so, a simulated damage detection example will be presented and each step of the damage detection process will be explained in detail.

3.1 Continuous Span Test Structure

Damage will be detected in the two span continuous beam shown in Figure 3.1 to illustrate the use of the algorithm.
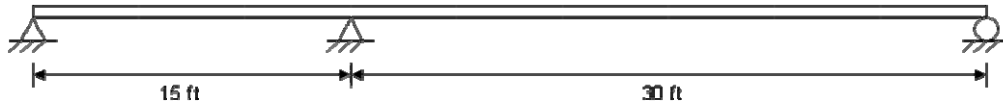
Figure 3.1 Continuous Beam Test Structure Used for Algorithm Illustration

This structure is chosen for illustration because of its intuitive response behavior. This structure will give the reader a solid base on the use of the algorithm without being clouded by issues that are specific to any one type of structural system.

The continuous beam of Figure 3.1 is assumed to be constructed of steel with modulus of elasticity 29000 ksi. Next, although not good engineering practice, a beam splice is located at the middle support connecting two different wide flange sections. The beam over the 15 ft span is a W14X53 (I_x=541 in.^{4}, A=15.6 in.^{2}) and the 30 ft span is a W14X90 (I_x=1000 in.^{4}, A=26.5 in.^{2}).

3.2 Steps for Damage Detection of the Two Span Test Structure

With the topology, material, and cross section properties known, the steps presented in Section 0 can be performed.

Create a preliminary model of the test structure:

A model of the test structure of Figure 3.1 will be created using 9 two dimensional beam elements with stiffness matrices presented in Section 2.7.1. In practice, the number of elements used to create the mathematical model will vary depending on the level of localization desired. Nine elements are used here to provide illustration on the use of the algorithm. An elevation view of the finite element model with global degrees of freedom (DOF) is shown in Figure 3.2.
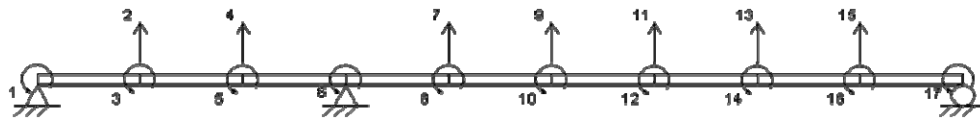
Figure 3.2 Finite Element Model of the Continuous Beam Test Structure

When creating the preliminary model it is important to assemble the elements so that a DOF is available at all possible loading points. It is assumed that the vertical DOFs of Figure 3.2 correspond to the possible load locations of the test structure.

Determine the optimal load cases for damage detection:

The possible load locations are given by DOFs 2, 4, 7, 9, 11, 13, and 15 of Figure 3.2. To find the optimal load cases, the strain energy contribution matrix of Eqn 2.33 must be calculated. Starting with the first possible load location, DOF 2, a simulated 1 kip load is applied to the mathematical model, shown in Figure 3.3.
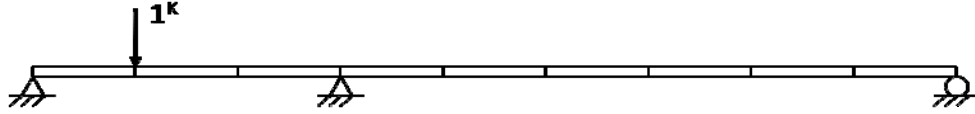
Figure 3.3 First Possible Load Case used for Calculating the Strain Energy Contribution Matrix

With the unit load applied, the resulting displacement field of the model can be used to calculate the strain energy of each element. The strain energy of each element for the first load case defines the first column of the elemental strain energy matrix. The strain energy values are given in Eqn 3.1.

$$ESE_{11} = 0.2064 \times 10^{-5} \, k * in$$

$$ESE_{21} = 0.2975 \times 10^{-5} \, k * in$$

$$ESE_{31} = 0.0231 \times 10^{-5} \, k * in$$

$$ESE_{41} = 0.0356 \times 10^{-5} \, k * in$$

$$ESE_{51} = 0.0238 \times 10^{-5} \, k * in$$

$$ESE_{61} = 0.0145 \times 10^{-5} \, k * in$$

$$ESE_{71} = 0.0074 \times 10^{-5} \, k * in$$

$$ESE_{81} = 0.0027 \times 10^{-5} \, k * in$$

$$ESE_{91} = 0.0004 \times 10^{-5} \, k * in$$

3.1

Following the same procedure for each possible load location, the elemental strain energy matrix can be fully defined. The full matrix is shown in Eqn A.1 in Appendix A.

A decision must now be made as to how many load cases can be applied for the testing procedure. For this example we will allow 4 possible load cases. The possible load combination matrix must be defined. A binary matrix is generated with every combination of the 7 load cases taken 4 at a time. The resulting matrix contains 35 columns, each of which represents a possible load combination for damage detection. For example, the first three columns of the matrix may look like,

$$PLC = \begin{bmatrix} 1 & 1 & 1 \\ 1 & 1 & 1 \\ 1 & 1 & 1 \\ 1 & 0 & 0 \\ 0 & 1 & 0 \\ 0 & 0 & 1 \\ 0 & 0 & 0 \end{bmatrix} \cdots$$

The full PLC matrix is given in Eqn A.2.

The strain energy contribution matrices must now be created by multiplying the ESE matrix by a diagonal matrix formed by each of the columns of PLC. For example, the first SEC matrix is show in Eqn 3.2.

$$SEC_1 = ESE * diag(PLC_1)$$

$$= 1 \text{X} 10^{-5} * \begin{bmatrix} 2.064 & 0.357 & 0.111 & 0.141 & 0 & 0 & 0 \\ 2.975 & 2.498 & 0.776 & 0.985 & 0 & 0 & 0 \\ 0.231 & 1.07 & 2.106 & 2.674 & 0 & 0 & 0 \\ 0.356 & 0.556 & 0.715 & 0.611 & 0 & 0 & 0 \\ 0.239 & 0.373 & 1.988 & 2.152 & 0 & 0 & 0 \\ 0.145 & 0.226 & 1.206 & 4.132 & 0 & 0 & 0 \\ 0.074 & 0.116 & 0.619 & 2.122 & 0 & 0 & 0 \\ 0.027 & 0.043 & 0.228 & 0.782 & 0 & 0 & 0 \\ 0.004 & 0.006 & 0.033 & 0.112 & 0 & 0 & 0 \end{bmatrix}$$

<div align="right">3.2</div>

A separate SEC matrix is formed for each possible load case combination defined by the columns of PLC. The SEC matrices show the total strain energy contribution of each element for the given load case combination.

Next, to determine the optimal load case combition a vector of maximum strain energies for each element is assembled for the available SEC matrices. The first vector of maximum strain energy contributions is given by:

$$MSEC_1 = \max\left(\left(SEC_q\right)^T\right)$$

$$= (1 \times 10^{-5}) * [2.064 \quad 2.975 \quad 2.674 \quad 0.7151 \quad 2.152 \quad 4.132 \quad 2.122 \quad 0.782 \quad 0.112]$$

The MSEC vectors provide a sense of the contribution each element has to the total strain energy of the system. Damage can be detected much more easily if most of the elements participate in the structural response and the $MSEC$ gives a sense of the contribution of each element. The final step

to determine the optimal load case combination is to find the *MSEC* vector with the largest vector norm. For this problem the optimal load case combination is the one that loads DOFs 2, 9, 11, and 13. The maximum strain energy contribution norm (MSECN) is 1.077×10^{-4} k-in.

Apply static points loads to test structure (Step 1 of Section 1.2)

With the optimal load cases found, the test structure can now be loaded. All data in this example is simulated and absent of error. Using the mathematical model as the test structure, the load cases are simulated. Each load case applies a single 10 kip load to DOFs 2, 9, 11, and 13 in sequence.

Measure displacements resulting from the applied point loads (Step 2 of Section 1.2):

For each of the 4 load cases, displacements must be measured. As a general rule, displacements are only able to be measured at degrees of freedom that are also able to be loaded. The load case and measurement schedule is shown in Table 3.1 along with the measurement value.

Table 3.1 Healthy Load Case and Measurement Schedule with Displacement Measurement Values

Load Case	DOF Loaded	DOF measured	Measurement (in.)
1	2	2	-0.04821
2	9	9	-0.05835
		11	-0.09165
3	11	9	-0.09165
		11	-0.16946
		13	-0.18897
4	13	11	-0.18897
		13	-0.23747

Use the measurement data and the simulated loads of Step 2 to update the stiffness parameters of the mathematical model:

After obtaining the baseline healthy measurements of the previous step, the mathematical model should be updated so that the simulated response using the optimal load cases matches the measured displacements. For this example, both modeling error and measurement error are absent from the

measurements, therefore adjusting the stiffness parameters of the mathematical model is not necessary.

Repeat Steps 3 and 4 periodically using the same load cases and measurement locations to monitor changes in the static response (Step 6 of Section 1.2)

Now imagine time has elapsed since the last time the testing procedure was executed. Since that time damage has occurred in the left span of the beam, in the vicinity of the middle support. To simulate this damage, the moment of inertia of the third element of the test sructure is reduced by 15%. The moment of inertia of element 3 is reduced from 540 in.⁴ to 459 in.⁴. The testing procedure is then repeated for the damaged structure. The results are shown in Table 3.2.

Table 3.2 Damaged Load Case and Measurement Schedule with Displacement Measurement Values

Load Case	DOF Loaded	DOF measured	Measurement (in.)
1	2	2	-0.04854
2	9	9	-0.0609
		11	-0.09535
3	11	9	-0.09535
		11	-0.17484
		13	-0.1944
4	13	11	-0.1944
		13	-0.243

Use optimization to adjust the stiffness parameters of the mathematical model to match the change in static response of the model with the measured change in response (Step 7 of Section 1.2)

The collected data now provides all the information necessary to detect damage in the structure. First the optimization problem will be defined, then the OC algorithm will iterate to determine the location of damage. From Eqns 2.1 and 2.2 the objective and constraint equations are:

$$\min \Phi = \sum_{a=1}^{4} \frac{1}{2} \mathbf{u}_a^T \mathbf{K} \mathbf{u}_a \tag{a}$$

$$g_1 = \frac{\Delta u_{2,1}}{0.04821} - \frac{-0.04854-(-0.04821)}{0.04821} = 0$$

$$g_2 = \frac{\Delta u_{9,2}}{0.05835} - \frac{-0.0609-(-0.05835)}{0.05835} = 0$$

$$g_3 = \frac{\Delta u_{11,2}}{0.09165} - \frac{-0.09535-(-0.09165)}{0.09165} = 0$$

$$g_4 = \frac{\Delta u_{9,3}}{0.09165} - \frac{-0.09535-(-0.09165)}{0.09165} = 0 \qquad \text{(b)} \qquad \mathbf{3.3}$$

$$g_5 = \frac{\Delta u_{11,3}}{0.16946} - \frac{-0.17484-(-0.16946)}{0.16946} = 0$$

$$g_6 = \frac{\Delta u_{13,3}}{0.18897} - \frac{-0.1944-(-0.18897)}{0.18897} = 0$$

$$g_7 = \frac{\Delta u_{11,4}}{0.18897} - \frac{-0.1944-(-0.18897)}{0.18897} = 0$$

$$g_8 = \frac{\Delta u_{13,4}}{0.2374} - \frac{-0.2430-(-0.2374)}{0.2374} = 0$$

$$541 \ in.^4 \geq x_i \geq 0 \qquad for \ i = 1,2,3 \tag{c}$$

$$1000 \ in.^4 \geq x_i \geq 0 \qquad for \ i = 4,5,6,7,8,9$$

Using the healthy moment of inertia values as the first approximation for the stiffness of the structure, the strain energy objective function and constraints can be calculated.

The value of the objective function is given by Eqn 3.4.

$$\Phi = \sum_{a=1}^{4} \frac{1}{2} \mathbf{u}_a^T \mathbf{K} \mathbf{u}_a = 0.2411 + 0.2918 + 0.8473 + 1.187 = 2.567 \ k * in \qquad \mathbf{3.4}$$

where

$$\mathbf{u}_a = \mathbf{K}^{-1} \mathbf{P}_a$$

and $\mathbf{P}_a$ is the ath load case.

Because the initial stiffness parameters are the healthy moment of inertia values, the initial change in calculated displacement, $\mathbf{\Delta u}$, is zero. Thus, the intial constraint values are:

$$g_1 = \frac{0}{0.04821} - \frac{-0.04854 - (-0.04821)}{0.04821} = 0.006845$$

$$g_2 = \frac{0}{0.05835} - \frac{-0.0609 - (-0.05835)}{0.05835} = 0.0437$$

$$g_3 = \frac{0}{0.09165} - \frac{-0.09535 - (-0.09165)}{0.09165} = 0.0404$$

$$g_4 = \frac{0}{0.09165} - \frac{-0.09535 - (-0.09165)}{0.09165} = 0.0404$$

$$g_5 = \frac{0}{0.16946} - \frac{-0.17484 - (-0.16946)}{0.16946} = 0.0317$$

$$g_6 = \frac{0}{0.18897} - \frac{-0.1944 - (-0.18897)}{0.18897} = 0.0287$$

$$g_7 = \frac{0}{0.18897} - \frac{-0.1944 - (-0.18897)}{0.18897} = 0.0287$$

$$g_8 = \frac{0}{0.2374} - \frac{-0.2430 - (-0.2374)}{0.2374} = 0.0236$$

Recall from Eqn 2.6 that the gradient of the objective function and constraint equations is needed to check for optimality. The equations for each gradient are as follows:

$$\frac{\partial \Phi}{\partial x_i} = \frac{\partial \mathbf{u}_a}{\partial x_i}^T \mathbf{K} \mathbf{u}_a + \mathbf{u}_a^T \frac{\partial \mathbf{K}}{\partial x_i} \mathbf{u}_a + \mathbf{u}_a \mathbf{K} \frac{\partial \mathbf{u}_a}{\partial x_i}$$

and

$$\frac{\partial g_j}{\partial x_i} = \frac{\partial}{\partial x_i} \left(\Delta u_j^* - \Delta u_{j,measured}^* \right) = \frac{\partial u_j}{\partial x_i} \bigg/ u_{j,healthy}$$

The displacement derivative is found from the force displacement equation, Eqn 1.1,

$$\mathbf{P} = \mathbf{Ku}$$

Taking the derivative of both sides with respect to the ith stiffness parameter gives:

$$\frac{\partial}{\partial x_i}(\mathbf{P}) = \frac{\partial}{\partial x_i}(\mathbf{Ku}) \qquad \textbf{3.5}$$

Note that $\mathbf{P}$ is the load vector that remains constant regardless of the stiffness of the structure. Thus, the left side of Eqn 3.5 vanishes. Utilizing the product rule for the right side, we arrive at Eqn 3.6:

$$0 = \frac{\partial \mathbf{K}}{\partial x_i}\mathbf{u} + \mathbf{K}\frac{\partial \mathbf{u}}{\partial x_i} \qquad \textbf{3.6}$$

Eqn 3.6 can now be solved for the desired quantity:

$$\frac{\partial \mathbf{u}}{\partial x_i} = -\mathbf{K}^{-1}\frac{\partial \mathbf{K}}{\partial x_i}\mathbf{u}$$

The gradient of the stiffness matrix with respect to each design variable can be easily calculated by setting the ith design variable to unity and assigning zero stiffness to the remaining variables. It must be recognize that this method of calculating the stiffness gradients is only valid for finite element models that behave linearly with respect to each stiffness parameter. For non-linear finite element models a more traditional way of calculating gradients is necessary. Models used in this research maintain linear behavior with respect to each design variable.

For illustration, a vector of gradient components of the objective and the first constraint are shown in Eqns 3.7 and 3.8, respectively.

$$\nabla \Phi = \begin{bmatrix} \dfrac{\partial \Phi}{\partial x_1} & \dfrac{\partial \Phi}{\partial x_2} & \dfrac{\partial \Phi}{\partial x_3} & \dfrac{\partial \Phi}{\partial x_4} & \dfrac{\partial \Phi}{\partial x_5} & \dfrac{\partial \Phi}{\partial x_6} & \dfrac{\partial \Phi}{\partial x_7} & \dfrac{\partial \Phi}{\partial x_8} & \dfrac{\partial \Phi}{\partial x_9} \end{bmatrix}^T$$

$$= 1 \times 10^{-3} * \begin{bmatrix} -0.1903 \\ -0.490 \\ -0.7654 \\ -0.1145 \\ -0.2718 \\ -0.6306 \\ -0.5428 \\ -0.19999 \\ -0.0285 \end{bmatrix}$$

<div align="right">3.7</div>

$$\nabla g_1 = \begin{bmatrix} \dfrac{\partial g_1}{\partial x_1} & \dfrac{\partial g_1}{\partial x_2} & \dfrac{\partial g_1}{\partial x_3} & \dfrac{\partial g_1}{\partial x_4} & \dfrac{\partial g_1}{\partial x_5} & \dfrac{\partial g_1}{\partial x_6} & \dfrac{\partial g_1}{\partial x_7} & \dfrac{\partial g_1}{\partial x_8} & \dfrac{\partial g_1}{\partial x_9} \end{bmatrix}^T$$

$$= 1 \times 10^{-3} * \begin{bmatrix} 0.6262 \\ 0.8915 \\ 0.0729 \\ 0.0595 \\ 0.03988 \\ 0.02419 \\ 0.01242 \\ 0.00458 \\ 0.00065 \end{bmatrix}$$

<div align="right">3.8</div>

As explained in Section 2.5.2, the constraint gradients are used to determine the active design variables for the current iteration. Only the elements that have the largest affect on the constraints are retained during the optimization process. Take for example the gradient of the first constraint given in Eqn 3.8. Elements 1 and 2 have the largest components of the gradient, while element 9 has a gradient component nearly 3 orders of magnitude smaller than either element 1 or 2. As explained in Section 2.5.2 in order to avoid the scenario where the algorithm will attempt to eliminate an element because it does not contribute to satisfying the constraint equations, only the elements with the largest constraint gradients will remain active. Therefore, the first constraint will retain elements 1 and 2 as active. Two elements are chosen from each constraint gradient to remain active. After performing the subroutine for each constraint, elements 1, 2, 3, 5, 6, and 7 remain active for this iteration. Even though elements 4, 8, and 9 are set as inactive in the OC algorithm, they are still subjected to a steepest descent algorithm to minimize the objective function, as will be explained.

With the active variables set and all gradients calculated, optimality can be checked. Utilizing Eqn 2.14, the Lagrange multipliers are found. Using a least squares approximation, the following Lagrange multipliers are calculated for the first iteration:

$$\lambda_1 = 0.2952$$

$$\lambda_2 = 0.3990$$

$$\lambda_3 = -0.7098$$

$$\lambda_4 = -0.7098$$

$$\lambda_5 = 4.0250$$

$$\lambda_6 = -1.9706$$

$$\lambda_7 = -1.9706$$

$$\lambda_8 = 3.0714$$

Knowing all Lagrange multipliers, T_i of Eqn 2.6 can be calculated for each active variable to assess the optimality of the current stiffness values.

$$T_1 = 1.1117$$

$$T_2 = 0.91794$$

$$T_3 = 0.69128$$

$$T_4 = 1.0000$$

$$T_5 = 1.00000$$

$$T_6 = 0.9999$$

$$T_7 = 0.99999$$

$$T_8 = 1.00000000$$

$$T_9 = 1.00000000$$

Judging from the calculated values for T_i, nearly all of the active variables are close to optimal. Element 3 is the least optimal for the current iteration. Using the recursion relation from Eqn 2.9, a

new set of design variables is calculated to better satisfy optimality. Elements 4 through 9 remain virtually unchanged, however elements 1 through 3 are shown below.

$$x_1^{k+1} = 541 + \frac{1}{2}(1.1117 - 1) * 541 = 571 \qquad \textbf{(a)}$$

$$x_2^{k+1} = 541 + \frac{1}{2}(0.9179 - 1) * 541 = 519 \qquad \textbf{(b)} \qquad \textbf{3.9}$$

$$x_3^{k+1} = 541 + \frac{1}{2}(0.69128 - 1) * 541 = 457 \qquad \textbf{(c)}$$

It is important to notice that the optimality criterion value for the first element is greater than 1, signifying that it must be increased to better satisfy optimality. However, Eqn 3.9(a) shows that the new design variable has increased the stiffness of element 1 beyond its healthy value. This is not possible due to the side constraint of Eqn3.3(c). Therefore this iteration must be repeated with element 1 set as an inactive variable. Once the new set of Lagrange multipliers and optimality values are calculated, the reults must again be inspected for elements that violate the side constraints. Once all values remain within the side constraints, an unconstrained steepest descent optimization is performed on the inactive variables to minimize the objective function. For example, element 9 is inactive, but it will be adjusted using the steepest descent equations:

$$x_i^{n+1} = x_i^n - \alpha \frac{d\Phi}{dx_i^n}$$

The derivative of the objective function with respect to element 9 can be found in Eqn 3.7. Ideally a one dimensional line search can be used to determine α, but to reduce computation time a static value will be employed for damage detection. A value of 2% of the healthy parameter value will be used. In this case, because all of the inactive variables are already at the upper limit of the side constraints and have negative objective gradients, the steepest descent equation will attempt to increase the elemental stiffness of all inactive variables beyond the upper limit of the side constraints. Therefore, the steepest descent method is not needed for the first iteration. Nevertheless, the steepest decent method should be applied to all inactive variables and the final results should be checked to assure that they remain within the side constraints.

The iteration data is shown in Table A.1. The objective and constraint optimizations are shown in Figure 3.4 and Figure 3.5, respectively.

51
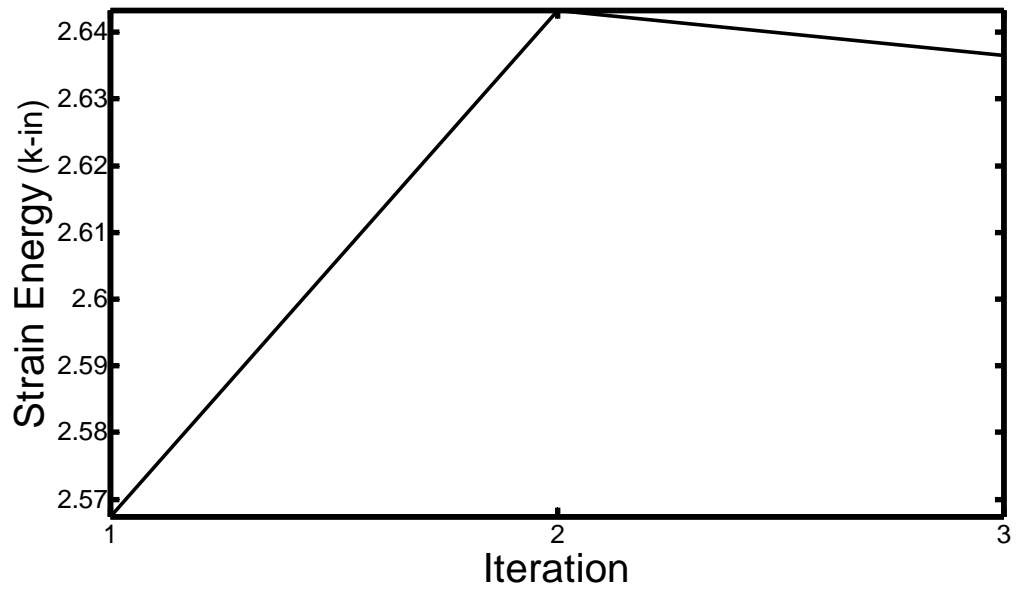
Figure 3.4 Objective Function Optimization Results
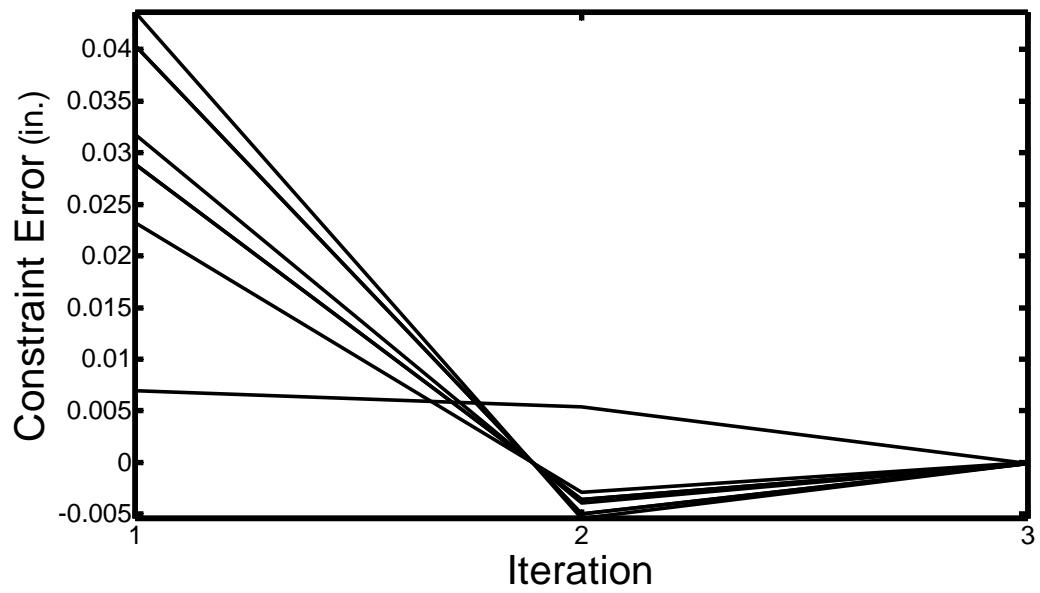
Figure 3.5 Constraints Optimization Results

Note that the constraint optimization exactly satisfied all constraint equations. This was expected since the measurement data was absent of errors and so an exact solution was able to be found. Due to the size of the structure and the number of constraints, it took only 3 iterations to find an optimal solution. The objective optimization shows an initial increase as the algorithm approached a feasible solution and then decreased with the second iteration. The final caculated element damage is shown in Figure 3.6.
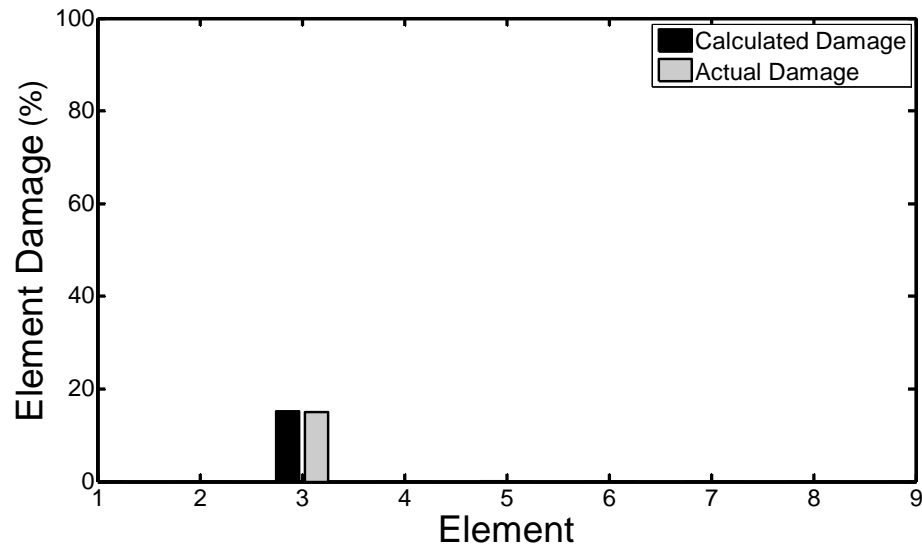
Figure 3.6 Damage Detection Results for Continuous Beam Structure

The algorithm was able to detect the 15% decrease in the moment of inertia of element 3. Again, the absence of error in the measurement data provides conditions were the algorithm can exactly satisfy all constraints and can locate and quantify damage exactly. When modeling and measurement errors are incorporated, it is expected that the damage detection data will be less exact, but will still provide a good approximation for the location and extent of damage.

The presented example has shown the process executed for damage detection. Each step was explained explicity in order to illustrate the calculations necessary to recreate the damage detection results that will be presented in subsequent chapters. The remaining examples will focus on presenting the nuances of each specific example, rather than the details of each individual calculation. The reader should recognize that the procedure and calculations presented in this chapter are similar for all examples and any changes to the process or algorithm will be fully explained within each damage detection problem.

4 Damage Detection in a Steel Moment Frame using Experimental Test Data

Previous work done by the author has attempted to establish the capabilities and limitations of the damage detection algorithm under ideal conditions, where both modeling and measurement errors are absent from the damage detection problem. It is important to thoroughly test the algorithm in the absence of error so that when error is added, there will be no ambiguity as to whether complications that arise are due to data error or are simply limitations of the algorithm.

Now that the performance of the algorithm under simulated conditions has been well documented (see [57]-[63]), its reliability in the presence of error must be established. To do this, a damage detection problem will be solved using the OC algorithm and test data presented by Bakhtiari-Nejad [2]. The results of the OC algorithm will be compared to the results presented in the literature to assess the performance of the current algorithm relative to an alternative static based method. The results presented in [2] are chosen for comparison because, one, very little raw test data has been published in the static damage detection literature and, two, the damage detection method in [2] uses a constrained optimization algorithm for damage detection. Recall that most researchers employ unconstrained methods and so the opportunity to compare results against a similar algorithm is highly beneficial in gauging the progress of the current research.

4.1 Test Structure

Damage will be detected in a one bay, one story steel moment frame using experimentally measured displacements. The experimental apparatus is shown in Figure 4.1. The frame is made of steel with an elastic modulus of 29000 ksi and density 487 lb/ft^3. The structural members are 1.57X0.39 in. hollow bars with 0.08 in. wall thickness. The healthy moment of inertia for all members is 0.0065 in.^{4} and the cross sectional area is 0.285 in.^{2}. Although not specifically stated, it is assumed that the base

of the columns are designed to mimic fully restrained boundary conditions. Both the bay width and story height are 39.37 inches. Even though the structure seems simple in nature, the results of the experimental test will help to establish the validity of the algorithm as a tool for damage detection. Only static displacement measurements will be used to detect damage in the test structure. The load case combinations have been determined by the authors of [2] and therefore will not be chosen using the method of Section 2.8. A list of section and material properties is shown in Table 4.1.

Figure 4.1 One Bay, One Story Steel Moment Frame Test Structure (reproduced from Bakhtiari-Nejad [2])

Table 4.1 Material and Cross Section Properties of Moment Frame Test Structure

Material and Cross Section Property	Columns	Beam
Weak axis moment of inertia, I_z	0.0065 in.^{4} (0.2685 cm^4)	0.0065 in.^{4} (0.2685 cm^4)
Strong axis moment of inertia, I_y	0.072 in.^{4} (3.0 cm^4)	0.072 in.^{4} (3.0 cm^4)
Cross sectional area, A	0.285 in.^{2} (1.84 cm^2)	0.285 in.^{2} (1.84 cm^2)
Modulus of elasticity, E	29000 ksi (200 Gpa)	29000 ksi (200 Gpa)
Density, ρ	487 lb/ft^3 (7800 kg/m^3)	487 lb/ft^3 (7800 kg/m^3)

4.1.1 Experimental Setup

A support frame is erected adjacent to the test structure in order to provide a static reference point to mount displacement sensors. Four displacement sensors will measure displacements resulting from three load cases. Each of the three load cases applies a combination of static point loads. Both vertical and horizontal loads are able to be applied using the test set up shown in Figure 4.1. It was deemed that a maximum of 3 static point loads is able to be applied for each load case. The support frame allows the displacement sensors to be moved so that different displacements locations can be measured for each load case. The loading and measurements are designed to characterize the in plane structural response of the steel moment frame. Therefore the test will only be used to detect stiffness reductions that affect the in plane static response.

4.2 Analytical Model

The loading and measurements are meant to characterize only the in plane structural response, therefore a two dimensional finite element model is sufficient to encompass the structural behavior. Using the two dimensional beam element of Section 2.7.1 the finite element model shown in Figure 4.2 is created.
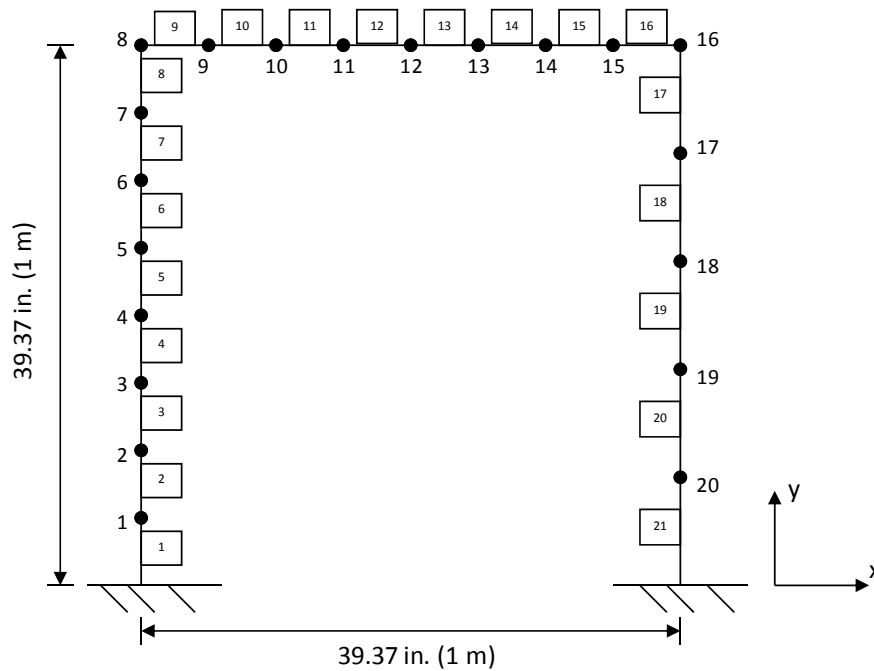
Figure 4.2 Twenty-One Element Analytical Model of the Moment Frame Test Structure

The experimental structure is approximated using a 21 member finite element model. The element layout and numbering scheme was chosen to match the model created in [2]. By creating a similar model, comparison of the damage detection results can be made much more easily. The model of the healthy structure is created using the parameters of the healthy test model given in Table 4.1. Both the modulus of elasticity, length, and cross sectional area are assumed to remain constant both pre and post damage. Moment of inertia is chosen as the design variable for optimization because the structural response is dominated by flexural stiffness. The length of the structural members is sufficiently slender so that shear deformations are assumed negligible compared to deflections due to bending. It is also assumed that the structure is loaded through the centroid of each member and therefore deflections due to torsion are not significant. The finite element model was checked for accuracy by assembling an identical model in RISA-3D. Using arbitrary loading conditions, the static responses of both the analytical model and the RISA-3D model were compared. Once the two response behaviors matched, the finite element model of Figure 4.2 was deemed acceptable for damage detection.

4.3 Baseline Data with Loading and Measurement Schedule

A baseline response must be recorded to provide a reference frame that all subsequent readings can be compared. To do this, three load cases are applied to the moment frame structure. The load locations will be described in reference to their location on the finite element model of Figure 4.2. The loading schedule is shown in Table 4.2.

Table 4.2 Loading Schedule for Damage Detection of Moment Frame Test Structure

Load Case 1			Load Case 2			Load Case 3		
Node	**Load** (lbs)	(N)	**Node**	**Load** (lbs)	(N)	**Node**	**Load** (lbs)	(N)
8	10.8	48.09	15	-22.04	-98.06	21	-4.99	-22.21
			18	-4.99	-22.21	18	-22.04	-98.06
			21	-22.04	-98.06			

Note the sign convention on the loads is relative to the axis shown in Figure 4.2. Loading points that lie along a vertical member, for example node 8 of load case 1, will apply the load magnitude in the horizontal direction. You will notice that the load cases shown in Table 4.2 do not fit the paradigm established in Section 2.8 for maximum practicality of the testing procedure. Recall, the loading conditions for damage detection attempts to use only gravity loads to increase the ease at which loads can be applied. The load cases employed here apply lateral loads to the moment frame. Application of lateral loads in real testing conditions can be challenging and often requires large equipment that is difficult and expensive to operate. Even though the load cases do not comply with the theory of Section 2.8, the purpose of this example is to assess the effectiveness of the damage detection algorithm and compare the results to a similar methodology. Therefore use of the load cases of Table 4.2 is beneficial for comparison purposes. If the load case combinations were determined using the algorithm of Section 2.8, assuming lateral loads are acceptable and 4 loading points are able to be employed, the optimal loading scheme would load nodes 10, 12, 14, and 18.

4.3.1 Steel Moment Frame Baseline Data

Next, the measurement locations must be set. Complying with the measurement locations established in the literature, the measurement schedule is shown in Table 4.3. The displacement measurements resulting from each of the load cases is also shown in Table 4.3. Similar to the applied loads, measurement locations along vertical members are lateral displacement measurements.

Table 4.3 Measurement Schedule and Baseline Data for Healthy Test Structure

Load Case 1			Load Case 2			Load Case 3		
Node	Displacement (in.)	(mm)	Node	Displacement (in.)	(mm)	Node	Displacement (in.)	(mm)
6	0.052	1.333	5	-0.008	-0.208	5	-0.007	-0.175
11	0.063	1.589	9	-0.024	-0.599	9	-0.019	-0.475
12	0.081	2.07	10	0.021	0.543	10	-7E-04	-0.019
18	-0.01	-0.265	20	-0.047	-1.198	20	-0.036	-0.909

The data presented in Table 4.3 represents the healthy or baseline data that is used for comparison of the damaged and undamaged states. Now that the baseline data has been obtained, the quality of the model must be assessed. To do so, the same load cases are simulated on the finite element model of Figure 4.2. The model has been created so that a nodal displacement can be calculated at each one of the measurement locations. The calculated response data is shown in Table 4.4 with the corresponding experimental displacement measurement.

Table 4.4 Analytical and Experimental Measurement Data Comparison

	Node	Analytical		Experimental		Error
		(in.)	(mm)	(in.)	(mm)	(%)
Load Case 1	6	0.055	1.398	0.052	1.333	4.65
	11	0.068	1.72	0.063	1.589	7.62
	12	0.087	2.213	0.081	2.07	6.46
	18	-0.011	-0.269	-0.01	-0.265	1.49
Load Case 2	5	-0.008	-0.196	-0.008	-0.208	-6.12
	9	-0.021	-0.524	-0.024	-0.599	-14.31
	10	0.021	0.536	0.021	0.543	-1.31
	20	-0.043	-1.104	-0.047	-1.198	-8.51
Load Case 3	5	-0.006	-0.152	-0.007	-0.175	-15.13
	9	-0.018	-0.449	-0.019	-0.475	-5.79
	10	-7E-04	-0.019	-7E-04	-0.019	-2.15
	20	-0.033	-0.834	-0.036	-0.909	-8.99

Also contained in Table 4.4 is the percent error between the experimental measured displacements and the analytical displacements calculated from the finite element model. As can be seen, many of the displacement measurements match the experimental values (within ±5%). However there are also many measurements that differ by more than 10% of the analytical value.

4.4 Model Validation and Updating

At this point it is beneficial to adjust the stiffness parameters of the mathematical model to better match the experimental data of the healthy structure. Reducing the difference between the healthy experimental data and calculated analytic data will make it easier to monitor changes in the response

behavior and reduce the overall error in the damage detection problem. Even though the focus of this work is on damage detection and not parameter identification, a preliminary identification step can help reduce the modeling error of the problem. As stated earlier, this step can be performed either manually or by an automated process. The number of elements used for this mathematical model is relatively small and so manual adjustment would be possible for this problem, however an automated process has been chosen. A parameter identification algorithm is presented in [57], and is employed here. The current model, using the parameters of Table 4.1, is used to initialize the identification process. The stiffness parameters are allowed to be adjusted by ±10% of the healthy moment of inertia values, with the exception of elements adjacent to connections. These elements are able to be increased by as much as 20% of the original moment of inertia values. This is to account for the difficulty in modeling connection stiffness. The algorithm is allowed to iterate to best match the calculated response data with the experimental measurement data. The identified stiffness parameters are shown in Table 4.5 along with the percent change from the stiffness value of Table 4.1. The resulting response data with experimental error are shown in Table 4.6.

Table 4.5 Stiffness Parameters of Updated Model

Element	I_x (in.^{4})	I_x (cm^4)	% Change
1	0.0071	0.295	9.757
2	0.0071	0.295	9.987
3	0.0071	0.295	9.993
4	0.0071	0.295	9.925
5	0.007	0.291	8.317
6	0.0058	0.242	-9.912
7	0.0071	0.295	9.980
8	0.0058	0.242	-9.985
9	0.0058	0.243	-9.531
10	0.0065	0.269	0.043
11	0.0058	0.243	-9.635
12	0.0059	0.246	-8.304
13	0.0062	0.259	-3.431
14	0.0058	0.242	-9.943
15	0.0058	0.242	-9.896
16	0.0059	0.245	-8.937
17	0.0058	0.242	-9.968
18	0.0058	0.242	-9.971
19	0.0058	0.242	-9.905
20	0.0058	0.243	-9.549
21	0.0077	0.319	18.921

Table 4.6 Comparison of Static Response Measurements of Updated Model

	Node	Analytical		Experimental		Error
		(in.)	(mm)	(in.)	(mm)	(%)
Load Case 1	6	0.053	1.3473	0.0525	1.333	-1.06
	11	0.0636	1.6158	0.0626	1.589	-1.66
	12	0.0825	2.0949	0.0815	2.07	-1.19
	18	-0.011	-0.273	-0.01	-0.265	-2.97
Load Case 2	5	-0.008	-0.204	-0.008	-0.208	1.91
	9	-0.022	-0.565	-0.024	-0.599	6.01
	10	0.021	0.5336	0.0214	0.543	1.76
	20	-0.046	-1.173	-0.047	-1.198	2.10
Load Case 3	5	-0.006	-0.155	-0.007	-0.175	12.86
	9	-0.018	-0.47	-0.019	-0.475	1.15
	10	-9E-04	-0.024	-7E-04	-0.019	-20.54
	20	-0.035	-0.892	-0.036	-0.909	1.87

The new calculated response data matches the experimental data more closely. There was an increase in error for two displacement values in load case 3, however you will notice that those two displacements are the smallest of all the displacement measurements and so small differences appear as very large errors. Therefore the large calculated error for these displacements is not of immediate concern.

4.5 Damaged Structure Response Data

The test structure is damaged using a saw cut to remove a portion of the cross section along element 16. It was determined by the authors that the saw cut induced a 62% reduction in the bending stiffness of the structure in the vicinity of the cut. A picture of the damage is shown in Figure 4.3.
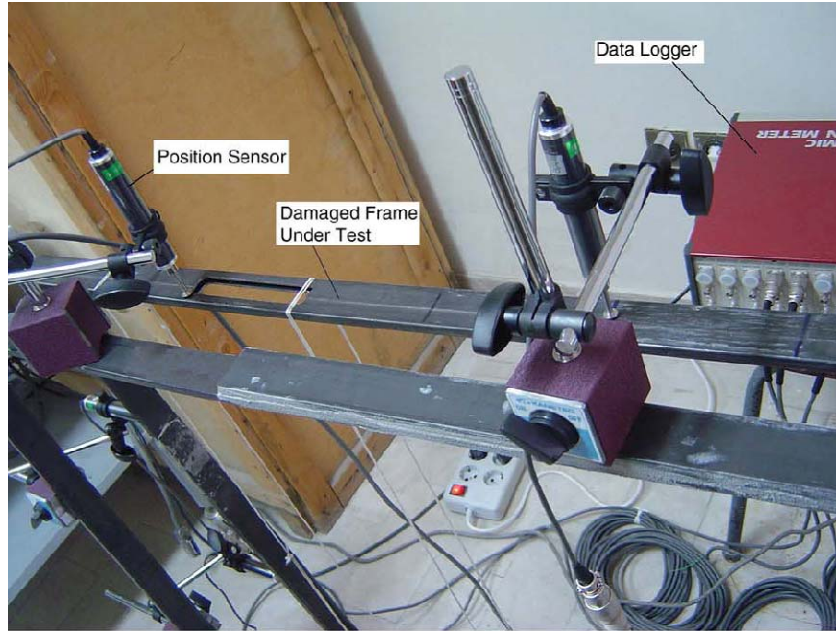
Figure 4.3 Saw Cut of Test Structure for Induced Damage (reproduced from Bakhtiari-Nejad [2])

Using the same experimental setup, load cases, and measurement locations as the healthy state, the response data of the damaged structure is obtained. The measurement data is shown in Table 4.7.

Table 4.7 Experimental Response Measurements of Damaged Structure

	Load Case 1				Load Case 2				Load Case 3		
Node	**Displacement**		**% Change**	**Node**	**Displacement**		**% Change**	**Node**	**Displacement**		**% Change**
	(in.)	(mm)			(in.)	(mm)			(in.)	(mm)	
6	0.0544	1.383	3.75	5	-0.008	-0.215	3.37	5	-0.006	-0.155	-11.43
11	0.0659	1.675	5.41	9	-0.025	-0.647	8.01	9	-0.019	-0.483	1.68
12	0.0855	2.171	4.88	10	0.0239	0.606	11.60	10	-7E-04	-0.019	0.00
18	-0.012	-0.297	12.08	20	-0.048	-1.225	2.25	20	-0.036	-0.917	0.88

You can see that the relative change in displacement from the healthy data ranges from 0% to a maximum of 12.08%. The optimization algorithm will adjust the stiffness parameters of the mathematical model to mimic these changes in the static response. All of the preliminary steps have now been taken for damage detection. The finite element model has been validated to reduce

modeling error and the data obtained in Table 4.3 and Table 4.7 provides all the information necessary for the algorithm to detect damage.

4.6 OC Algorithm Damage Detection Results

The response data are used as constraints in the optimization problem and the upper side constraints are set equal to the healthy stiffness values, preventing any of the elements from increasing in stiffness. The objective function being minimized is the cumulative strain energy given by Eqn 2.1. Two exit criteria are employed for this damage detection problem. The algorithm will deem that the problem has converged if either all of the optimality criterion values of Eqn 2.6 are within ±1% of unity or the change in the cumulative error of the constraint equations and the total strain energy changes by less than 1% of the previous iteration for 3 consecutive iterations. The final calculated damage is shown in Figure 4.4 along with the actual damage location.
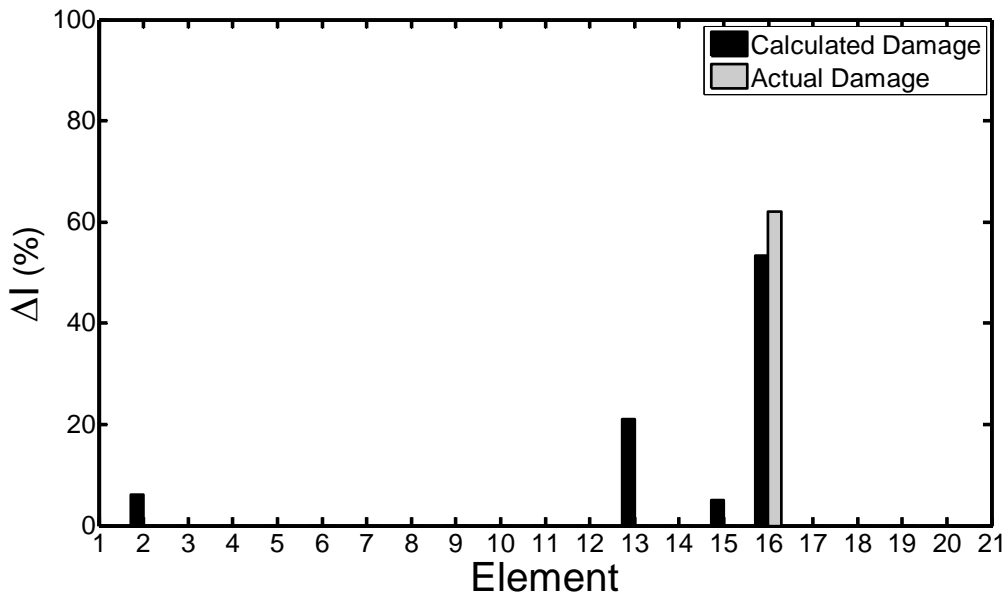
Figure 4.4 Moment Frame Damage Detection Results Using OC Algorithm

The algorithm was able to detect significant damage in element 16. The calculated damage identifies two areas of significant damage. A reduction of 53.4% in the moment of inertia is observed in element 16 and a 21% reduction in element 13. Although slightly under predicted, the damage

calculated in element 16 gives a very good indication of the extent of damage present in the system. The slight damage calculated in element 15 can be attributed to its close proximity to the real damage location. The discrepancy in the actual and calculated damaged values can be attributed to errors in modeling of the structure and the accuracy of the test data. Of concern is the damage calculated in element 13. First, it should be noted that false positives in damage detection are much more desirable than lack of detection of true damage. However, false positives can be frustrating during implementation of monitoring procedures as inspection crews will necessarily be required to inspect areas identified by the algorithm. Notice that most of the areas of false positive damage identification, i.e. elements 2 and 13, are adjacent to structural connections. Connection details are not provided in the literature so the behavior of the structure in the vicinity of connections is not well known. The finite element model assumes the connections are fully fixed, but it is possible that the true connection behaves more as a rotational spring rather than a fully fixed connection. In turn, the experimental response behavior may appear as though damage is present in the connection since it is modeled as fully fixed. The connection detail may also lead to nonlinear response behavior. Significant nonlinear behavior is unlikely due to the small load magnitudes applied, but any nonlinearities that are present could be interpreted as damage by the optimization algorithm. In any case, one should be suspicious of damage calculated in the vicinity of connections but at the same time realize that connection damage is often the most likely form of damage. Therefore calculated damage in these areas should be taken seriously. A new element will be presented in Chapter 5 that will better model and detect damage in connections.

4.7 SQP Model Updating and Damage Detection

The experimental data has already been presented in Sections 4.3 and 4.5. A finite element model is created in the literature that is similar to the one presented in Figure 4.2, with identical node and element numbering scheme. The authors perform a model validation step, much like Section 4.4, to improve the accuracy of the initial finite element model. To do so the authors deviate slightly from the static based method and use experimental natural frequencies to update the structural model. Using the first 8 natural frequencies of the structural system, the authors use a Sequential Quadratic Programming (SQP) software package to match the measured healthy static response data with the calculated data of the mathematical model, while minimizing the error between the measured dynamic response data and the calculated natural frequencies of the finite element model. A sample of the updated parameters is presented in the literature.

Once the model has been updated, the test data of the damaged structure can now be used to calculate areas of stiffness reduction. Again, utilizing a Sequential Quadratic Programming algorithm, the change in the static displacements are used as constraints and the objective function attempts to minimize the error between the calculated damaged load case combinations and the healthy load case combinations. Ideally the load cases are identical both pre and post damage so the objective function attempts to match the applied load vector both before and after damage. The results of the optimization algorithm are shown in Figure 4.5 and Figure 4.6.
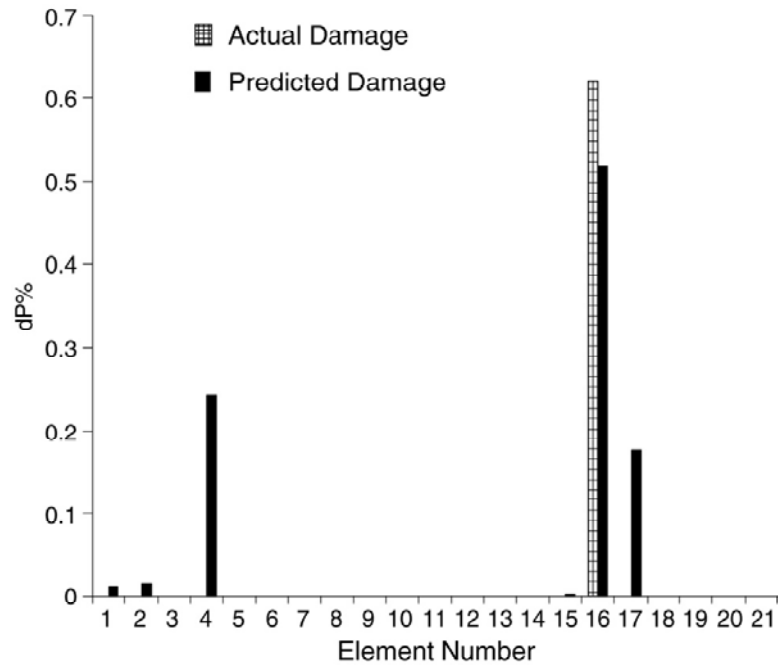
Figure 4.5 SQP Damage Detection Results Using Load Cases 1 and 2 (reproduced from Bahktiari-Nejad [2])
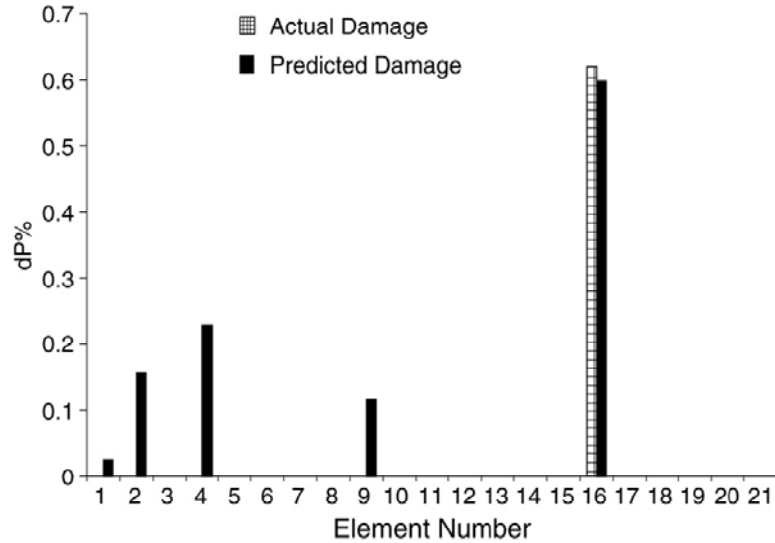
Figure 4.6 SQP Damage Detection Results Using Load Cases 2 and 3 (reproduced from Bahktiari-

Nejad [2])

The results of Figure 4.5 and Figure 4.6 show that the SQP algorithm is able to correctly detect damage in element 16. Both results also provide a reasonable prediction of the extent of damage in the structural element. The algorithm also detects an array of false positive damage locations. One possible reason for this is that the authors did not use all 3 load cases for detecting damage. Each result only uses two load cases at a time.

4.7.1 Result Comparisons of the Damage Detection Algorithms

Both algorithms detected damage in the correct element. The SQP algorithm better quantified damage as both presented results were within ~10% of the true reduction in stiffness of element 16. The OC algorithm also correctly identified stiffness reduction in element 16 and also quantified damage within 10% of the true damaged value. One advantage of the Optimality Criterion algorithm is that the validation step only utilized the static data already collected. Additional dynamic tests were not needed to reduce the error in the model. The number of false positive damage locations was much higher for the SQP algorithm because the authors only utilized two load cases at any one time. It is unclear why the authors did not use all 3 load cases, but it is suspected that algorithm stability may have been a factor in determining the number of load cases used. To reiterate the underlying theme from previous sections, constrained methods often suffer from stability issues when

experimental data is used for damage detection. The error inherent in the measurements often creates inconsistent constraints where a feasible solution does not exist. The modified OC algorithm is able to maintain stability even when many constraints are used that contain error because of the least squares subroutine. This fact allows for the use of all three load cases as well as all measured displacement data for damage detection. As a result, the OC algorithm had far fewer false positive damage locations than the SQP algorithm.

Unfortunately the authors did not comment on the computation time and effort required for damage detection so direct comparison of the algorithms cannot be made. Comment can be made, however, on the choice of the SQP method as a damage detection tool. SQP is a constrained optimization method built on the framework of Newton's Method. Essentially SQP is Newton's method applied to the condition of optimality given in Eqn 2.5 (repeated here for convenience).

$$\frac{\partial L}{\partial x_i} = \frac{\partial \Phi}{\partial x_i} + \sum_{j=1}^{p} \lambda_j \frac{\partial g_j}{\partial x_i} = 0 \quad for\ i = 1,2,3,\dots,n$$

At each iteration the objective is approximated using a quadratic function. The minimum of that function is found subject to linear constraints (or linear approximated constraints). The quadratic approximation at each iteration requires the calculation of the mixed partial derivatives of the objective function, a very time consuming and computationally expensive step. The beauty of the method, however, is its fast convergence in very few iterations. Therefore the increased computing effort can be somewhat justified by the reduction in the number of iterations to find an optimal solution. The fast convergence is contingent upon the accuracy of the quadratic approximation of the objective function at each step.

It was the goal of this research to avoid using the Hessian matrix in order to minimize the computing effort and maintain the ability to solve larger scale problems. Iteration data is not provided by the authors but it is speculated that use of the SQP algorithm is not overly burdensome for this example. Larger structures, however, may require a more computationally efficient algorithm. It would not be surprising if the SQP algorithm converges in fewer iterations that the OC algorithm for this example, however for larger scale problems the OC algorithm has the advantage of requiring only first derivatives of the constraint and objective functions. Further, the OC algorithm is also known for its fast convergence in the presence of nonlinear constraints and objectives and so it presents characteristics favorable for both fast convergence and computation efficiency.

4.8 Conclusion

A damage detection method must be accurate even when test data contains errors. The performance of the OC algorithm for this example is encouraging. The algorithm was able to detect damage with very little knowledge of the testing procedure or the characteristics of the test structure. All data used in this chapter was obtained from the published literature. The author did not assist in the testing procedure or have firsthand knowledge of the test structure. The modeling choices were made based on written descriptions of the test structure. Further, the load cases and measurement locations in the literature did not exactly match those determined by the theory of Sections 2.8 and 2.9, yet the algorithm was still able to accurately locate and quantify damage. False positive damage locations did appear in the results, however many of these false positives can be explained by the lack of knowledge of the connection detail of the structure and the difficulty in modeling connection stiffness. Contrasting the results presented in the literature, the OC algorithm results had far fewer false positive damage identifications. The accuracy of damage detection in the true damaged element was comparable, as both methods were able to quantify damage in the correct element to within 10% of the true damage value. The SQP method was only able to use two load cases at any one time for damage detection, while the OC algorithm was able to use all three load cases at once. Direct comparison of the algorithm efficiencies was not possible, but in a general sense, both algorithms contain their own inherent advantages under certain conditions for damage detection. The SQP algorithm requires more computing effort due to calculation of the Hessian, but often exhibits fast convergence, while the OC algorithm uses only first derivatives and may require additional iteration for smaller scale problems. The OC algorithm has the advantage for large scale damage detection problems and superior stability characteristics. The performance of the algorithm under the presented conditions is promising and warrants further testing and exploration of the algorithm's ability to detect damage in other structures and testing conditions.

5 Damage Detection in a Three Dimensional Grid Structure - A Benchmark Problem

Independent damage detection experiments are instructive in assessing an algorithm's potential to detect damage in real world structures. However, once the damage detection procedure and algorithm has been finalized, it becomes necessary to compare results to other methodologies. The problem with comparisons, however, is that they are difficult unless experiments are performed on a common structure. Fortunately, the International Association for Bridge Maintenance and Safety (IABMAS) has supported an international effort to create a benchmark structure for the evaluation of structural health monitoring methodologies of bridges. The benchmark structure has been created at the University of Central Florida that is representative of a typical two span highway overpass. The goal of the benchmark problem is to assess the reliability of current SHM methodologies and to promote wider acceptance of these methodologies among bridge owners and engineers. A complete description of the structure and provided software is given in [11] and an abbreviated description is presented herein.

In this chapter, the damage detection methodology will be tested using the provided benchmark program provided by the benchmark organizers. The goal is to test the algorithm's ability to identify structural connections that have sustained damage. Detection of connection damage is particularly important for civil structures as they play a vital role in the transfer of loads between members and provide a load path from the point of application down to the foundation. Connections must resist very large loads and require careful fabrication as well as good design. Errors in either design or fabrication can leave a connection susceptible to damage. Three separate damage scenarios will be tested for the benchmark problem. Each scenario will have an increased level of damage over the previous scenario. The methodology will be asked to detect both reductions in the moment capacity of connections as well as reductions in the flexural stiffness of members in the vicinity of

connections. In Section 5.2 a new finite element is presented that better models changes in rotational stiffness and will aid in the detection of connection damage. The element will also exhibit characteristics well suited for optimization.

5.1 Test Structure

Damage detection data will be generated using a simulation program created by the benchmark organizers. The program is based on experimental data obtained on an actual grid structure built at the University of Central Florida. The test structure is shown in Figure 5.1.

Figure 5.1 Benchmark Test Structure used to Develop Simulation Problem (reproduced from

Catbas[13])

The structure, a schematic shown in Figure 5.2, has two spans and is continuous over the center support. The two continuous span girders are connected by 9 transverse beams spaced at 3ft on center. The superstructure of the bridge system is constructed of S3X5.7 steel members. The six column supports are W12X26 sections.
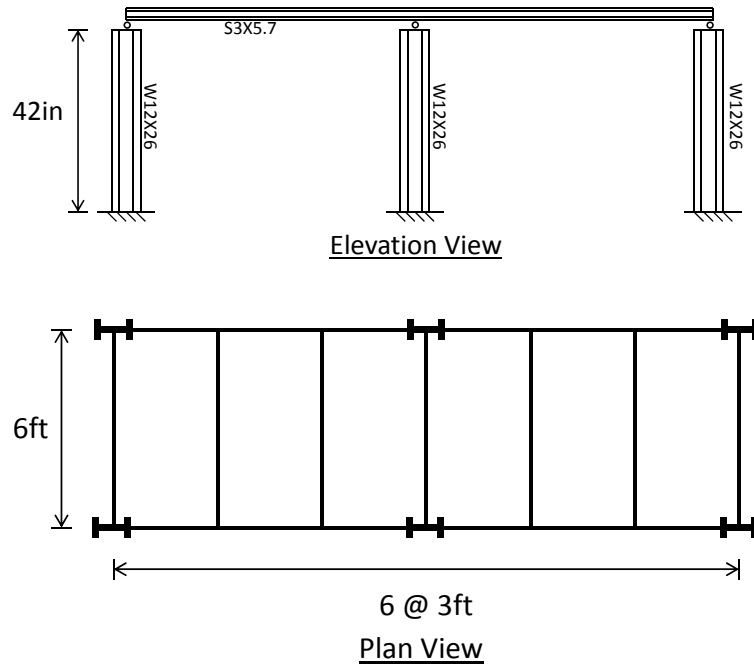
Figure 5.2 Schematic Diagram of Benchmark Structure

The superstructure is connected to the substructure at each of the six columns. A simple roller support, as shown in Figure 5.3(a), is used to transfer load from the superstructure to the base. The six supports are mounted along the centroidal axis of all support columns and plates are welded to the upper face to ensure uniform stress distribution across the column cross sections. The columns are welded to large steel base plates, which are in turn affixed to the rigid laboratory floor. It is assumed that the base connections are sufficient to simulate fully fixed boundary conditions.

(a)   (b)

Figure 5.3 (a) Roller Support between Pier and Superstructure (b) Typical Connection between

Girder and Transverse Beam Elements (reproduced from Catbas[13])

The members of the superstructure are attached using bolted flange, bolted web moment connections. Figure 5.3(b) shows a typical connection of the girder and transverse beam. A schematic of the connection is shown in Figure 5.4. Shear is transferred from the transverse member to the girder through the shear clip attached to the web of both members. The connection plates attached to the top and bottom flanges provides the moment resistance in the connections. A total of 30 bolts are used in each typical connection.
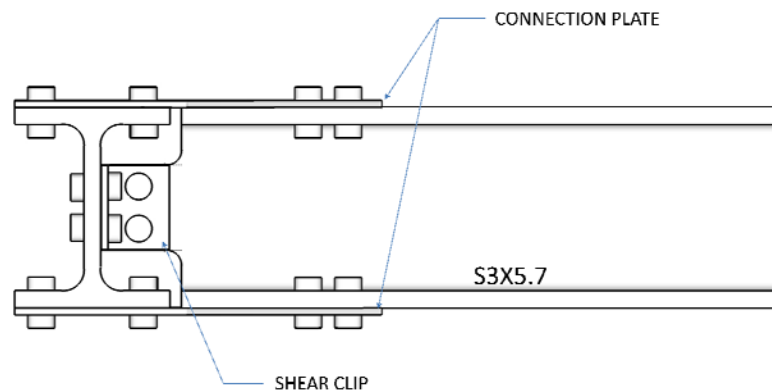
Figure 5.4 Typical Moment Connection of the Benchmark Structure

Little information is provided on the exact connection details of the structure, for example connection plate thickness and bolt sizes are not provided. Therefore it is difficult to validate that the connection is able to fully transfer the moment produced by the loading. However, it is assumed that the load magnitudes used for testing are small enough to be well within the capacity of the connections. Thus it is safe to assume that the connections behave as full moment resisting connections.

5.1.1 Simulation Program

The benchmark organizers have created a virtual testing environment to provide researchers the ability to test their damage detection methodologies on a common structure. The simulation is based on a finite element model of the test structure built in SAP2000 and imported in to MATLAB. The simulation can accommodate both static and dynamic based methodologies, but only the static simulation will be described here. The finite element model uses 177 nodes with 182 frame elements, resulting in a total of 1062 degrees of freedom. The level of refinement of the model is chosen to give researchers an ample number of simulated loading points to test their methodologies. Particular attention was paid to modeling the moment connections of the super structure. It should be noticed that the connection plates do more than just provide moment resistance to the connections; they also effectively increase the major axis moment of inertia of the girders in the region of the connections. The finite element model used for simulation has increased the flexural stiffness in the vicinity of each connection.

The user is able to specify as many load cases as desired and displacement sensors can be mounted at virtually any point on the superstructure. Loads can be applied in any direction. Likewise displacements can be measured in all three orthogonal directions. The structure behaves linearly both before and after damage and the material remains isotropic for all simulations. Efforts were made to mimic experimental error in the generated response of the model. Random error is added to the applied forces of each load case. The random error is normally distributed with a standard deviation of 0.2% of the applied load. This is to reflect the uncertainty in the applied load during real testing. Measurement error is incorporated by adding a normally distributed random vector with an RMS value of 0.1% of the maximum displacement measurement of the load case tested. Modeling error is inherent as the finite element model created for damage detection and used in the OC algorithm is created separately from the simulation model created by the benchmark organizers. A general description of the simulation model is provided by the organizers, but exact modeling parameters

have not been included. Due to the lack of knowledge of the finite element model, as well as the connection details, modeling error is a natural result of the benchmark problem. All added errors can be incorporated in the generated structural response using Eqn 5.1.

$$\mathbf{u} = \mathbf{K}^{-1}(\mathbf{P} + \mathbf{v}_f) + \mathbf{v}_u \qquad \mathbf{5.1}$$

where $\mathbf{K}$ is the structural stiffness matrix of the simulation model, $\mathbf{P}$ is the applied load vector, $\mathbf{v}_f$ is the random vector simulating load uncertainty, $\mathbf{v}_u$ is the random vector simulating measurement error, and $\mathbf{u}$ is the simulated static response of the structure. The inclusion of the two error terms simulates the two most common error models used by researchers for simulated data, proportional error and absolute error. The simulation program generates 100 sets of data for each load case so that researchers can assess the effectiveness of their damage detection methodologies with multiple sets of randomly perturbed data.

5.1.2 Damage Scenarios

The benchmark simulation program has the ability to induce 3 types of structural damage. The first type is damage to the connections between the girders and transverse beams of the superstructure. The second type of damage is to the boundary conditions of the superstructure. Damage to the roller supports between the piers and the deck are replaced with fixed connections to simulate seizing of the supports. The last type of damage is scour, where the spring stiffness at the base of the piers is reduced. Even though the benchmark problem has the capability of testing these three damage scenarios, the OC algorithm will be employed for only the first damage scenario, connection damage.

Within this damage scenario, three levels of damage are tested. First, the moment capacity of a single connection is eliminated by removing the bolts that attach the connection plates to the transverse beam (Figure 5.5(a)). The connection still has full shear capacity as the shear clip remains intact and the girder still has increased flexural stiffness in the vicinity of the connection. The second level of damage is tested by removing the connection plates completely (Figure 5.5(b)). Like the first level of damage, there is no moment capacity in the connection, but now there is also reduced flexural stiffness of the girders as the connection plates no longer provide the increased moment of inertia in the vicinity of the connection. The third level of damage removes the connection plates at two separate locations. The OC algorithm will be used to detect both types of damage in the benchmark structure.

(a)   (b)
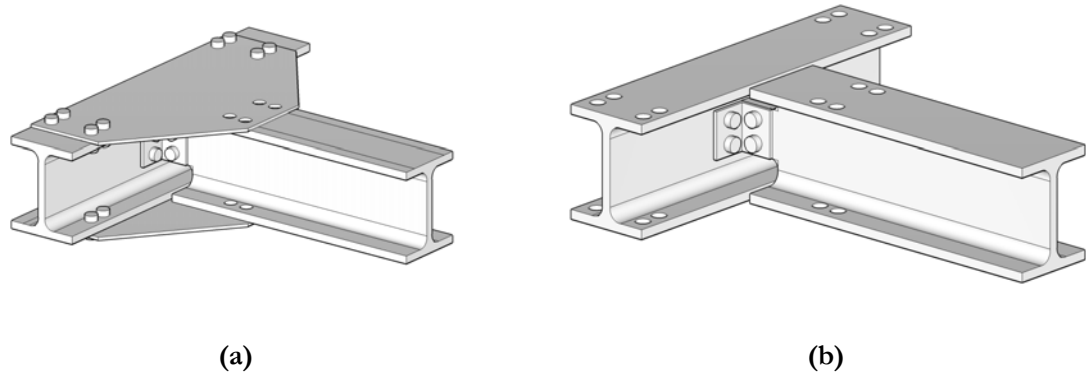
Figure 5.5 Moment Release of Typical Connection (a) Full Removal of Connection Plates

5.2 Analytical Model

The analytical model is the model used by the OC algorithm to pinpoint areas of suspected damage. Earlier damage detection problems have been able to be simplified by restricting the model to two dimensions. The applied loads and measured displacements only required a two dimensional model to capture all of the pertinent response characteristics. That luxury does not exist for the current structure. The structural advantage of a grid system is that all of the members in the system participate in the resistance of a load. Therefore, it is vital that all portions of the structure be accurately modeled in order to truly simulate the test structure.

Using the description of the physical system given in Section 5.1, the finite element model was created using the three dimensional frame elements of Section 2.7.2. The finite element model is created using the section properties obtained from the AISC Steel Construction Manual. The pertinent material and cross section parameters are shown in Table 5.1. It should be noted that the torsional stiffness of the members has a significant effect on the static response of the structure. Unfortunately the torsional stiffness of wide flange sections is not easily calculated. Only for a circular cross section is the torsional stiffness coefficient, K_T of Eqn 2.31, equal to the polar moment of inertia. For wide flange sections the coefficient is much less than the polar moment of inertia. As a result, the torsional stiffness will be chosen during the updating step after the initial baseline data is obtained.

Table 5.1 Member Properties of Benchmark Structure

Material and Cross Section Property	S3X5.7	W12X26
Strong axis moment of inertia, I_x	2.50 in^4	204 in^4
Weak axis moment of inertia, I_y	0.383 in^4	17.3 in^4
Cross sectional area, A	1.66 in^2	7.65 in^2
Modulus of elasticity, E	29000 ksi	29000 ksi
Shear Modulus, G	11154 ksi	11154 ksi
Poison Ratio	0.29	0.29
Effective Shear Area Factor	1.2	1.2

The model is discretized using a total of 70 finite elements. The superstructure is comprised of 64 elements while each of the piers is a single frame element. Short, 6 inch long, elements were used in the vicinity of each connection in order to model the connection plates. The moment of inertia of these shorter elements can be adjusted to reflect the increased stiffness provided by the connection plates. The base of the piers was modeled as a rigid connection and all connections between the piers and the deck were modeled as roller supports. Again the model was checked for accuracy using RISA-3D. A representative model is shown in Figure 5.6 with the global coordinate system.
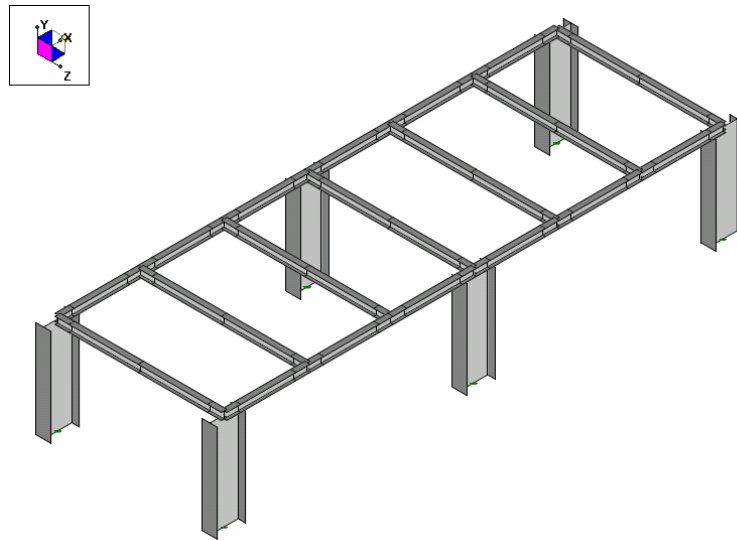
Figure 5.6 Illustration of the Analytical Model used for Damage Detection (created in Risa3D)

The numbering scheme for the elements comprising the deck is shown in Figure 5.7. The goal in using this test structure is to detect different levels of damage to structural connections, therefore the active elements for all problems presented in this chapter are the small, 6 inch long elements in the vicinity of each connection.
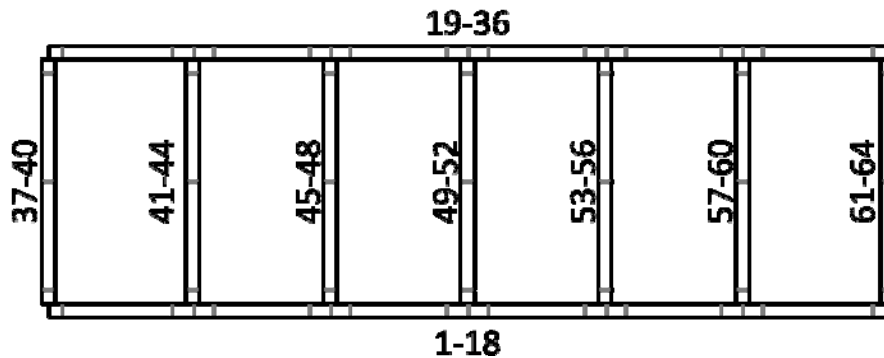
Figure 5.7 Element Numbering Scheme of Analytical Model

The current analytical model is only able to mimic rigid connections where the full internal moment in the transverse beams is transferred to the girders. In order to accurately model the loss of moment resistance in the connections, the finite element model and algorithm needs to be altered. It was originally thought that the loss of moment resistance in the connections could be simulated by reducing the moment of inertia near the joint. However the reduction in moment of inertia does not account for the redistribution of the internal shear and moment until the flexural stiffness of the entire element is nearly eliminated. The problem with this is that once an element's flexural stiffness is nearly eliminated, structural instability becomes an issue as the structural stiffness matrix becomes nearly singular. Further, as the structure nears instability the optimization problem becomes ill-conditioned. This proves problematic for the algorithm since the true damage is not being accurately model. A better model must be developed that can accurately mimic the behavior of semi-rigid connections, but also have "well behaved" stiffness gradients in order to maintain the stability of the optimization algorithm.

Common Approach to Modeling Semi-rigid Connections

Many finite element models have been created to mimic the behavior of semi-rigid connections (see [17], [19], [32], and [44]), however the majority of these developed models do not easily lend

themselves to optimization. The most common approach is to represent the structural connection as a torsional spring, as shown in Figure 5.8, where k_θ is the torsional stiffness of the spring. The moment equation in Figure 5.8 is used to develop a rigidity index for the each end of the beam. This rigidity index is used to calculate the moment resistance of the spring based on the relative rotation of the end of the beam and the total connection.

$$M_A = k_\theta^* \theta_A$$
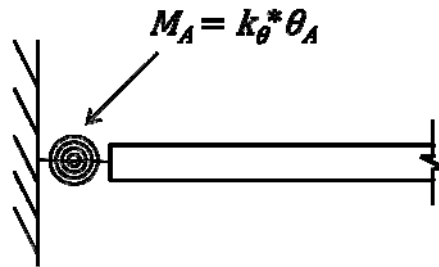
Figure 5.8 Common Modeling Approach for Semi-rigid Connections

These models have been shown to match experimental data very well, however these models cannot be easily used for optimization. The first reason for this is that these finite element models are nearly always nonlinear w.r.t. to the torsional stiffness of the connection, k_θ. Thus, the gradient of the connection element must be recalculated for every iteration, which slows the convergence rate of the algorithm. Second, the domain of the rigidity index is typically unbounded. A fully fixed connection is achieved as the rigidity index approaches infinity and a pinned connection is achieved when the rigidity index is zero. In practice the rigidity index does not have to be set to infinity to behave sufficiently close to a rigid connection, however determining the true value where modeling errors are small enough to be ignored is difficult and often requires an iterative approach. Further, if the rigidity index is initialized to a very large number, the optimization algorithm may take an unreasonable number of iterations to converge to the true value. This is especially true since the stiffness matrix is nonlinear w.r.t. to the rotational stiffness parameter, as stated above. A new finite element model must be created that, one, is linear w.r.t. changes in the rigidity of the connection and, two, uses a bounded domain for the stiffness parameter of the element.

A New Model for Semi-rigid Connections

Consider a two dimensional beam element, shown in Figure 5.9.
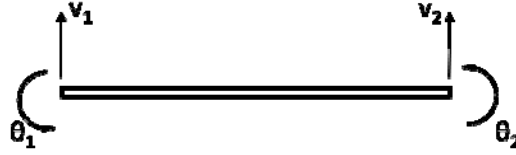
Figure 5.9 Two Dimensional, 4 DOF Finite Element

The element stiffness matrix shown in Section 2.7.1 and repeated here for convenience.

$$
K_F = \begin{bmatrix}
\dfrac{12EI}{L^3} & \dfrac{6EI}{L^2} & -\dfrac{12EI}{L^3} & \dfrac{6EI}{L^2} \\
\dfrac{6EI}{L^2} & \dfrac{4EI}{L} & -\dfrac{6EI}{L^2} & \dfrac{2EI}{L} \\
-\dfrac{12EI}{L^3} & -\dfrac{6EI}{L^2} & \dfrac{12EI}{L^3} & \dfrac{6EI}{L^2} \\
\dfrac{6EI}{L^2} & \dfrac{2EI}{L} & \dfrac{6EI}{L^2} & \dfrac{4EI}{L}
\end{bmatrix}
= \begin{bmatrix}
k_{11} & k_{12} & k_{13} & k_{14} \\
k_{21} & k_{22} & k_{23} & k_{24} \\
k_{31} & k_{32} & k_{33} & k_{34} \\
k_{41} & k_{42} & k_{43} & k_{44}
\end{bmatrix}
\qquad \textbf{5.2}
$$

The member end forces and local displacements are related by the equation:

$$
\begin{Bmatrix} V_1 \\ M_1 \\ V_2 \\ M_2 \end{Bmatrix}
= \begin{bmatrix}
k_{11} & k_{12} & k_{13} & k_{14} \\
k_{21} & k_{22} & k_{23} & k_{24} \\
k_{31} & k_{32} & k_{33} & k_{34} \\
k_{41} & k_{42} & k_{43} & k_{44}
\end{bmatrix}
\begin{Bmatrix} v_1 \\ \theta_1 \\ v_2 \\ \theta_2 \end{Bmatrix}
\qquad \textbf{5.3}
$$

For the element represented by Eqn 5.2, full shear and moment are transferred to each adjacent element in the assembled structure. A pin connected element can be created by eliminating the moment resistance at one end. Note that end releases are a property of the element and not the boundary conditions. The matrix notation of Eqn 5.3 is expanded and a right end moment release is included by forcing M_2 to be zero, as shown in Eqn 5.4(d).

$$V_1 = k_{11}v_1 + k_{12}\theta_1 + k_{13}v_2 + k_{14}\theta_2 \qquad \textbf{(a)}$$

$$M_1 = k_{21}v_1 + k_{22}\theta_1 + k_{23}v_2 + k_{24}\theta_2 \qquad \textbf{(b)}$$

$$\textbf{5.4}$$

$$V_2 = k_{31}v_1 + k_{32}\theta_1 + k_{33}v_2 + k_{34}\theta_2 \qquad \textbf{(c)}$$

$$0 = k_{41}v_1 + k_{42}\theta_1 + k_{43}v_2 + k_{44}\theta_2 \qquad \textbf{(d)}$$

The end forces are now recalculated and, by static condensation, θ_2 is eliminated from the expressions for V_1, M_1, and V_2. Solving for θ_2 from Eqn 5.4(d) gives:

$$\theta_2 = \frac{-1}{k_{44}}(k_{41}v_1 + k_{42}\theta_1 + k_{43}v_2) \tag{5.5}$$

Plugging Eqn 5.5 into Eqn 5.4(a)-(c), combining like terms, and noting that $k_{ij}=k_{ji}$ gives:

$$V_1 = \left(k_{11} - \frac{k_{14}^2}{k_{44}}\right)v_1 + \left(k_{12} - \frac{k_{14}k_{42}}{k_{44}}\right)\theta_1 + \left(k_{13} - \frac{k_{14}k_{43}}{k_{44}}\right)v_2$$

$$M_1 = \left(k_{21} - \frac{k_{14}k_{24}}{k_{44}}\right)v_1 + \left(k_{22} - \frac{k_{24}^2}{k_{44}}\right)\theta_1 + \left(k_{23} - \frac{k_{24}k_{43}}{k_{44}}\right)v_2$$

$$V_2 = \left(k_{31} - \frac{k_{34}k_{41}}{k_{44}}\right)v_1 + \left(k_{32} - \frac{k_{24}k_{34}}{k_{44}}\right)\theta_1 + \left(k_{33} - \frac{k_{34}^2}{k_{44}}\right)v_2$$

Thus the elemental stiffness matrix of a beam element with a right end moment release becomes:

$$K_{P_1} = \begin{bmatrix} \left(k_{11} - \frac{k_{14}^2}{k_{44}}\right) & \left(k_{12} - \frac{k_{14}k_{42}}{k_{44}}\right) & \left(k_{13} - \frac{k_{14}k_{43}}{k_{44}}\right) & 0 \\ \left(k_{21} - \frac{k_{14}k_{24}}{k_{44}}\right) & \left(k_{22} - \frac{k_{24}^2}{k_{44}}\right) & \left(k_{23} - \frac{k_{24}k_{43}}{k_{44}}\right) & 0 \\ \left(k_{31} - \frac{k_{34}k_{41}}{k_{44}}\right) & \left(k_{32} - \frac{k_{24}k_{34}}{k_{44}}\right) & \left(k_{33} - \frac{k_{34}^2}{k_{44}}\right) & 0 \\ 0 & 0 & 0 & 0 \end{bmatrix} \tag{5.6}$$

By similar derivation, the stiffness matrix of a beam element with a left end moment release is:

$$K_{P_2} = \begin{bmatrix} \left(k_{11} - \frac{k_{21}^2}{k_{22}}\right) & 0 & \left(k_{13} - \frac{k_{12}k_{23}}{k_{22}}\right) & \left(k_{14} - \frac{k_{12}k_{24}}{k_{22}}\right) \\ 0 & 0 & 0 & 0 \\ \left(k_{31} - \frac{k_{21}k_{32}}{k_{22}}\right) & 0 & \left(k_{33} - \frac{k_{23}^2}{k_{22}}\right) & \left(k_{34} - \frac{k_{32}k_{24}}{k_{22}}\right) \\ \left(k_{41} - \frac{k_{42}k_{21}}{k_{22}}\right) & 0 & \left(k_{43} - \frac{k_{42}k_{23}}{k_{22}}\right) & \left(k_{44} - \frac{k_{24}^2}{k_{22}}\right) \end{bmatrix} \tag{5.7}$$

where k_{ij} is as defined in Eqn 5.2.

The stiffness matrix of Eqn 5.2 represents the fixed-fixed case where the full internal shear and moment are transferred to and from each adjacent beam element. The stiffness matrices of Eqns 5.6 and 5.7 represent the fixed-pinned and pinned-fixed case, respectively, where moment transfer does not occur at one end of the element. These stiffness matrices are sufficient to model the behavior of a connection at the two extremes, fully fixed or pinned, but do not model the behavior of a semi-rigid connection. For the semi-rigid case, the true structural stiffness is a combination of the fixed and pinned condition. To model the semi-rigid case, a function must be created that combines the effects of both states, but at the same time must be defined on a bounded domain in order to support optimized.

A continuous function is created by assuming that the stiffness matrices form complementary pairs. The elemental stiffness matrix of a semi-rigid connection is calculated as:

$$K_S = C * K_F + (1 - C) * K_P$$

<div align="right">5.8</div>

where

$$0 \leq C \leq 1$$

Notice that when C, from here in termed the rigidity coefficient, is equal to unity the equivalent stiffness matrix is that of the fully fixed condition. Note that C is unitless. As C approaches zero the stiffness matrix approaches the pinned condition. In the optimization algorithm, the moment of inertia will no longer be the design variable for these connection elements. The algorithm will now adjust the rigidity coefficient. The benefit of using Eqn 5.8 for optimization is that the function is linear w.r.t. C and therefore recalculation of the gradient is unnecessary during the optimization process, thus minimizing computation effort. Expansion of the current two dimensional stiffness matrix into three dimensions requires replacing the corresponding DOF entries of Eqn 5.6 or Eqn 5.7 into Eqn 2.31. The process is straight forward and for brevity the 3D matrix is not presented here.

It should be noted that quantifying damage based on intermediate values of C is difficult as experimental tests have not been performed to establish the true relationship between C and connection damage. The developed model does however provide more accurate response gradients than the previous model used, which will better lead the algorithm to the true damage state. Future research should attempt to prove the validity of this semi-rigid model by determining the true form of the function for C.

5.3 Loading and Measurement Schedule

There are two main types of damage that must be detected by the algorithm, reduction in rotational stiffness of a connection and loss of flexural stiffness in the girders. The loading and measurements provide enough information to the algorithm to detect both types of damage. The loading schedule is defined using the theory of Section 2.8, however there is some room for customization in the measurement schedule of each load case. For clarity, the node numbering scheme shown in Figure 5.10 will be used to reference the loading and measurements.
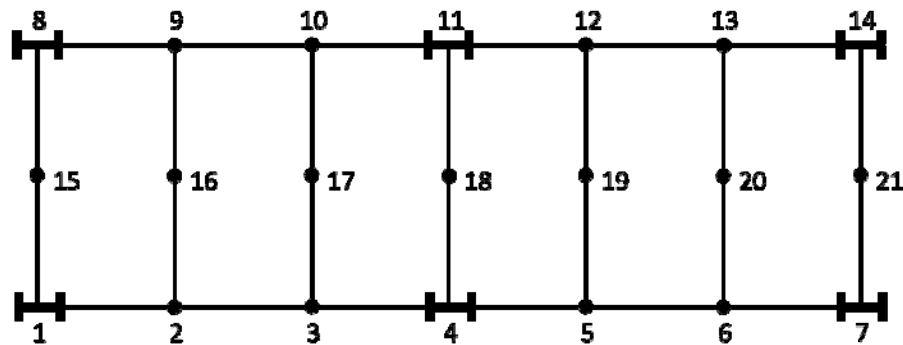
Figure 5.10 Node Numbering Scheme of Analytical Model

Following the guidelines for maximum practicality, only gravity loads will be applied to the test structure and each load case will apply a 150 pound point load. The load magnitude was chosen to match that used by the program organizers to perform initial experiments on the test structure. The first 8 load cases are used mainly to detect damage in the girders of the test structure, while the last 7 load cases help detect damage in the transverse beams. The complete loading and measurement scheme is shown in Table 5.2.

Table 5.2 Loading and Measurement Schedule for Damage Detection of Benchmark Structure

Load Case	Loading		Measured Node
	Node	Magnitude (lb)	
1	2	150	2, 3, 5, 6
2	3	150	2, 3, 5, 6
3	5	150	2, 3, 5, 6
4	6	150	2, 3, 5, 6
5	9	150	9, 10, 12, 13
6	10	150	9, 10, 12, 13
7	12	150	9, 10, 12, 13
8	13	150	9, 10, 12, 13
9	15	150	15
10	16	150	2, 9, 16
11	17	150	3, 10, 17
12	18	150	18
13	19	150	5, 12, 19
14	20	150	6, 13, 20
15	21	150	21

Load cases 1 through 8 measure deflections along the loaded girder. These measurements are necessary since the grid structure is statically indeterminate and even changes in stiffness that are far from the applied load can have a significant effect on the deflections near the load. The four sensor locations for each of the first 8 load cases are sufficient to detect damage in the girders. Load cases 9 through 15 help to detect damage to the rotational stiffness of a connection. By loading the transverse beams and measuring the deflection at 3 separate points, it is hoped that the deflection data is sufficient to detect any reductions in rotational stiffness of the end connections. If a single type of damage is known to be present, it might be possible to customize a loading and measurement scheme to exactly detect this damage; however in practice it is unknown beforehand what type of damage will be present in the structure. Therefore a single loading and measurement schedule must be robust in order to maximize the chance of detecting all types of damage that can occur in the structure.

5.4 Baseline Data and Updating of the Analytical Model

A baseline, healthy response must be established for the test structure in order to monitor changes in the static response due to damage. The loading schedule of Table 5.2 is applied to establish the healthy baseline. Later, the same loading will be applied to the test structure after damage has been induced. The same load and measurement scheme is used to detect damage for all damage scenarios. Using the simulation program provided by the organizers, the load cases are simulated one-by-one and the static response measurements are recorded. Recall that the static response data is calculated using Eqn 5.1. For each damage case to be tested, 100 data sets will be generated by the simulation program, thus the simulation program also generates 100 healthy data sets for direct comparison. A representative sample of the healthy deflection data is shown in Table B.1.

5.4.1 Updating the Analytical Model

Now that the baseline response has been recorded, the analytical model must be adjusted to best match the baseline data. The goal of the updating step of the analytical model is to minimize the initial modeling error of the damage detection problem in order to limit the propagation of error. The same load cases of Table 5.2 are applied to the analytical model and the structural response is compared to the healthy data generated by the simulation program. Two structural properties were targeted to best match the recorded measurement data. First, the moment of inertia of the elements in the vicinity of the connection plates is adjusted and, second, the torsional stiffness of all the elements is adjusted. It is assumed that the connections of the healthy structure are rigid and can transfer the full internal shear and moment of the transverse beams with very little relative displacement, therefore all rigidity coefficients are set to unity.

All model parameters are manually adjusted. The moment of inertia of the connection plate elements has the largest effect on the measurements for load cases 1 through 8, while the torsional stiffness of the girders has the largest effect on the displacements of the transverse beams. The moment of inertia of the connection elements was increased by 45% to match the baseline data. Then, after fine tuning the torsional stiffness of the girder elements, all calculated displacements were within 1.03% of the simulated measured data. The error between the calculated and measurement data is shown in Table B.1 of Appendix B. Now that the model has been updated to match the baseline data, the first damage case can be tested.

5.5 Damage Case 1 - Moment Release of one Connection

The first damage state will test the algorithm's ability to detect reduced moment resistance in a single connection. The rigid connection of the transverse beam connecting in to node 3 of Figure 5.10 will be replaced with a pin connection. In essence, element 45 will be replaced with the pin connected element derived in Eqn 5.6. This damage case simulates the removal of the bolts that attach the connection plates to the transverse beam. An illustration of the damage is shown in Figure 5.11.
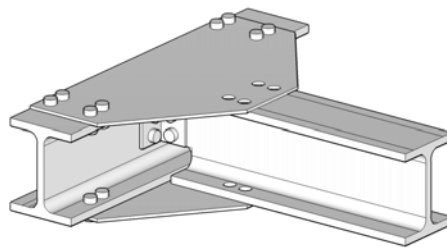
Figure 5.11 Connection Damage Illustrative of Damage Case 1

Note that the connection plates are still attached to the girder and therefore the algorithm should not detect a reduction in moment of inertia of the girder elements. For visualization the location of damage is shown in Figure 5.12.
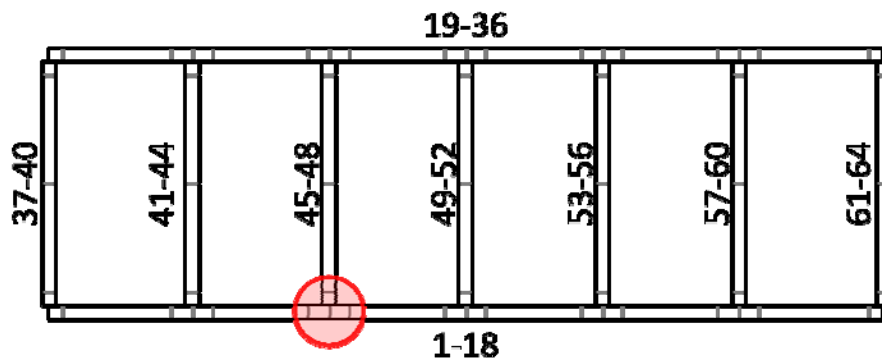
Figure 5.12 Location of the Damaged Connection for Damage Case 1

Before testing the damage case with experimental error, the algorithm must first prove that it can detect damage when error is not included in the measurements. Therefore, for this first damage case two different scenarios will be tested. First the damage detection problem will be solved when measurement error is excluded from the experimental data and then the problem will be repeated with data that contains simulated experimental error.

5.5.1 Damage Case 1 (No Experimental Error)

For the first case, experimental error must be eliminated from the test data. To do this $\mathbf{v}_f$ and $\mathbf{v}_u$ of Eqn 5.1 will be set to zero and the response data will be generated. With the damage induced, the load cases of Table 5.2 are again applied to the test structure and the simulation program generates the deflection data. The static response measurements of the damaged structure are then recorded. It should be mentioned that the baseline data and updating step have been performed again using errorless data.

After normalizing the response data with respect to the initial healthy deflections, all of the deflections show very little change except for the measurements of load case 11. The relative change in deflection is 0.194%, -0.194%, and -0.297% for measurements at nodes 3, 10, and 17, respectively. Although the change is slight, it is significant compared to all other changes in the deflection data which are nearly zero. From the deflection data it is already suspected that damage has occurred in the vicinity of the third transverse beam. The algorithm must now pinpoint the exact location of the damage.

Localization of Connection Damage

It is expected that the algorithm can detect reductions in moment of inertia relatively easily; however detection of reduced moment resistance in connections may be a challenge. The reason for this suspicion is that changes in the deflection data due to reduced moment capacity are much smaller than those of reduced flexural stiffness of an element. Even the data for the current damage state shows only a maximum of 0.297% change in the midspan deflection due to the connection damage. Therefore a preliminary localization procedure is needed to limit the number of connection elements that remain active for optimization. The localization techniques presented in Section 2.6 will be employed here. The DLAC algorithm will simulate various damage states using the analytical model and rank the correlation of the calculated response of each simulated damage state with the measured

response recorded from the simulation program. For example, the first DLAC is calculated by first replacing the rigid connection of element 37 with a pin connected element of Eqn 5.6. The load cases of Table 5.2 are then applied to the structure and the static deflection measurements are recorded. Next, the test data and the calculated data are used to find the DLAC value of Eqn 2.27. The resulting DLAC value is the correlation of the two response vectors. A higher DLAC value implies a greater correlation between the simulated data and measured test data, signifying a greater likelihood that the induced connection damage is the true damaged connection. The DLAC procedure is repeated by replacing all rigid connections with pin connections one-by-one. The resulting DLAC values for each simulated damaged connection are shown in Figure 5.13.
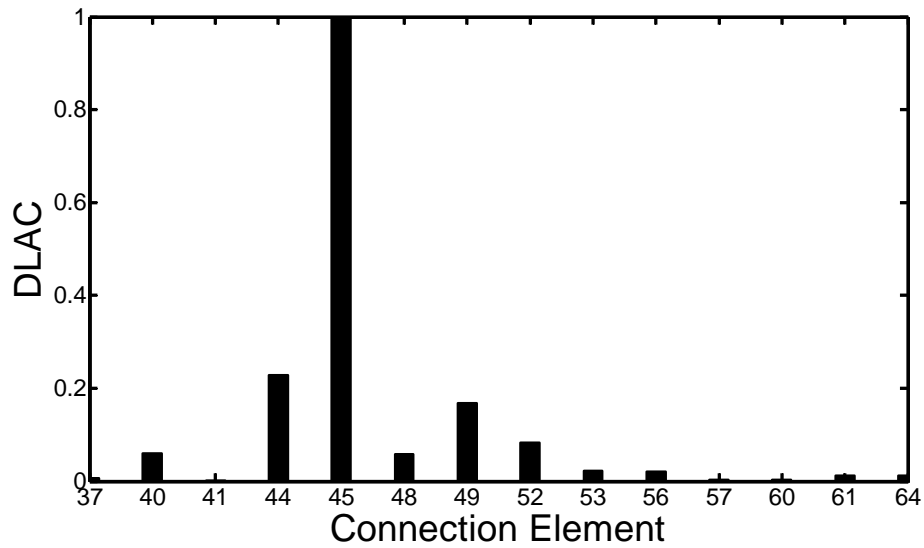
Figure 5.13 DLAC Values used for Localization of Damage Case 1

The DLAC values show a near perfect correlation between the measured data and the calculated data for connection damage in element 45. Therefore, when the OC algorithm is executed using the measurement data, all of the girder elements will remain active, but only element 45 of the transverse beams will be set as active. When error is incorporated in the measurement data, it is possible that several elements will have large DLAC values and so typically more than one connection element should remain active during optimization. Therefore the OC algorithm will keep up to 3 connection elements active that have DLAC values within 50% of the maximum DLAC value. For the results of Figure 5.13 only element 45 will remain active since no other DLAC value is within 50% of the maximum value. Keeping up to 3 elements will also give the algorithm a chance to detect damage in

multiple connections. It may be asked why the optimization algorithm is even necessary since the DLAC algorithm seems to pinpoint damage well. The reason the DLAC method is not used exclusively for damage detection is because, one, quantification of damage is difficult with the method, and two, for large structures with many elements and many measured displacements, the computation effort can become burdensome since all possible damage scenarios must be simulated separately for the DLAC method. As such, the method is only utilized as a localization technique on a subset of the total elements in the structure.

Damage Detection Results for Damage Case 1 (No Experimental Error)

Now that the active connection elements have been determined, the OC algorithm can be used to solve the general damage detection problem of Eqn 2.3. All constraint equations can be fully defined using the obtained displacement data. The exit criteria of the algorithm are a maximum of 40 iterations or all design values come within 2% of optimality. The constraint convergence is set to 10% of the maximum violated constraint and two member groups are used in the active parameter selection subroutine. The girder elements are one group and connection elements are the other. The optimization variable for the girder elements is the major axis moment of inertia and the optimization variable for the connection elements is the rigidity coefficient, C, given in Eqn 5.8. Note that the variables available for optimization are only those in the vicinity of each connection, i.e. elements 1, 3, 4, 6, 7, 9, 10, 12,13, 15, 16, 18, 19, 21, 22, 24, 25, 27, 28, 30, 31, 33, 34, 36, 37, 40, 41, 44, 45, 48, 49, 52, 53, 56, 57, 61, and 64 of Figure 5.7. Although for the current case it has already been determined by the localization procedure that only element 45 is active among the connection element 37, 40, 41, 44, 45, 48, 49, 52, 53, 56, 57, 61, and 64. One minor modification has been made to the algorithm. The constraint handling now operates along load case groups. What this means is that if one constraint within a load case is active, all of the other constraints within that same load case are also set active. This modification is made so that the algorithm, when adjusting the design variables, must take in to account the global changes in the static response rather than only the local changes at the site of the most violated constraint. The optimization problem is initialized to the updated parameters previously calculated using the baseline data. The algorithm is allowed to iterate until one of the exit criteria is reached. The damage detection results are shown in Figure 5.14.
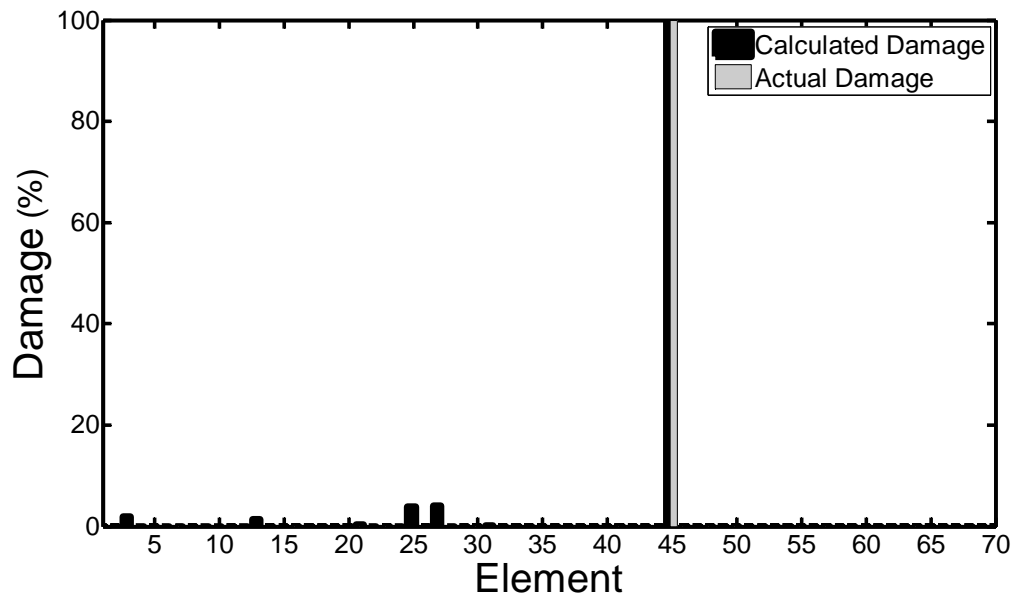
Figure 5.14 Damage Detection Results for Damage Case 1 (No Error)

The algorithm required a total of 27 iterations to satisfy optimality. It is calculated that 100% damage occurred in element 45, matching the true damage state of the structure. The 100% damage calculated by the algorithm implies that the rigidity coefficient of element 45 was reduced from one, which signifies a rigid connection, to a value of zero, which corresponds to the pinned condition. Therefore a complete loss of moment capacity has occurred at the connection of element 45. The algorithm also calculated very slight damage in elements 25 and 27. This damage is due to the increase in displacement at node 6 of load case 11. However the increase in displacement is not due to damage in the girder elements, it is due to the redistribution of reaction forces at the ends of the transverse beam because of the change in stiffness of the connection. The damage calculated in these two elements is very minor and is not nearly significant enough to be deemed a potential damage location.

In the absence of error the algorithm is able to accurately detect damage in the correct element. Next, experimental error must be introduced so that the performance of the algorithm can be judged for testing conditions that are closer to real conditions. It is suspected that detection of connection damage will be largely dependent on the level of error present in the measurements. As can be seen in the current case, the change in the static response behavior is very subtle when one connection is damaged and therefore errors in experimental data may mask the effects of this damage.

5.5.2 Damage Case 1 (with Experimental Error)

Experimental data inevitably contains errors. As such, detecting damage based on a single simulated data set reveals little on an algorithm's ability to detect damage in real world conditions. Fortunately, the simulation program can generate 100 data sets for each damage scenario. Each data set incorporates random error according to Eqn 5.1. Next, the damage detection problem is solved for each randomly perturbed data set. The results will provide a sense of the affect measurement error has on the algorithm's ability to detect damage.

Damage Detection Results for Damage Case 1 (with Experimental Error)

The procedure for damage detection is identical to that of the errorless case, except that it will be repeated for all generated data sets. First, 100 healthy data sets will be generated using the simulation program. The load error, $\mathbf{v}_f$ in Eqn 5.1, is normally distributed with a standard deviation of 0.2% of the applied load. Once the displacements are calculated using the new load vectors, measurement error is then incorporated. The measurement error is normally distributed with zero mean and a standard deviation of 0.1% of the maximum displacement measurement for each load case. Due to the large volume of data sets, it is impractical to update the model for each newly perturbed data set. Therefore the updated model used for the errorless case will be used for all 100 damage detection problems. Next, 100 damaged data sets are generated using the same error distributions just described. Each of the generated data sets represents a unique damage detection problem that must be solved by the algorithm. Each set of data is used to formulate the damage detection problem of Eqn 2.3.

Each time the damage detection problem is solved, the algorithm will first perform the localization step to eliminate as many connection elements as possible and then the OC algorithm will detect damage based on the remaining active parameters. Both the convergence and exit criteria are unchanged from the errorless case and the localization step still retains the 3 elements with the largest DLAC values that are within 50% of the maximum. The calculated damage for all data sets is compiled and the sample mean is plotted in Figure 5.15.
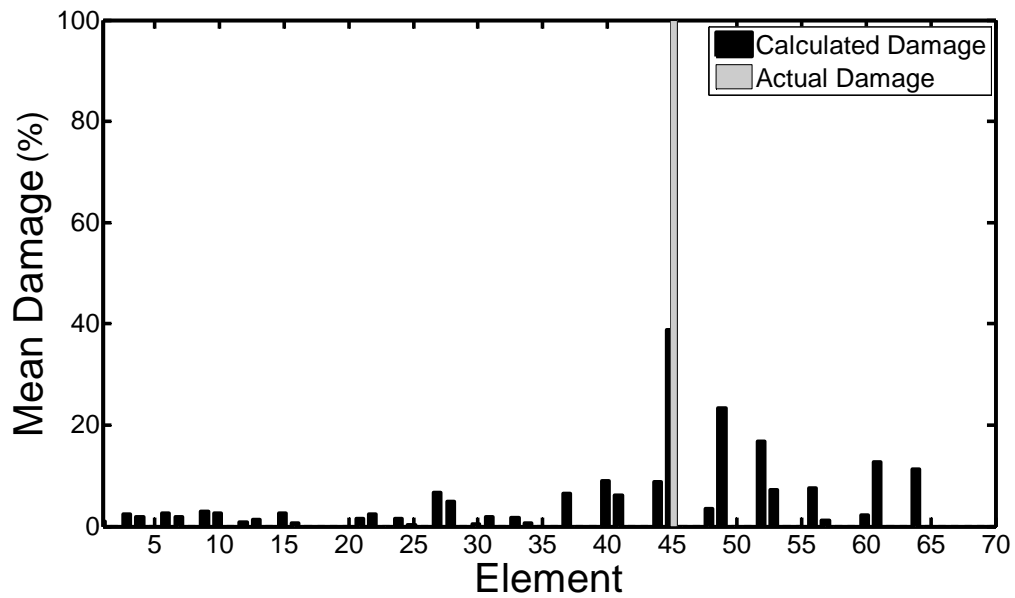
Figure 5.15 Mean Damage Detection Results for Damage Case 1 (with Error)

The algorithm detected damage in element 45 more than any other element. This is reflected in the fact that the mean damage detected was highest in element 45. The mean value is a 39% reduction in the rigidity coefficient of element 45. The sample standard deviation is 0.46 which correlates to a standard error of ±4.6%. The true damage is a 100% reduction in the rigidity coefficient of element 45. Any time damage was calculated in a connection element, the algorithm had a tendency to force the rigidity coefficient to one extreme, either 1 or 0. Rarely was an intermediate value of the rigidity coefficient calculated. Assuming a reduction of at least 15% in any design variable signifies the possible presence of damage, damage was detected in 47 of the 100 data sets and damage was detected in the correct element a total of 43 times. Within those 43 instances, additional false positive damage was calculated 32 times.

5.5.3 Discussion

It is obvious that measurement error has a significant effect on the algorithm's ability to detect the current damage scenario. For the errorless case of Section 5.5.1 the algorithm was able to detect the correct damage case to a very high level of accuracy. When error is included, the algorithm is able to accurately detect damage in the correct element 43% of the time. Using the standard error approach,

there is a 95% chance that the true population mean falls in the range of 29.8%-48.2% reduction in the rigidity coefficient of element 45, which is not close to the true damage of 100%. False positive damage was also detected in the majority of these cases. These results are not entirely unexpected, however. As shown in the errorless case, loss of moment resistance in one connection translates to only a 0.297% change in the midspan deflection of the 3rd transverse beam. This is problematic for two reasons. First, simulated error in the measurement data can easily drown out the effects of such connection damage. Second, the maximum change in deflection occurs at the midspan of the transverse beam. If all other changes in displacement are drowned out by measurement error, the midspan deflection does not provide enough information to determine which end of the beam has experienced connection damage. It is the displacement measurements near the connections that best determine which end of the transverse beam is damaged. Unfortunately it is suspected that once flexural stiffness reduction is introduced in the girder elements, the effects of connection damage will be even further lost in the deflection data. One possible remedy to this situation is to include rotational measurements at the connections. These measurements can be achieved by mounting tiltmeters near each connection. It is expected that connection damage will be much more apparent if such measurements are obtained. However these measurements are not used for the current damage case because, one, the simulation program does not allow for such measurements, and two, this measurement scheme should be tested for the combined case of rotational stiffness reduction in the connection and flexural stiffness reduction in the girder before alterations to the measurement schedule are considered.

5.6 Damage Case 2 - Moment Release of One Connection with Reduced Flexural Stiffness of Girder

The next damage scenario to be tested will remove the top and bottom connection plates at the same location as damage case 1 (node 3 of Figure 5.10). Removal of the connection plates induces both a complete loss of moment resistance of the connection as well as a reduction in the flexural stiffness of the girder in the vicinity of the connection. It is expected that the change in deflections due to damage case 2 will be much more pronounced than that of damage case 1. The induced damage is similar to that shown in Figure 5.16.
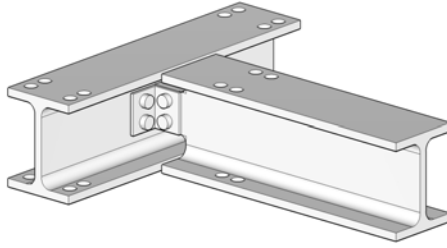
Figure 5.16 Illustration of Removed Connection Plates for Damage Case 2

The testing procedure is identical to that previously presented. There is no need to regenerate the baseline displacement data as it has already been performed for damage case 1. All of the same load cases and measurement locations of Table 5.2 are employed. Using the simulation program, 100 data sets are generated incorporating random error. Again the incorporated error is normally distributed with standard deviation 0.1% and 0.2% for the displacements and applied loads, respectively.

After analyzing the simulated data, the current damage case shows much more variation in the deflections from the healthy structure to the damaged structure. The maximum change in deflection again occurs in load case 11, but this time at node 3 rather than node 10 of the previous damage case. This measurement location corresponds to the vertical displacement of the node at the location where the connection plates are removed. After averaging all 100 data sets, an increase of 9.8% in this measured deflection is observed. A representative sample of the data is shown in Table B.3.

Now that the test data has been generated and the measurements recorded, the OC algorithm can be used to locate the damaged areas. To reduce computing time, the model updating step is again omitted and the updated model for the errorless case will be used to initialize all 100 problems. The simulated damaged data is used to define all constraints of the damage detection problem of Eqn 2.3. The localization step described in Section 2.6 is still employed to reduce the number of active connection elements. Once the localization step is completed, the OC algorithm solves the damage detection problem using the remaining active parameters. With the removal of a connection plate there is not only a reduction in the moment capacity of a connection but also a reduction in the moment of inertia of the girder in the vicinity of the connection. Since the analytical model contains two separate elements in these areas, linking is employed to ensure equal damage is imparted to both of these elements during optimization. For example, removal of the connection plates at node 2 of Figure 5.10 would reduce the moment of inertia of elements 3 and 4 of Figure 5.7. Therefore elements 3 and 4 are linked to assure that equal damage is imparted to both elements. The same

93

pattern is repeated for all girder elements in the vicinity of each connection. The convergence and exit criteria are identical to the previous damage case. The damage detection results of each data set have been compiled and the average of the compiled data is shown in Figure 5.17.
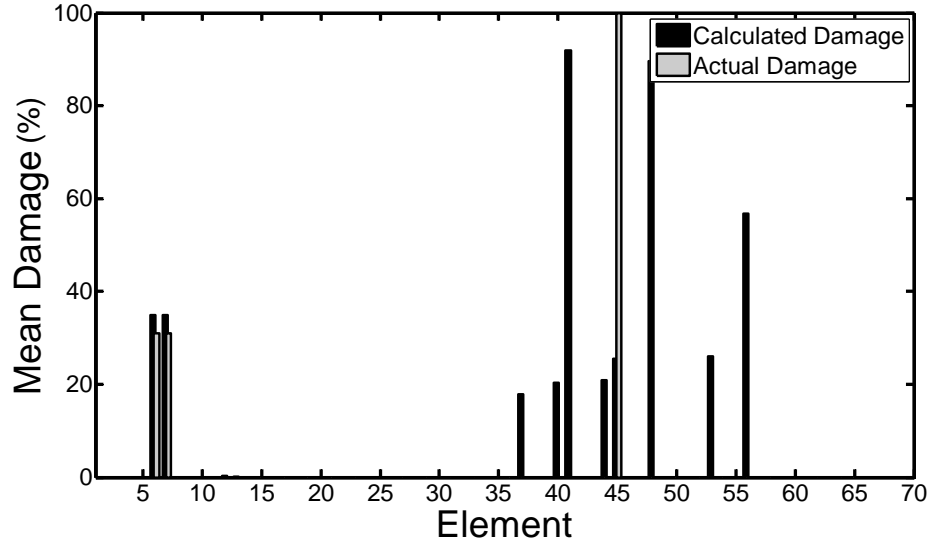
Figure 5.17 Mean Damage Detection Results for Damage Case 2

The algorithm accurately detected the reduction in moment of inertia of elements 6 and 7, but had difficulty detecting the correct damage in element 45. The 34.8% damage calculated in elements 6 and 7 reflects the loss of flexural stiffness resulting from the removal of the connection plates. The true reduction in stiffness in these elements was 31.0%.Unfortunately the large increase in deflection due to this damage made the detection of the loss of moment capacity in element 45 nearly impossible. Of the 100 data sets, damage was identified in element 45 only 16 times. Damage was detected most often in the connections at elements 41 and 48. The OC algorithm determined that element 41 had experienced damage 93 times and that element 48 experienced damage 91 times. On a positive note, the algorithm was able to detect damage in elements 6 and 7 in all 100 data sets. Further, the level of variation in the compiled data for these elements was astoundingly small. The standard deviation in the results for elements 6 and 7 was 0.0052 in.[4], or approximately 1.5% of the mean.

5.6.1 Damage Case 2 Results with Rotational Displacement Measurements

The presented results reveal that there is difficulty detecting the loss of moment resistance in the connection element. Both damage case 1 of Section 5.5 and the results just presented show large variations in the calculated damage of the connections. It is now necessary to discern whether the inability to detect this damage is due to the measurement data, or if it is a limitation of the algorithm. It was hoped that damage would be detected utilizing only vertical deflection measurements as they are the easiest to obtain. However it has become apparent that the deflection data is not sufficient to detect both losses in flexural stiffness of the girder and rotational stiffness of the connections. Therefore damage case 2 will be repeated with rotational displacement measurements to see if the algorithm can accurately detect all damaged elements. The new measurement schedule is shown in Table 5.3.

Table 5.3 Load and Measurement Schedule for Damage Case 2 with Rotation Measurements

Load Case	Loading		Measured Node	
	Node	Magnitude (lb)	Deflection	Rotation*
1	2	150	2, 3, 5, 6	
2	3	150	2, 3, 5, 6	
3	5	150	2, 3, 5, 6	
4	6	150	2, 3, 5, 6	
5	9	150	9, 10, 12, 13	
6	10	150	9, 10, 12, 13	
7	12	150	9, 10, 12, 13	
8	13	150	9, 10, 12, 13	
9	15	150	15	1, 8
10	16	150	2, 9, 16	2, 9
11	17	150	3, 10, 17	3, 10
12	18	150	18	4, 11
13	19	150	5, 12 , 19	5, 12
14	20	150	6, 13, 20	6, 13
15	21	150	21	7, 14

* Rotations are measured about the global X-axis

As explained in previous sections, measuring rotational displacements can be difficult as it is often necessary to mount tiltmeters directly on steel members of the structural frame adjacent to the connection. Deflections, on the other hand, can be measured globally and sensors do not necessarily

have to be mounted directly on the structural steel. It is for this reason that previous examples attempted to only utilize deflection measurements. However rotations are used here to judge whether or not rotational displacement measurements can improve the accuracy of damage detection.

The simulation program does not have the ability to measure rotations; therefore the analytical model will be used as the test structure. It is recognized that by using the analytical model as both the test structure and the mathematical model for optimization that modeling error is essentially eliminated from the problem. To account for this, the standard deviation of the measurement noise will be increased by a full order of magnitude and the noise in the applied load vector will be increased as well. Both $\mathbf{v}_f$ and $\mathbf{v}_u$ of Eqn 5.1 remain normally distributed but will both have a standard deviation of 1% of the applied load and deflection, respectively. This increase in experimental error will help to better account for the lack of modeling error in the problem. Again 100 data sets are generated for the healthy and damaged response data.

After analyzing the data sets, the deflection measurements are all within 1% of the previous data generated by the simulation program. Matching the deflection data of the previous case is important because it shows that the analytical model is accurately modeling the test structure. Now turning our attention to the change in the rotational displacements, again load case 11 shows the most significant change in the data as the change in rotation at node 7 is dramatic. It is hoped that the change in rotational displacement will help pinpoint that the rigidity coefficient of element 45 has been reduced. Again, using the static data to formulate the damage detection problem, the OC algorithm is used to pinpoint areas of potential damage. The damage detection procedure is still the same. The initial localization step will be employed using both the deflection and rotation displacement data and then the OC algorithm will solve the damage detection problem using the remaining active variables.

The localization step is the first step in assessing whether the new measurements help detect connection damage. The localization step using the measurement schedule of Table 5.2 often didn't even pinpoint element 45 as a possible damage location. Thus, element 45 was not even an active variable during the optimization problem. To check whether the localization step is retaining element 45 as an active variable, a data set is chosen at random and the DLAC values are plotted. The 67th data set was chosen and the DLAC values are shown in Figure 5.18.
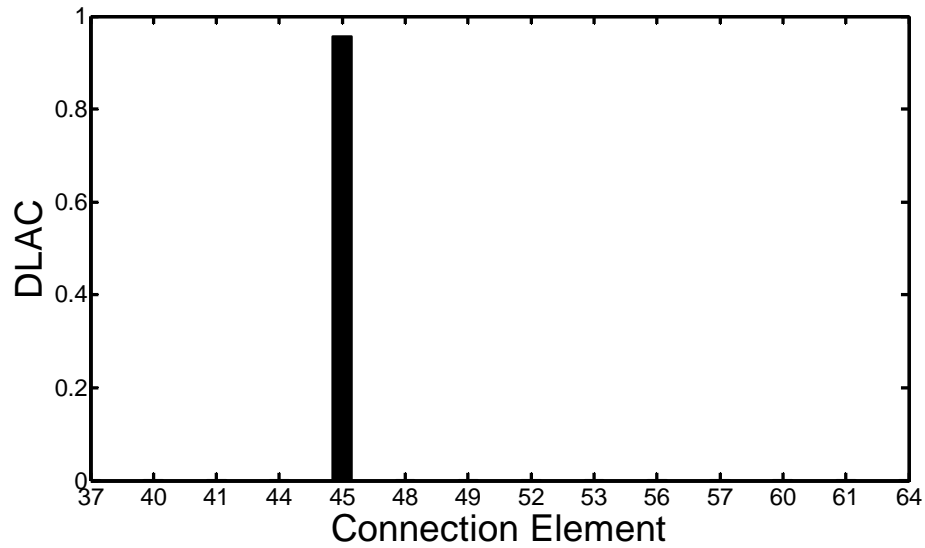
Figure 5.18 DLAC Values for Data Set 67 with Rotational Measurements

It is apparent that the rigidity coefficient of element 45 is the most likely candidate for damage in this data set. Therefore element 45 will be retained as an active parameter in the optimization problem. The reason that the DLAC value is so high for element 45 is because the largest change in rotational displacement of the generated data occurred at the connection of element 45. Naturally this rotation is most affected by the change in the rigidity coefficient of element 45. All of the other connections have a very small influence on the rotation of this connection. Even though the DLAC results presented in Figure 5.18 represent only a single data set, the level of correlation of element 45 is encouraging and it is hoped that this is a common trend for all data sets.

The localization step is executed for all data sets and then the OC algorithm is used to solve the damage detection problem. The results of each data set are recorded and plotted in Figure 5.19.
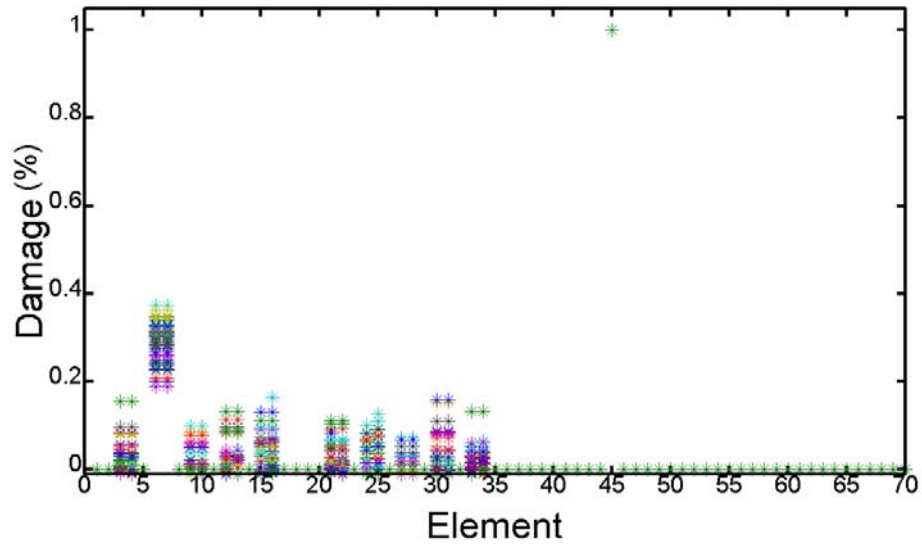
Figure 5.19 Damage Detection Results for Damage Case 2 with Rotation Measurements

The damage detection results show that the rigidity coefficient of element 45 was the sole connection element that was damaged. No other connection was calculated to have any damage for any of the data sets. The girder elements showed some variability in calculated damage, but the most significant damage was concentrated in elements 6 and 7. To better see the calculated damage, the sample mean of the calculated data is shown in Figure 5.20.
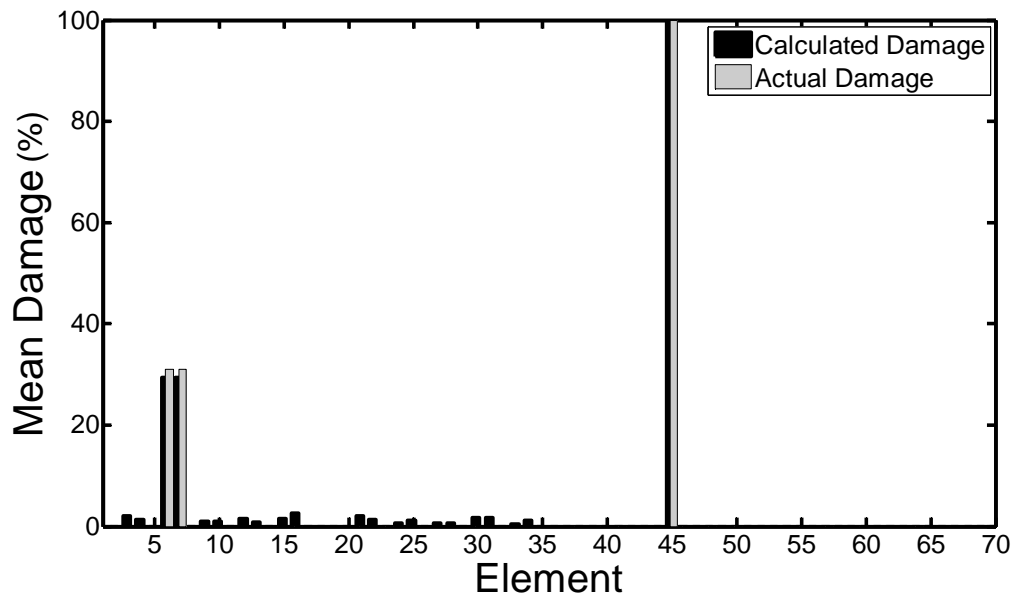
Figure 5.20 Mean Damage Detection Results for Damage Case 2 with Rotation Measurements

The mean damage is very close to the true damage of the structural system. Assigning a threshold of 10% reduction in stiffness for damage detection, element 45 was detected in all 100 of the test cases. This is a drastic improvement to the previous case using the simulation program. Damage in elements 6 and 7 was also detected in all 100 data sets. Of the girder elements, damage was always largest in elements 6 and 7. However using the 10% threshold, false positive damage was calculated in 20 of the test cases. False positive damage was not detected in any of the connections.

The use of rotational measurements produces much more accurate damage detection results. The deflection data is still sufficient to detect damage in the girder elements, while the rotation data give the added ability to detect loss of moment resistance in the connections. Plus, the convergence of the algorithm is much faster when rotational displacements are used as 68% of all the tested cases required fewer than 20 iterations to satisfy optimality, compared to only 31% of the cases when rotational measurements were not used.

The damage detection results are quite impressive, however it can be argued that one reason for this marked improvement is that the analytical model is being used as both the test structure and the optimization model and so modeling error is not present. An attempt was made to account for modeling error by increasing the standard deviation in the normally distributed error models, but it is possible that this increase is still not sufficient to fully incorporate modeling error. Therefore, the

current damage case will be repeated one last time with an even larger standard deviation for the error models.

5.6.2 Damage Case 2 Results with Rotational Displacement Measurements and Increased Measurement Error

The previous results used Eqn 5.1 with $\mathbf{v}_f$ and $\mathbf{v}_u$ both normally distributed with a standard deviation of 1%. The standard deviation of both variables will now be increase to 2.5%. The increased error level will further assure that the lack of modeling error in the simulated data is accounted for. The results should also provide insight on the algorithm's performance under varying error levels.

The 100 healthy and damaged data sets are again generated but now use the increased error level. The same loading and measurement schedule of Table 5.3 is employed, and the damage detection procedure is identical to the previous cases. The results of each data set are plotted in Figure 5.21.
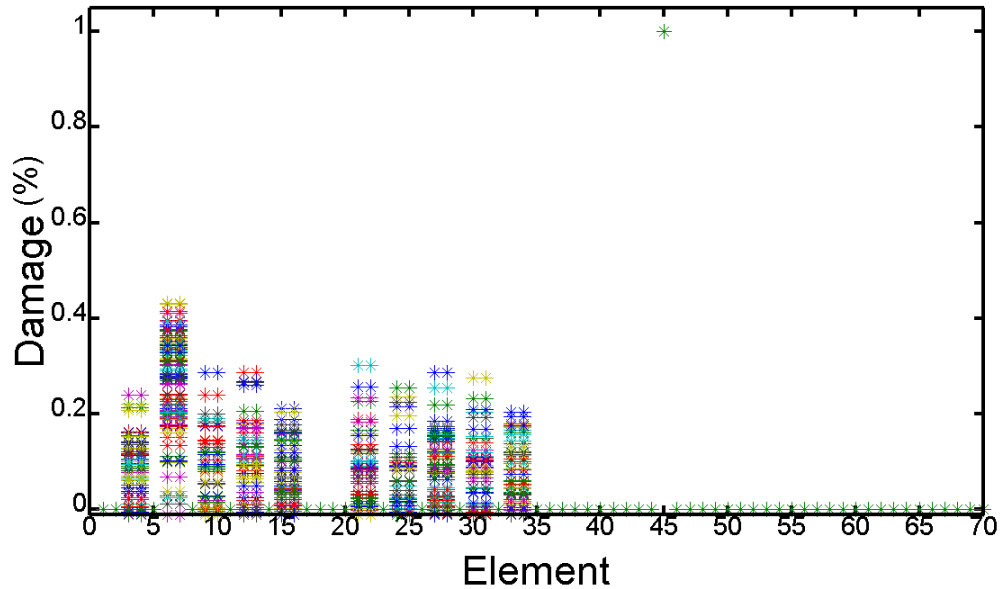
Figure 5.21 Damage Detection Result for Damage Case 2 with Rotation Measurements and Increased Error

Once again the reduced rigidity coefficient was detected for all 100 data sets, and the results show significant damage concentration in elements 6 and 7. It also appears as though the algorithm has detected significant damage for many of the active girder elements. To gain a better sense of the level of damage detected, the mean of the damage detection results are plotted in Figure 5.22.
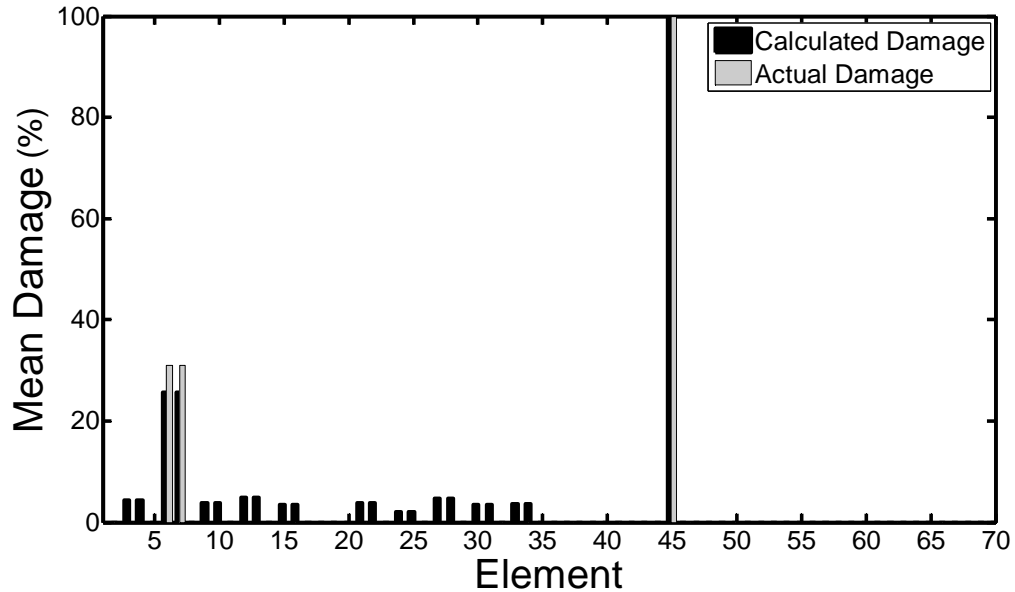
Figure 5.22 Mean Damage Detection Results for Damage Case 2 with Rotation Measurements and Increased Error

Figure 5.21 makes it appear that widespread damage was calculated for a many of the data sets, however Figure 5.22 reveals that the algorithm detected damage mainly in elements 6, 7, and 45, which are the true damage locations. Using the same 10% threshold for damage detection as the previous results, damage was detected in elements 6 and 7 for 91 of the 100 data sets. False positive damage was detected for 82 of the 100 data sets. False positive damage was more prevalent for this case compared to the 1% damage case. However there were still no false positives detected for the rigidity coefficients. If the damage threshold is increased to 15% reduction in a stiffness parameter to pinpoint damage, damage is still detected in element 45 for all 100 data sets. Damage is detected in elements 6 and 7 for 87 of the data sets and false positive damage is detected for 51 of the data sets. It is seen that the increased threshold does not significantly affect the number of times that the correct damage state was detected by the algorithm as it decreased from 91 times to 87 times. But the increased threshold did eliminate a significant number of the false positives detected as it decreased

from 82 to 51. In future work, a study should focus on establishing a systematic approach to determine the correct damage threshold that will accurately detect damage and minimize the number of false positives in damage detection.

Hjelmstad [30] developed two damage indices based on the results of Monte Carlo samples. One index is normalized with respect to the healthy parameter values while the second is normalized by the standard deviation of the Monte Carlo sample. Together they are used to evaluate a parameter's sensitivity to measurement noise and are also used to detect damage. The limit thresholds for these indices are determined from the Monte Carlo simulations themselves and can be useful for subsequent simulations or experiments.

Ideally the limit thresholds would be determined without the heavy use of preliminary simulation, but Monte Carlo simulations may provide the most insight to the sensitivity of each parameter to experimental error. Even without a solid limit threshold established, the results of Figure 5.22 are encouraging. The algorithm was able to detect the correct damage state even though the measurement error was increased significantly.

5.6.3 Discussion

It is obvious from the results of Figure 5.17 that the reduction in stiffness of elements 6 and 7 has such a dramatic affect on the static response of the structure that the loss of moment resistance in the connection could not be detected from deflection measurements alone. Even the localization procedure was unable to determine that the rigidity coefficient of element 45 was the most likely damage candidate as element 45 was rarely included as an active parameter by the DLAC algorithm. Even though measurement error can prove a challenge in detecting connection damage, as evidenced in damage case 1, it is suspected that the difficulty experienced in the current damage case is due to the disproportionate affect the girder elements have on the deflection measurements compared to the rigidity coefficient of a connection. This result was somewhat expected due to the minor changes in the static response data that results from the loss of moment resistance in a single connection. The change in deflection from damage case 1 showed a maximum change of 0.297% while the maximum change for the current damage case was 9.8%. Deflection changes due to reduced moment capacity of a single connection are overshadowed by the significant changes induced by the damage in the girders.

The difficulty in detecting loss of moment resistance is not due to the OC algorithm or the applied load cases, it is due to the type of measurements used to detect damage. When rotational displacements were measured, as in Section 5.6.1, the likelihood of detecting connection damage increased significantly. The two data types (deflection and rotation) are each able to provide enough information for the algorithm to detect both types of damage. The rotation data is able to provide information on which connection has lost moment capacity while the deflection data pinpoints areas where there is a loss of flexural stiffness. It was hoped that the damage detection procedure would accurately detect damage using only deflection measurements, however it became readily apparent that rotation data is necessary to detect changes in rotational stiffness of connections.

It is also encouraging that even with increased error levels in the generated response data, the algorithm was still able to detect damage at the correct locations. Reduction in the rigidity coefficient of element 45 was still detected in all 100 test cases and the correct girder damage was detected for 91 of the test cases. As expected, there was an increase in the number of false positive damage cases. With further research a systematic method in determining a good damage threshold can be created that will minimize the number of false positive damage locations calculated.

5.7 Damage Case 3 – Moment Release of Two Connections with Reduced Flexural Stiffness of Girder

The final tested damage case will induce damage at two separate locations in the structure. The goal in testing this damage state is to assess the algorithm's ability to detect multiple damage locations. Just as the reduction in flexural stiffness clouded the effects of loss of moment resistance in a connection, it is feared that the reduction of flexural stiffness at one location will cloud the effects of changes in flexural stiffness at another location. The connection plates are removed at node 2 and node 10 of Figure 5.10. The removal of the connection plates at these two locations essentially replaces the rigid connections with a pinned connection and also reduces the moment of inertia of the girder elements adjacent to the connections. The two damage locations in reference to the theoretical model are shown in Figure 5.23.
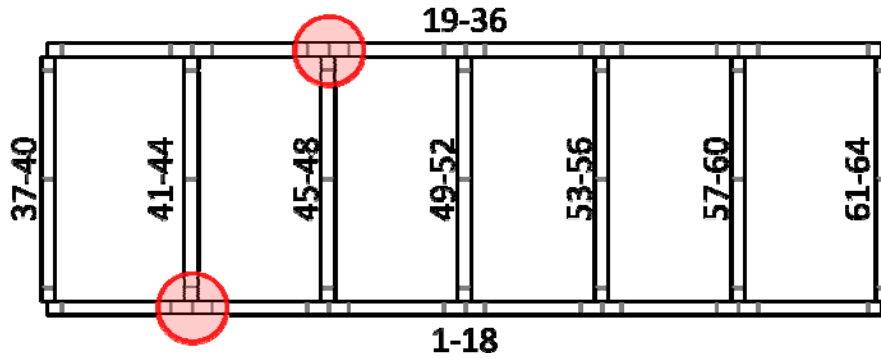
Figure 5.23 Location of Damaged Connections for Damage Case 3

It is apparent from the previous damage case that the loss of moment resistance can only be detected if rotational displacements are measured at the connections. Therefore the simulation program will not be used to generate the test data for this final damage case. To accurately detect damage, the algorithm must calculate a significant decrease in the rigidity coefficient of elements 41 and 48 and also detect a reduction in the flexural stiffness of elements 3 and 4 as well as elements 24 and 25. The analytical model is used to generate 100 randomly perturbed data sets with the same error levels as used in the previous damage cases. The data is generated by applying the load cases of Table 5.3 and the same measurement locations are used, which now include rotational displacement measurements for load cases 9 through 15. The damage detection procedure is identical to the previous cases. The localization procedure is executed prior to optimization in order to reduce the number of active rigidity coefficients in the optimization problem. Evidenced by the results of the previous damage cases, it is expected that the algorithm will be able to detect the reduced flexural stiffness of the girders as well as the reduction in rigidity coefficient of both connections. The optimization results for the 100 data sets are shown in Figure 5.24.
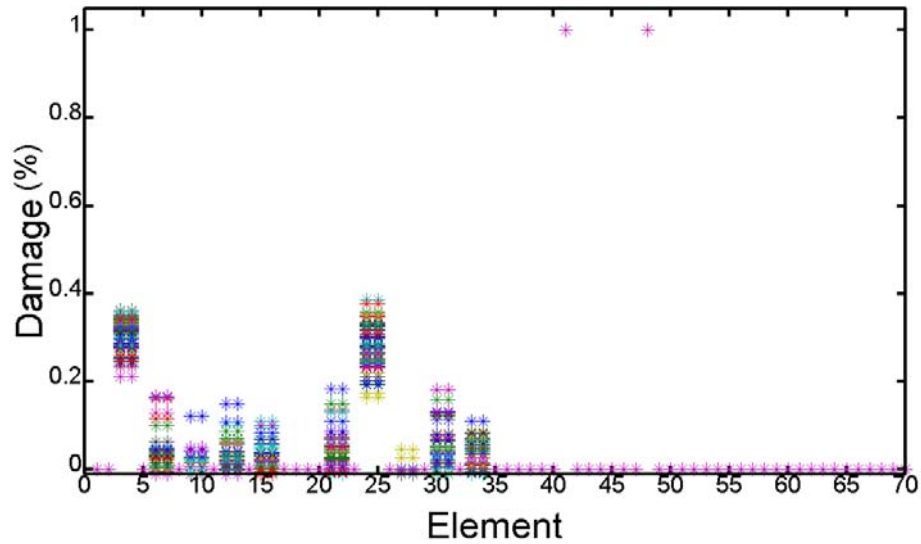
Figure 5.24 Damage Detection Results for Damage Case 3

It must be noted that the data presented in Figure 5.24 has been filtered. The optimization results for twenty five of the data sets showed immediate instability as the algorithm was forced to terminate after only the second iteration. The instabilities exhibited are most commonly a result of the algorithm attempting to make large changes to the stiffness parameters of the model in the first iteration. Many Lagrange multiplier methods exhibit a large jump in the constraints and objective during the first iteration. This jump is often interpreted as a calibration step for the algorithm and smooth convergence is typically witnessed for the following iterations. In these 25 cases, however, the calibration step attempted to adjust the variables too severely and the algorithm was unable to recover. The initial jump was too large and many of the variables became inactive due to violation of the side constraints. The good news is that these "bad" damage detection results are easily identified by the large number of inactive variables and the divergence witnessed in the constraint values. This instability can almost always be eliminated by increasing the convergence control parameter, r, of Eqn 2.20. The bad news is that determining the value of r that is large enough to avoid instability is accomplished by trial-and-error. It is not possible to adjust the convergence control parameter during the automated process of calculating the damage location for all 100 data sets. An alternative would have been to assign a convergence control parameter large enough to maintain stability for all data sets. However the larger parameter, in effect, slows convergence for the optimization of all 100 data sets and therefore would significantly increase the runtime of the algorithm. Instead it was decided

that it is more practical to not adjust the parameter and then simply filter out the data that is determined to be inaccurate.

The damage detection results show a significant reduction of the rigidity coefficient of elements 41 and 48. No other connections were calculated to have any damage for any of the data sets. Once again the girder elements showed some variability in calculated damage, but the most significant damage was calculated in elements 3, 4, 24, and 25. This result corresponds perfectly with the true damage state. The mean of the results is shown in Figure 5.25.
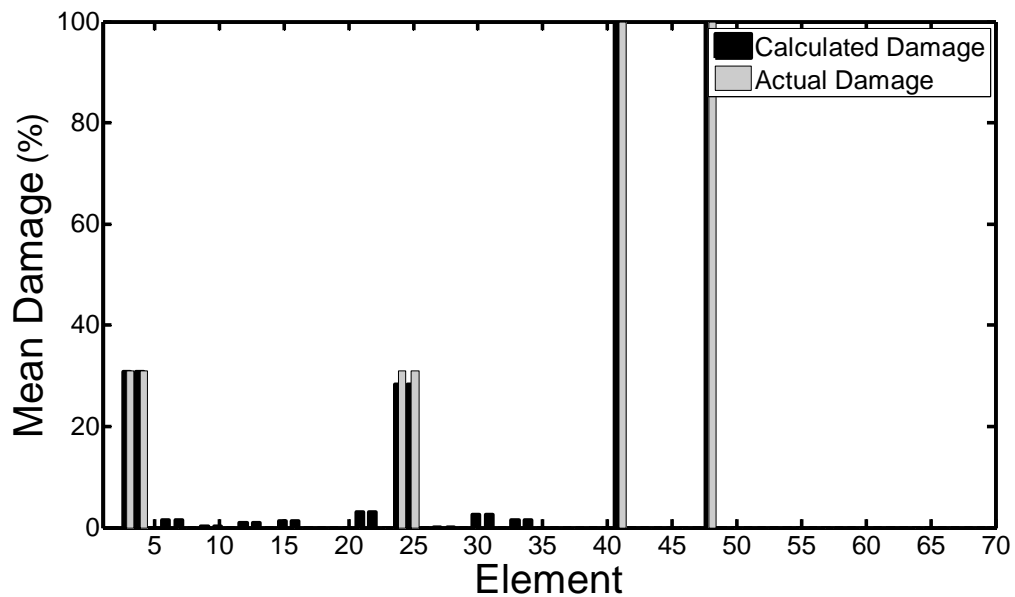
Figure 5.25 Mean Damage Detection Results for Damage Case 3

The algorithm detected the correct reduction in the rigidity coefficient for both damaged connections and the average damage of 30.8% in elements 3 and 4 is close to the true damage value of 31.0%. The sample standard deviation of these elements was 0.034 in⁴. Damage calculated in elements 24 and 25 was accurate as well. The average damage in these elements was 28.2%. The range of calculated damage for these elements was a bit higher as the sample standard deviation was 0.049 in⁴, or 2% of the mean. Greater than 10% damage was calculated in these elements for all 75 of the remaining data sets. False positive damage was calculated in 22 of the data sets. The correct reduction in the rigidity coefficients was also detected in all data sets. If the damage threshold is raised to 15% percent, the damaged elements are still detected in all 75 data sets, but the number of times false

positive damage is detected is reduced from 22 to 5. Once again, further studies are needed to establish a method of choosing an optimal damage threshold for damage detection.

5.7.1 Discussion

It was feared that the effects of damage at multiple locations would be interpreted by the algorithm as widespread damage over a large area of the structure. Instead the algorithm was able to use the measured response data to detect acute damage at 2 separate locations. Prior to including rotational displacements for damage detection, the detection of changes in rotational stiffness of the connections was largely affected by measurement error. Once rotational displacements are included, the accuracy of damage detection improves dramatically. The algorithm detected the correct reduction in rotational stiffness for every data set. Instabilities in the algorithm were more prevalent for the current damage case as 25 calculated results needed to be filtered out of the final presented results. Even though the instabilities are readily seen in the calculated data, the simple fact that instabilities are present shows that the algorithm has more trouble detecting damage cases with multiple points of damage. Again, the convergence control parameter can be used to limit these instabilities.

Several issues must still be addressed for the current structure. First, it wasn't until rotational displacements were included that the algorithm could accurately, and repeatedly, detect the correct damage state. Ideally only deflection data would be used to identify all damage locations and types. Therefore, further study must be done to determine if there is an alternate measurement scheme or if patterns in the deflection data can pinpoint rotational stiffness reductions. It is also possible, using the Betti-Maxwell Reciprocal Theorem, that rotational displacements can be calculated from deflection measurements and a combination of applied point loads and concentrated moments. A derivation of the formula is shown in Appendix C. The damaged rigidity coefficients for all damage cases were always at the extremes, either 1 or 0. It is desirable in real conditions to detect connection damage before there is a complete loss of moment resistance. A study must be done to determine if intermediate values for the rigidity coefficient can be used to detect such damage. In order to do this however, an accurate model must be developed for the relationship between the rigidity coefficient and the rotational stiffness. It is suspected that the true function is not truly linear. Lastly, if rotational measurements are deemed necessary a study must be performed to determine the accuracy of such measurements. It was assumed that the rotational measurements comply with the level of accuracy of the deflection measurements, which may or may not be true. If it turns out that rotational

measurements are significantly less accurate than deflection measurements, then a separate error model must be included in the generated data. Alternatively, the uncertainty of error models can be avoided altogether if real test structures are used.

5.8 Conclusion

With the support of IABMAS, a benchmark structure and simulation program was created to provide researchers a common platform to test their SHM methodologies. The benchmark structure simulates a common highway bridge structure. The two span grid system was composed of two main girders linked by 7 transverse beams with full moment connections at each end. The objective of this chapter was to assess the ability of the methodology and algorithm to detect damage in structural connections. Three damage cases were tested. The first damage case released the moment resistance of a single connection. The second damage case released the moment resistance as well as reduced the moment of inertia of the girder elements in the vicinity of the connection. The last damage case released the moment resistance at two connections and reduced the moment of inertia of the girders at these same locations.

To better model changes in rotational stiffness of connections, a modified finite element was developed that included a rigidity coefficient to describe the end fixity. This new element is much better suited for optimization as a linear relationship was developed between the rigidity coefficient and the redistribution of internal forces. Further, the new connection element was defined on a bounded domain, thus limiting the search space of the optimization problem. The newly developed element reduces the computation effort and improves the stability of the algorithm compared to preliminary trials when other connection element models were used.

The damage detection results varied greatly depending on the damage case tested. Deflection data proved able to detect changes in flexural stiffness of the girder elements to a high degree of accuracy, but was often not sufficient to detect changes in the rotational stiffness of connections. It is concluded that the inability to detect this connection damage is not a limitation of the algorithm, but rather a result of the type of measurements obtained during testing. Changes in rotational stiffness simply do not produce a large enough change in the deflection data to accurately detect damage. This is especially true when damage to the girders is also present. Rotational displacement measurements were included for both damage states 2 and 3. Once these rotational displacements were measured at the connection locations, the accuracy of damage detection improved dramatically. The changes in rotational stiffness were detected in 100% of the cases and the reduction of flexural stiffness was detected to an almost equally high level. Some false positive damage locations were recorded and

thus a better, more systematic approach needs to be developed to discern real damage from false positive damage.

Finally, three main achievements were presented in this chapter and deserve recognition. First, a finite element better suited for optimization and detection of connection damage was created. Next, the OC algorithm, coupled with the DLAC localization, was able to detect changes in rotational stiffness of connections as well as reductions in flexural stiffness of structural members. The algorithm was also able to detect stiffness reductions when the damage was contained at two separate locations in the structure. Finally the algorithm showed tremedous accuracy even when the error levels in the simulated response data were increased.

6 Damage Detection in a 14 Bay Truss Bridge Structure

Experiments performed using simulated data are instructive in assessing the capabilities of a damage detection methodolgy, but true acceptace cannot be gained until the methodology is performed using experimental test data. The objective of Chapter 4 was to illustrate the power of the OC algorithm, particularly its stability and accuracy. Chapter 5 established the optimal loading and measurement scheme and illustrated its effectiveness under simulated conditions. The current chapter is the culmination of these presented ideas using experimental test data. In this chapter damage will be detected in a 14 bay truss structure using the proposed damage detection methodology and algorithm. The structure is located at the University of Illinois Urbana-Champaign in the Smart Structures Technology Laboratory.

6.1 Test Structure

The test structure is a steel three dimensional truss with 14 bays. The structure consists of two parallel trusses joined by a series of connection members along the top and bottom chords. Each bay is 0.4 meters long and 0.4 meters tall. The structure is simply supported with all three translational degrees of freedom restrained at the left supports and the vertical and out of plane translation restrained at the right supports. The test structure is shown in Figure 6.1.

Figure 6.1 Fourteen Bay Three Dimensional Truss Test Structure in the Smart Structures Technology Laboratory at the University of Illinois Urbana-Champaign

The structural elements are hollow steel bars with tubular cross section. A total of 53 truss members comprise the front panel of the test structure. The bottom chord of the truss sits approximately 0.6 meters off the ground. Structural members are able to be removed and replaced with members of different cross sectional properties. Damage is simulated by installing members with reduced cross sectional area. Properties of the healthy test structure are shown in Table 6.1.

Table 6.1 Material and Cross Section Properties of Healthy Test Structure

Material and Cross Section Property	
Member Inner Diameter, D_i	0.43 in. (10.9 mm)
Member Outer Diameter, D_o	0.67 in. (17 mm)
Cross sectional area, A	0.336 in.^{2} (2.17 cm^2)
Moment of inertia, I	0.0118 in.^{4} (0.492 cm^4)
Torsional Moment of Inertia, J	0.0197 in.^{4} (0.819 cm^4)
Modulus of elasticity, E	29000 ksi (200 Gpa)
Density, ρ	487 lb/ft^3 (7800 kg/m^3)

6.2 Experimental Set Up

The test structure is excited using a series of static point loads, each applying a force of 80 lb at the center of the elements connecting the two truss panels. Two weights are hung side by side to apply the necessary load. Damage is only induced on the front truss panel and so displacement measurements are only taken at the nodes of the bottom chord of the front truss. Displacements are measured using displacement dial gauges with a total lead of 1 in. and a precision of 0.001 in. A total of 9 displacement dial gauges were obtained for use in the damage detection procedure. For illustration, a portion of the measurement set up is shown in Figure 6.2. Following the premise of maximizing practicality of the method, only gravity loads will be applied to the structure, therefore it was deemed that only vertical displacements would be used for damage detection. The benefit of testing a scale model structure is that displacement gauges can be easily mounted on a stationary reference point and so differential displacements from that reference point represent the absolute displacements of the structure. Testing on full scale structures does not often present this convenience. Alternate methods of displacement measurement are necessary. A brief explanation of these methods is contained in Section 1.1.1. Fortunately the presented damage detection theory, with the exception of the model updating step, is largely dependent on the change in displacements relative to the healthy displacements. Therefore, if an accurate initial model can be developed, a stationary reference frame is not always needed.

Figure 6.2 Experimental Set up for Damage Detection in 14 Bay Truss Structure

As stated earlier, only gravity loads are applied to the structure. These loads are applied to the center of the connecting elements along the bottom chord of the truss. The structure is meant to imitate a highway truss bridge and so the applied gravity loads simulate a large vehicle that is parked at specific locations to induce displacements for damage detection. Only vertical displacements are measured using the dial gauges. Figure 6.3 shows a typical load case used for damage detection.

Figure 6.3 Typical Load Case Used for Damage Detection in Test Structure

The loading and measurement schedule will be presented in Section 6.4. At this point a brief comment on measurement error is necessary. The displacement gauges are mounted by hand and leveled by eye. Precise leveling devices were not available and so it is possible that the displacement gauges were not plumb. It is estimated that vertical alignment of the gauges can be achieved to within 10 degrees with respect to both horizontal axes. The estimate of 10 degrees may appear as an overestimate, but is meant to provide a worst case scenario as well as encompass cumulative leveling errors such as floor slant, skew of the mounting stands, as well as the levelness of the structure itself. Assuming the maximum error of 10 degrees about both axes of the horizontal plane, a maximum measurement error of 3.1% is calculated for the experiment.

6.3 Analytical Model

The static response of truss structures is dominated by the axial stiffness of each element. An idealized model can be created by assuming that all connection nodes resist little to no moment and the internal force distribution is defined purely by axial tension or compression of the structural members. In reality, the connection nodes inevitably have some level of moment resistance, however due to the abrupt reduction in moment of inertia of the elements at each connection node (seen in Figure 6.3), axial displacements define the response more than flexural stiffness. A three dimensional truss element can be created using the truss element given in Section 2.7.1 in conjunction with a three dimensional transformation matrix. Each three dimensional element contains 6 translational degrees of freedom, resulting in a total of 158 unrestrained degrees of freedom for the entire structure. A representative model was created in RISA-3D and is shown in Figure 6.4 for illustration. The RISA-3D model was created to check the finite element assembly algorithm written in Matlab. Once the response of the two models matched under arbitrary loading conditions, the assembly algorithm was deemed sufficient for damage detection.
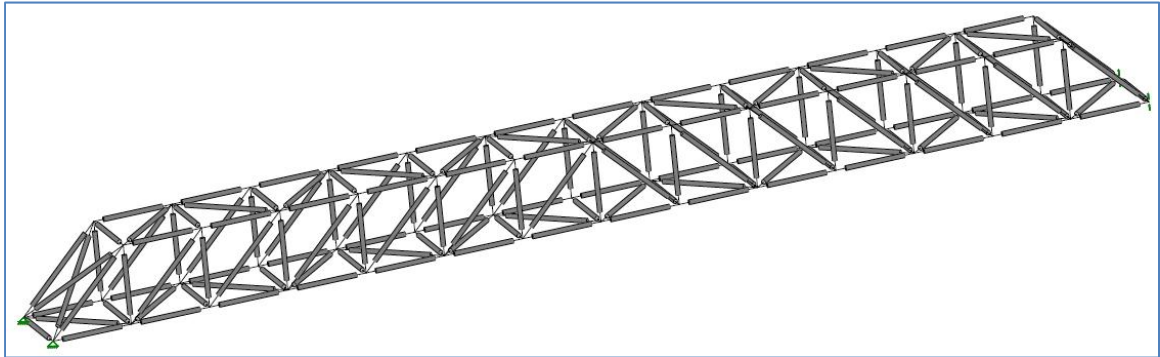
Figure 6.4 Representative Finite Element Model Used for Damage Detection in Test Structure

A total of 164 elements are used to build the truss model. All elements contain identical cross sectional characteristics and are initialized using the healthy cross sectional area given in Table 6.1. Damage will be detected by identifying elements with reduced cross sectional area. Both the modulus of elasticity and the length of each member remain constant pre and post damage. Damage will only be induced in the front panel of the structure therefore all element and node references will be made in accordance with Figure 6.5 to avoid confusion and to aid in visualization. The dimensions and the global coordinate system are also included in the figure.
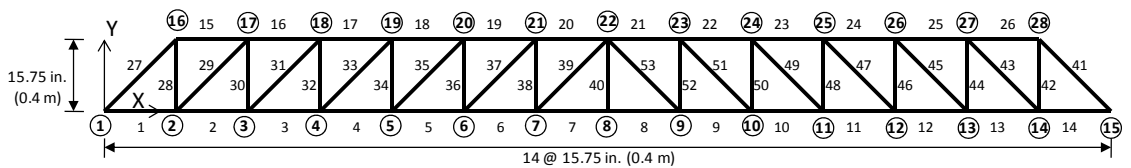
Figure 6.5 Node and Element Numbering Scheme of Truss Panel with Global Coordinate System

6.4 Truss Structure Baseline Data with Loading and Measurement Schedule

Nine load cases are used for damage detection at the nine displacement gauge locations. The loading schedule is shown in Table 6.2 along with the measurement schedule and baseline displacement data. Note that the loaded node in the loading schedule refers to the element connecting into the node listed and not the actual node. It was earlier explained that all load cases apply loads to the connecting element between the truss panels, a sample photo is shown in Figure 6.3.

Table 6.2 Loading Schedule and Baseline Measurements for the 14 Bay Test Structure

	Loading			Measurement		
Load Case	Node	Magnitude (lb)	(N)	Node	Displacement (in.)	(cm)
1	4	80	356	4	-0.0137	-0.0348
2	5	80	356	5	-0.01902	-0.0483
3	6	80	356	6	-0.02724	-0.0692
4	7	80	356	7	-0.03051	-0.0775
5	8	80	356	8	-0.03016	-0.0766
6	9	80	356	9	-0.03039	-0.0772
7	10	80	356	10	-0.02598	-0.066
8	11	80	356	11	-0.01961	-0.0498
9	12	80	356	12	-0.01772	-0.045

The nine displacement gauges were mounted at nodes 4 through 12. These locations were chosen because the measurement locations must remain constant for the entire test to limit the amount of time needed to execute the testing procedure. Thus the measurement locations must extract the most pertinent data for the loading schedule as a whole. Measurement of nodes 2, 3, 13, and 14 were avoided due to the small displacement magnitudes near the supports. The displacement data shown in Table 6.2 matches the expected trend. Displacements are nearly symmetric about load case 5 with the largest displacements being recorded for load cases 4, 5, and 6.

Similar to the previous damage detection examples, a model updating step is performed to match the experimental baseline data with the calculated healthy response. Manual adjustment of the parameters is chosen as the updating technique. After updating of the structural parameters, displacement errors

ranged from 2.8% for load case 7 and 9.2% for load case 4 to a high of 19.24% for load case 9. The response error is noticeably higher for this structure than those of previous problems. This is not unexpected however. The main source of error in previous examples was due to unknown stiffness parameters of the elements. Most other parameters such as load magnitude and load locations were well defined. This structure on the other hand has many unknowns. The exact stiffness value of each element is still a source of error, but other sources include the measurement error discussed previously, the modeling error associated with the moment resistance of each connection, and finally the load distribution. Each of the load cases applies a load by hanging two weights on a connection element between the two truss panels. Care was taken in applying the loads, but if these loads were not applied symmetrically, then one of the truss panels will carry a larger portion of the load than the other. This is not accounted for in the mathematical model. Thus with all of these sources of error present, a certain level of discrepancy must be tolerated. Precautions were taken to minimize the experimental error, but it is the role of the algorithm to be robust enough to handle data error and still detect damage.

6.5 Damage States

With the baseline data collected the damage states can now be tested. Two damage states will be tested to assess the algorithm's ability to detect damage using experimental data. The two damage states are shown in Table 6.3. The first damage state replaces elements 10, 49, and 50 of Figure 6.5 with elements that have reduced cross sectional area. Notice all three of these elements are contained in the same bay.

Table 6.3 Tested Damage States for the 14 Bay Truss Structure

Damage State	Damaged Element	Area Reduction (%)
	10	51.1
1	49	48.9
	50	40.9
	10	51.1
2	49	48.9
	50	40.9
	20	40

It must be noted that after performing the testing procedure, during reinstallation of the healthy members, it was noticed that the damaged member in position 10 contained additional unintended damage. The weld on the threaded connector at one end of the member was cracked. The crack was severe enough that the threaded connector was not fully secure on the damaged element. The exact quantification of this additional damage is very difficult to determine, however it was clear that the damage was much greater than the 51.1% stiffness reduction given in Table 6.3. A picture of the damaged element is shown in Figure 6.6.

Damaged weld on threaded connection element
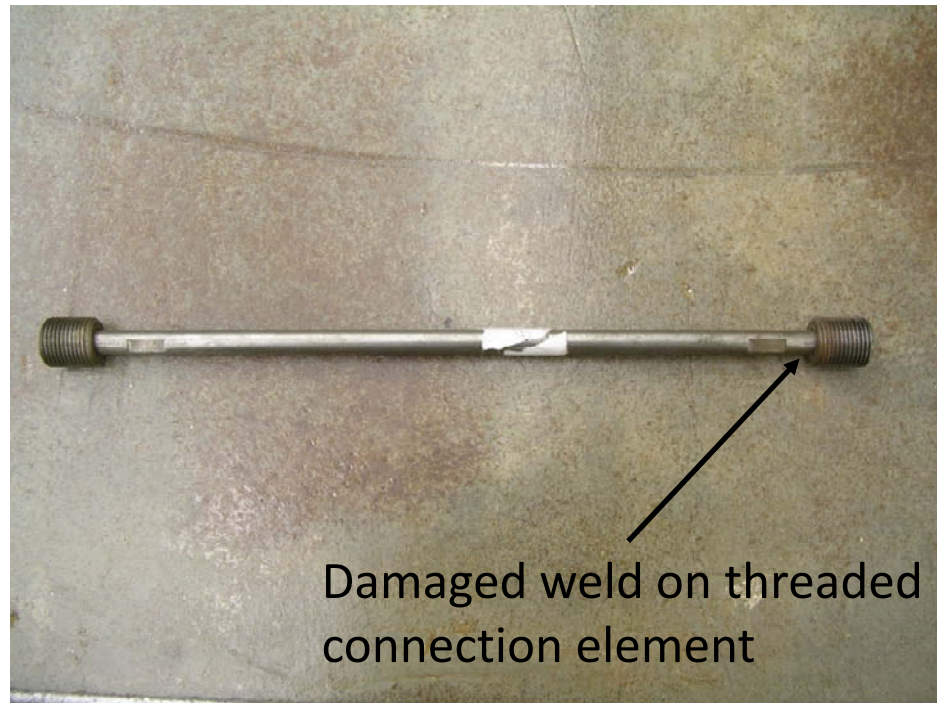
Figure 6.6 Damaged Element at Position Ten of the Test Structure

The intended goal of testing the first damage state is to assure that the algorithm is able to detect significant damage concentrated in a localized area of the test structure. The second damage state contains all of the damaged elements of the first damage state with additional damage induced in element 20. This damage state will assess the algorithm's ability to detect damage at multiple locations. It is feared that large damage concentrated in a portion of the structure will drown out the response characteristics of less severe damage in other parts of the structure. The second damage state will be discussed in Section 6.6. The experimental set up of the first damage state is pictured in Figure 6.7. The three damaged elements are shown and have noticeably reduced cross sectional areas than the surrounding healthy elements.
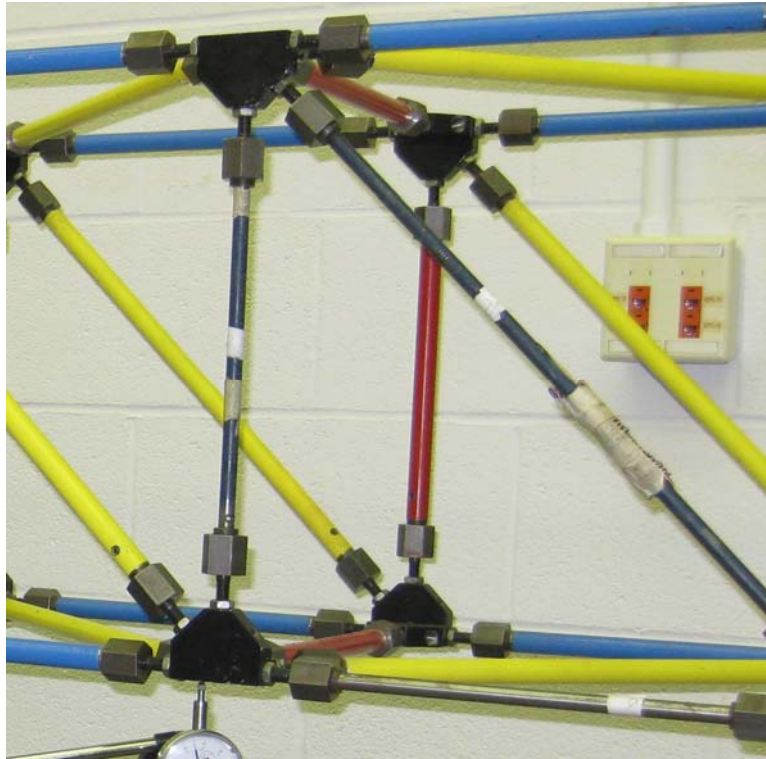
Figure 6.7 Installed Damaged Elements for Damage State 1

6.5.1 Detection of Severe Localized Damage (Damage State 1)

With the three damaged elements of damage state 1 installed in the structure, the damaged static response data can be obtained. The procedure for obtaining the baseline respone is repeated for the first damage scenario. The displacement gauges are mounted at nodes 4 through 12 and the load cases of Table 6.2 are applied. Again, it is known that damage is only induced in the front truss panel and so displacement measurements are only obtained along the bottom chord of the front truss. In practice, damage would not be known beforehand and displacement measurements would need to be taken along both panels. Due to the limited number of available displacement gauges, damage was concentrated in the front panel only. The response data of the damaged structure is shown in Table 6.4.

Table 6.4 Loading Schedule and Static Response Data of Damage State 1

Load Case	Loading			Measurement		
	Node	Magnitude		Node	Displacement	
		(lb)	(N)		(in.)	(cm)
1	4	80	356	4	-0.013	-0.032
2	5	80	356	5	-0.023	-0.057
3	6	80	356	6	-0.03	-0.076
4	7	80	356	7	-0.048	-0.122
5	8	80	356	8	-0.05	-0.127
6	9	80	356	9	-0.055	-0.139
7	10	80	356	10	-0.059	-0.151
8	11	80	356	11	-0.041	-0.104
9	12	80	356	12	-0.023	-0.058

The data presented in Table 6.4 shows a significant increase in displacement near the damage location when compared to the data contained in Table 6.2. For example, the displacement measurement for load case 7 has more than doubled compared to the healthy state, while the displacement of load case 1 increased by a modest 8.6%. The significant difference in response behavior near the damage location is an advantage of static reponse methods. Static response data is able to capture changes in response behavior locally and damage can be much more readily identified if response measurements can be obtained in the vicinity of damage.

Damage Localization (Damage State 1)

To aid in damage detection, a localization step is performed to reduce the number of active stiffness parameters used in the final optimization problem. The optimization problem is formulated in the same fashion as Eqn 2.3, but the optimization process will operate using parameter groups rather than the individual stiffness parameters of each element. This localization step can only be employed if the structure presents a logical method of grouping parameters for localization. Fortunately the truss structure can be partitioned into parameter groups that comprise each bay. To operate using parameter groups the linking algorithm of Section 2.4.5 must be used. The linked variables are shown in Table 6.5.

Table 6.5 Linked Elements for Damage Localization

Parameter Group	Linked Elements
1	1, 27, 28
2	2, 15, 29, 30
3	3, 16, 31, 32
4	4, 17, 33, 34
5	5, 18, 35, 36
6	6, 19, 37, 38
7	7, 20, 39, 40
8	8, 21, 53
9	9, 22, 51, 52
10	10, 23, 49, 50
11	11, 24, 47, 48
12	12, 25, 45, 46
13	13, 26, 43, 44
14	14, 41, 42

Note the active parameter selection subroutine of Section 2.5.2 is not employed for this initial localization step. Instead all parameter groups remain active for the entire optimization process. Using the measured response data of Table 6.2 and Table 6.4, the constraints are formed similar to Eqn 2.3. The exit criteria are $\pm 1\%$ satsifaction of opimality, less than 0.1% change in the constraint or objective functions for 3 consecutive iterations, or a maximum of 50 iterations. The side constraints remain unchanged, as the stiffness of any element must be greater than zero and cannot be greater than the healthy stiffness value. The results of the optimization problem are shown in Figure 6.8.
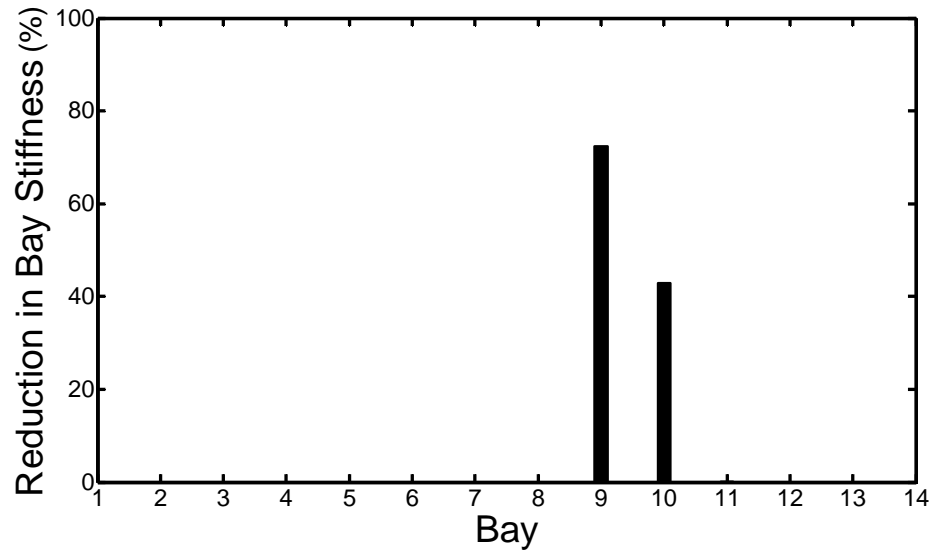
Figure 6.8 Damage Localization Results for Damage State 1

The algorithm localized damage in the region of bays 9 and 10. It was hoped that the algorithm would be able to localize damage to bay 10 alone rather than two seperate bays, however the results do accomplish the inteded goal of localizing damage and reducing the number of active design variables for the final damage detection problem. Now that the vicinity of damage has been determined through the preliminary localization step, the familiar damage detection problem can be solved.

Damage Detection (Damage State 1)

The damage detection problem is now repeated, but this time without linking. Only the elements contained in bays 9 and 10 of Table 6.5 will remain active for the damage detection problem. Also, the active parameter selection subroutine will be utilized during optimization. Four member groups are chosen for parameter selection. The four groups are the bottom chord elements, the top chord elements, the vertical elements, and the diagonal elements. From these groups, the element with the largest constraint gradient will be chosen to remain active for each iteration. The exit criteria are identical to the localization step and the constraint convergence is set to half of the maximum initial constraint error. The optimization results are shown in Figure 6.9.
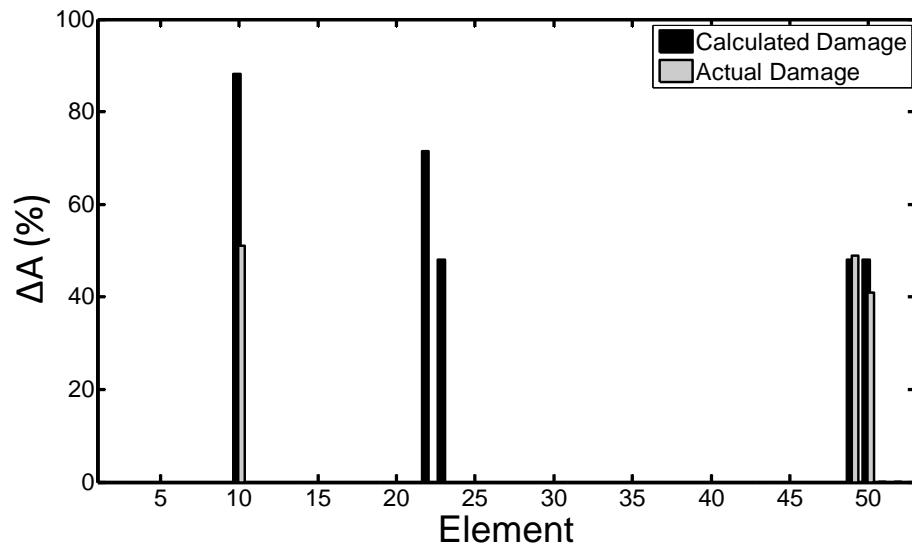
Figure 6.9 Calculated Damaged Elements for Damage State 1

The damage detection algorithm was able to locate and quantify damage in members 49 and 50 to a high level of accuracy. The algorithm calculated damage in both the top and bottom chord elements (elements 10 and 23) of bay 10. Approximately 90% damage was calculated for element 10 when the true reduction in crossectional area was 50%. Also, significant damage was calculated for elements 22 and 23 when no actual damage was present. The overprediction of damage can be attributed to the unintended damage in the threaded connection of element 10. Recall that exact quantification of this damage was not possible, but it was expected that the detected damage would be significantly higher than the 50.1% reduction in cross section. As can be seen, the algorithm has spread damage to the top chord elements in bays 9 and 10 to account for the additional damage in element 10. If alternate loads, such as lateral loads were able to be applied and horizontal displacements measured, the algorithm may have had a better opportunity to pinpoint damage to only element 10. However practicality of the testing procedure does not allow for these loads and measurements. Given the restrictions on measurement and loading, the results are encouraging. The algorithm was able to localize damage to a very small group of members using only vertical loads and vertical displacements.

6.6 Detection of Multiple Damage Locations (Damage State 2)

The second damage state contains all of the damaged elements of the first damage state with additional damage induced in element 20. This damage state intends to test the algorithm's ability to detect damage at multiple locations. The same load cases and measurement locations will be employed as shown in Table 6.2. It should be noted that the damaged element at position 10 is unchanged and still contains the additional damage in it's threaded connection, therefore it is still expected that additional damage will be detected in bay 10. After repeating the static tests the following response data was measured.

Table 6.6 Loading Schedule and Static Response Data for Damage State 2

Load Case		Loading			Measurement		
	Node	Magnitude		Node	Displacement	
		(lb)	(N)		(in.)	(cm)
1	4	80	356	4	-0.014	-0.036
2	5	80	356	5	-0.024	-0.061
3	6	80	356	6	-0.031	-0.079
4	7	80	356	7	-0.062	-0.157
5	8	80	356	8	-0.061	-0.155
6	9	80	356	9	-0.064	-0.163
7	10	80	356	10	-0.066	-0.167
8	11	80	356	11	-0.043	-0.109
9	12	80	356	12	-0.025	-0.064

Damage Localization (Damage State 2)

The displacements are all slightly larger than those measured for damage state 1, indicating that the structure has experienced additional damage. The same localization step of damage state 1 is employed here where all elements in a bay are linked. Again the linked elements are shown in Table 6.5. After performing the localization step, the results of Figure 6.10 are obtained.
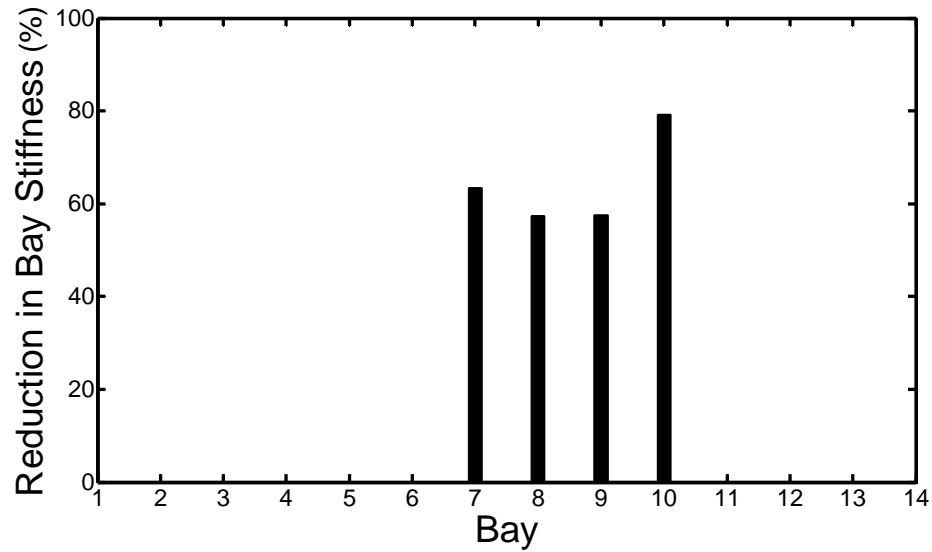
Figure 6.10 Damage Localization Results for Damage State 2

The localization step has pinpointed damage in the vicinity of bays 7, 8, 9, and 10. The algorithm was unable to pinpoint bays 7 and 10 exclusively and instead smeared damage across all bays spanning 7 to 10. Nevertheless, the number of active design variables used in the final damage detection algorithm has been reduced dramatically.

Damage Detection (Damage State 2)

The damage detection problem can now be repeated with the elements comprising bays 1 through 6 and 11 through 14 set inactive. Once again the active parameter selection subroutine is employed at each iteration on the remaining eligible design variables. The convergence criteria remain unchanged from the previous damage state. The damage detection results are shown in Figure 6.11.
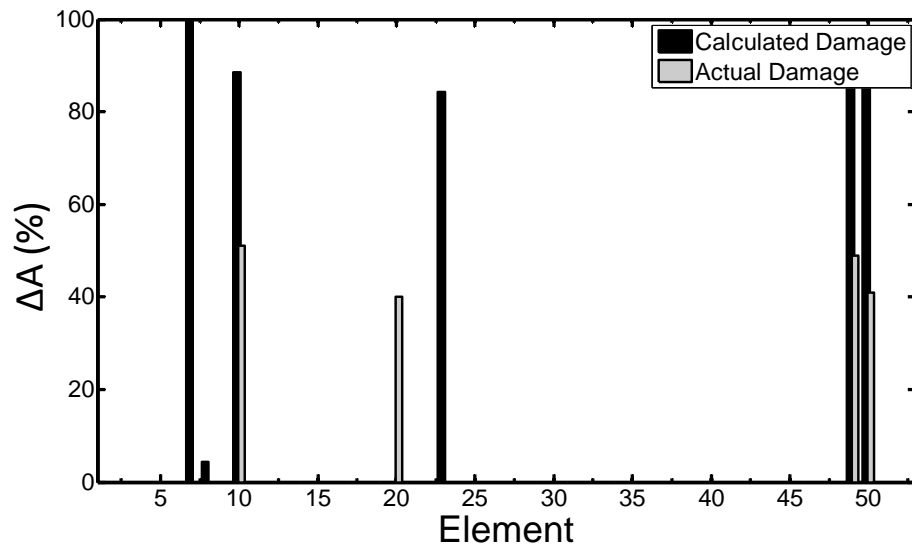
Figure 6.11 Calculated Damaged Elements for Damage State 2

The damage detection algorithm again correctly detects damage in elements 10, 49, and 50 but also detects significant damage in elements 7 and 23. Damage was not detected in element 20. At first glance the results may seem incorrect, but upon closer investigation the results do provide insight on the locations of damage. The detection of damage in elements 10, 49, and 50 is encouraging, but also the false identification of damage in element 23 is still contained in bay 10. It can be conjectured that the damage detected in element 23 is a result of the unintended damage in element 10, similar to the results of damage state 1. Therefore, significant damge has been localized to bay 10.

Unfortunately the algorithm did not detect damage in element 20, however there is damage detected in element 7. Note that element 20 is the top chord element of bay 7 and element 7 is the lower chord element of bay 7. The reason for this false identification is because the top and bottom chord elements have essentially the same affect on the constraint equations. Without measurement data for both the upper and lower chord nodes it is difficult for the algorithm to discern that damage has occurred in the top chord rather than the bottom chord. This shows that the accuracy of damage detection for the algorithm, and static based methods in general, are largely dependent on obtaining response measurements in the immediate vicinity of damage. The results also show that the algorithm does not necessarilly attempt to smear damage across all elements in a single bay. It was observed in previous research that the algorithm often smears damage over many elements rather than concentrating damage in few elements. It was the intent of the active parameter selection

subroutine to avoid this tendency of the algorithm. In this example the algorithm did damage all elements in bay 10, which can be explained by the unexpected additional damage in element 10, but then only calculated damage in one element of bay 7. Even though the calculated damage was not in the true damaged element, it does indicate promise that the algorithm can find multiple points of damage even when one damaged area is significantly more severe than the other.

6.7 Trends in the Calculated Results

Common to both damage state results is the level of overprediction in damage present in the system. It was initially thought that the algorithm became unstable and induced excessive damage, however inspection of the constraint optimization disproves this hypothesis. Looking at the constraint convergence of Figure 6.12, one can see that the optimization shows relatively smooth convergence with no instabilities. Instabilities are characterised by sharp "spikes" in the optimization data or large abrupt changes between successive iterations.
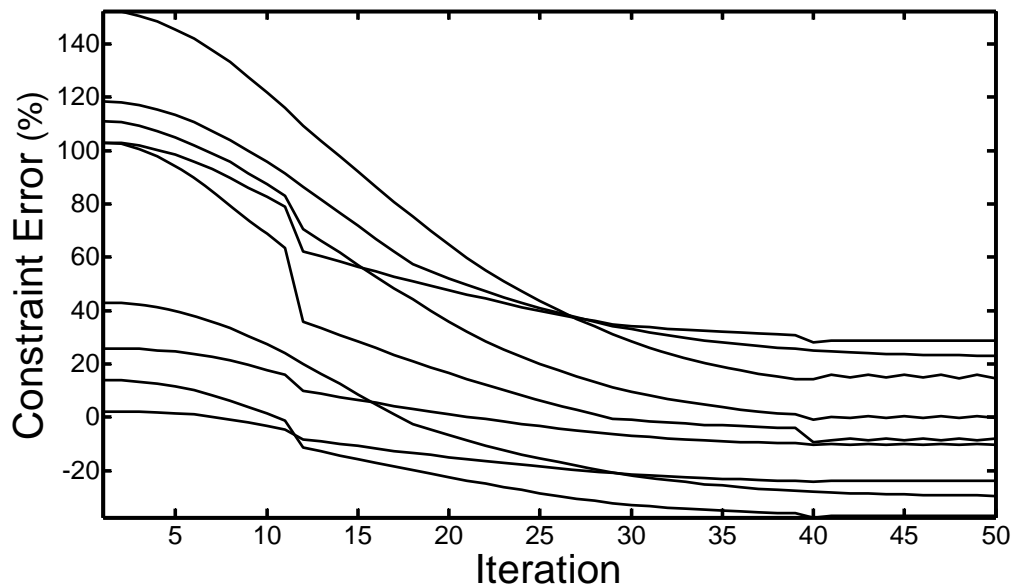
Figure 6.12 Constraint Convergence for Damage State 2

The majority of constraint values are greater than zero at the end of the optimization proces, which implies that the calculated displacements are still not as large as the measured displacements. This

127

means that the calculated damage, although large, is still not large enough to recreate the large displacments measured for the damaged structure. Therefore, the overprediction of damage is not a result of the algorithm, it is a result of the mathematical model of the structure. It becomes obvious once the deflection for each load case is plotted that either torsional deflections are induced that are not accurately reflected in the mathematical model or the damage in element 10 is so severe that it produces unexpected deflected shapes. The deflection plots are shown in Figure 6.13.
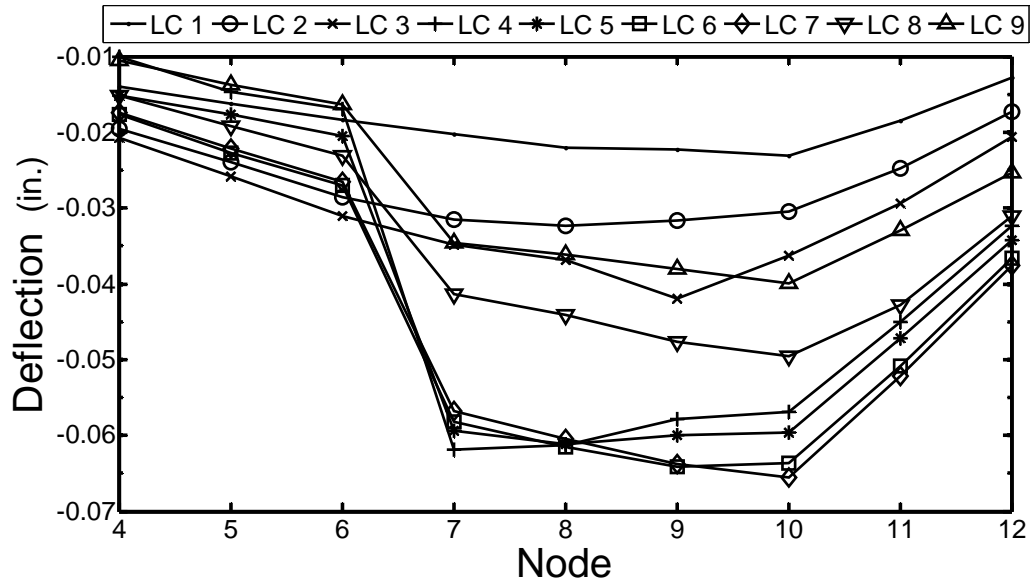
Figure 6.13 Plotted Displacement Data for each Load Case for Damage State 2

The deflection data is smooth for load cases 1, 2, and 3 but changes drastically beginning with load case 4. It can be seen that the structural response at nodes 4, 5, and 6 is significantly less than other deflection measurements in the same load case. Even though increased deflection is expected in the vicinity of damage, the drastic change in displacement from node 6 to node 7 is not expected. It is suspected that the applied load cases have induced torsion in the structural system. Recall that damage is induced in only the front panel of the structure, thus the stiffness of the structure is not uniformly distributed. Even though the three dimensional finite element model can account for torsion, the level of torsion measured could not be accurately mimicked by the model without inducing the severe damage calculated in Figure 6.11.

It is also possible that the damage in element 10 is much more severe than initially expected. It is possible that the damage to the weld essentially eliminates the stiffness of the element. It would be

128

impossible for the algorithm to eliminate element 10 because an unstable structure would result, but it is percieveable that the test structure can withstand the removal of a member. The reason is because the connection elements do have a certain capacity for moment resistance even though the finite element model was created using pin connections. Future tests should determine whether the deflected shape is a result of the damage in element 10 or is due to a torsional deflection that is not mimicked in the finite element model. Future work should also determine whether damage can be detected to the left of the inflection point where the structure was less responsive. Displacements should also be measured along both truss panels to assess the complete response of the structure.

6.8 Conclusion

Damage was detected in a scale model, 14 bay truss bridge using experimentally obtained static displacement measurements. The cross sectional area of each element was selected as the optimzation parameter to locate damage. A three dimensional finite element model was created using truss elements and was used in the optimization algorithm. The results show that stiffness reductions can be detected and localized to a specific bay in the truss structure using a limited number of load cases and displacement measurements. In specific cases, exact damaged elements were able to be detected.

Displacement measurements were taken using displacement dial gauges mounted at nodes 4 through 12 along the bottom chord of the structure. The static response data was obtained by employing the optimal load locations calculated using the theory from Section 2.8 and using the measurement guidelines of Section 2.9. After obtaining the static response data, the damage detection process required two steps. First, a localization step was performed where all elements contained in a bay were linked and the optimization algorithm detemined the bay(s) that was the most likely candidate for damage. The damage detection algorithm was then re-solved, but setting all the elements not contained in the likely damaged bay(s) as inactive. The active parameter subroutine was used to aid the algorithm in pinpointing the exact elements that contained damage. The algorithm was able to localize damage to specific bays, however the algorithm had trouble determining whether damage was contained in the top or bottom chord elements. The reason for this is because the top and bottom chord elements have very similar effects on the response behavior of the structure. Further, displacements were only measured along the bottom chord of the structure, making it very difficult to discern whether damage was contained in the top or bottom chord.

Modeling error may have played a role in the quantification of damage. It is possible that the damage and loading induced torsion in the structure that was difficult to mimic using the finite element model. The torsion magnifide the change in displacements in the vicinity of damage, leading the algorithm to calculate much more severe damage than was actually present. It is also possible that the additional unintended damage in element 10 may have contributed to the increased level of damage calculated. Despite the sources of error present in the test, the algorithm proved robust enough to localize damage to a very small region of the test structure. The algorithm was able to detect damage in a single area as well as a damage state with multiple damage locations. Promising results were obtained even for the damage state with multiple damage locations where one location contained severe damage and the other point contained lesser damage. Future work must concentrate on determining the level of damage able to be detected in the structure without sacrificing accuracy. The presented experimental test adds validity to the testing procedure and algorithm.

7 Conclusion

The research presented in this dissertation was a continuation of the masters level research performed by the author, see [57]. The masters level work aimed to establish the feasibility of using the classic OC algorithm and static response data for damage detection. Damage was detected using simulated data for two dimensional frame models. The simulated data was free of both measurement and modeling errors. The algorithm was able to accurately detect reductions in flexural stiffness of these two dimensional models with acceptable computing effort. The algorithm, however, did experience difficulties from ill-posed constraints and was at times unable to complete many damage detection problems. Despite this complication encountered during the masters level research, the results were promising and warranted further exploration of the method and development of the algorithm. The improvements developed in this Ph.D. research are now summarized.

7.1 Improvements

The goal of the current research was to address many of the questions left unaswered during the masters level research. First, the solution process for ill-posed constraints needed to be modified in order to make damage detection much more consistent. Second, experimental error needed to be incorporated in the test data and the algorithm shown to have the ability to detect damage even when experimental errors are present. Third, the methodology needed to detect damage in more complex structures than only two dimensional frame models. Lastly, the algorithm needed to go beyond simulated examples and use experimental test data for damage detection. The improvements made to address these points fall into three main categories; improvements made to the algorithm, improvements made to the methodology, and improvements made to modeling. A summary of each category are as follows:

Improvements made to the OC algorithm:

- Instability in the classic OC algorithm most often occurred when the system of equations used to solve for all Lagrange multipliers were inconsistent. To solve this issue, a least squares approximation was employed so that a "best fit" solution for the Lagrange multipliers could be found at each iteration. This modification to the algorithm is especially important when experimental error is included in the measurements. The least squares approximation improves the stability of the algorithm dramatically, all at a minimal cost in computation effort.

- Changes have been made in the handling of active paramters. An active parameter selection subroutine has been developed to prevent smearing of calculated damage. After eliminating converged constraints, the components of the constraint gradients are ranked by magnitude. Only the variables with the largest constraint gradient from each member group remain active during optimization. This active parameter subroutine prevents the algorithm from eliminating variables that do not contribute to the convergence of contraints, which is a characteristic of the classic OC algorithm.

- The active parameter selection subroutine was supplemented with a steepest descent algorithm for all inactive variables. Variables that are set inactive due to their small constraints gradients may still have a significant affect on the objective function and therefore should still participate in the damage detection problem. The steepest descent method adjusts all inactive variables to minize the objective function. Both the steepest descent and parameter selection subroutine are modifications made specifically for when the OC algorithm is applied to damage detection.

- An initial localization step was also employed for several of the damage detection problems presented. It is usually beneficial to limit the number of active parameters prior to using the OC algorithm for damage detection as it will reduce the computation time. Two methods of localization were employed in this dissertation, one of which was the DLAC algorithm, which had not previously been used for static response data. The method, originally developed for damage detection using dynamics data, performed exceptionally well for static data.

Improvements made to the methodology:

- The largest improvement to the methodology is the systematic approach to determine the optimal load cases for damage detection. The masters research relied heavily on trial-and-error simulations to determine the optimal load cases for damage detection. Now the load cases are chosen based on the distribution of strain energy in the system from simulated loads applied at each possible load location. The method also provides flexibility to the testing procedure as users are able to choose the possible load locations, thus allowing impractical load locations to be omitted from testing. Further the methodology need not be applied to the structure all at once. The computation effort can be divided by applying the optimal load case algorithm to subsections of the structural system.

- General guidelines were set forth to determine the optimal measurement locations for damage detection. Determining the optimal measurement locations is still largely dependent on mathematical simulations prior to performing the damage detection tests. The guidelines do, however, bring to attention many issues not previously considered for static based procedures. For example, the guidelines set out to avoiding loading and measurement schemes that can produce multiple solutions that satisfy the displacement data.

Improvements made to modeling:

- The most significant improvement made to modeling is the development of a finite element that is able to model semi-rigid connections. The element makes it possible to optimize the connection stiffness, allowing for detection of changes in the rotational stiffness of moment connections. Although not the first attempt at modeling semi-rigid connections by researchers, it is the first element that is well suited for optimization as it is defined on a bounded domain and is linear with respect to the rigidity coefficient.

7.2 Summary of Results

After incorporating the outlined modifications, the method and theory were tested on 3 different structures. First, damage was detected in a one bay, one story scale model steel moment frame using published data in [2]. Next, three separate damage cases were detected on a structural grid benchmark problem. Last, damage was detected using experimental data obtained from tests performed on a 14 bay truss bridge in the Smart Structures Technology Laboratory at the University

of Illinois Urbana-Champaign. The results of these damage detection tests revealed many positives as well as some areas for improvement.

Positives

- Damage was able to be detected in three different types of structures; a steel moment frame, a three dimensional steel grid, and a three dimensional steel truss, showing that the method and algorithm are robust.

- The computation effort required to execute the algorithm is not overly burdensome. All problems were solved on a personal laptop. Even the data perturbation trials of Chapter 5 required fewer than 6 hours to complete for each damage case.

- Connection damage was detected in the structural grid benchmark structure. Previous research performed by the author had only detected changes in moment of inertia and crossectional area of structural members.

- Damage was detected using experimental data, a feat that had not been previously accomplished in prior research using the algorithm. The use of experimental data showed that even in the precense of real modeling and measurement error, the algorithm and methodology performed exceptionally well.

Areas of Improvement

- The damage detection results of Chapter 5 required the use of rotation displacement measurements. It was originally hoped to detect damage using only deflection data. It was instructive, however, to show that connection damage is most easily detected with the use of rotational displacement measurements at the connections.

- Even though the least squares approximation drastically improved the robustness of the algorithm, there were still instances when stability was not maintained. For example, the results in Section 5.7 showed that a portion of the data sets were not useable due to instability of the algorithm. Even though these poor results are easily identified and can be corrected by adjusting the convergence control parameter of the algorithm, an automated correction process for the unconverged data sets would be helpful.

- The damage detection algorithm has trouble identifying damage in elements that are less responsive to deflection measurements. It has already been explained that the connection damage of Chapter 5 was difficult to detect with deflection measurements alone, but the algorithm also had difficulty detecting damage in the diagonal members of the truss structure in the Chapter 6.

7.3 Future Work

Improvements can always be made to the structural model as model development is a never ending task. The same is true for the current research. The semi-rigid connection element developed in Section 5.2 was an important step in developing an element that can be used for optimization methods that detect damage in connections, but the model must still be improved. Quantification of damage based on intermediate values of the rigidity coefficient is difficult. The model developed simply established the form of the equation that describes the stiffness of the element. The true relation of the rigidity coefficient must still be studied. It was assumed that the fixed and pinned condition form complimentary pairs, but the true relationship may not be so straightforward. It may even be necessary to create an empiracal formula derived from experimental tests performed on moment connectons that have sustained a range of damage.

Many of the parameters needed to establish the damage detection procedure are still dependent on preliminary simulations of the test structure. The most important of which are the number and locations of the measurement sensors and the number of load cases needed for accurate damage detection. The optimal load case algorithm is extremely useful once the user has identified the possible load locations and the number of applied loads. Also, the measurement guidelines provide a good general measurement strategy, but determining if a sufficient number of load cases and measurements have been used is more a process of simulation than mathematical reasoning. As a general rule it is better to use as many load cases and measurements as possible and let the algorithm sift through the data to choose the active constraints, but research must be performed to establish the minimum number of load cases and measurements that still produce accurate damage detection.

Additional experimental tests are always instructive in assessing a methodology. The damage detection examples presented were all performed on skeletal structures. All models were assembled using a single element type. It would be instructive to test the damage detection methodology on structures that contain an array of structural elements. For example the methodology could be tested

on a building system composed of steel frames and concrete floor slab or a cable-stayed bridge requiring several element types to model the bridge deck, towers, and support cables. The static method should show that it is able to detect damage in any of these structural elements.

Appendix A

Using the optimal load case algorithm of Section 2.8, the elemental strain energy matrix is assembled by applying a unit load to each of the possible load locations, one by one. The elemental strain energy matrix of the continuous beam in Figure 3.2 is given by:

$$ESE = 1 \times 10^{-5} * \begin{bmatrix} 0.206 & 0.036 & 0.011 & 0.014 & 0.014 & 0.009 & 0.003 \\ 0.298 & 0.250 & 0.078 & 0.099 & 0.101 & 0.063 & 0.019 \\ 0.023 & 0.107 & 0.211 & 0.267 & 0.274 & 0.171 & 0.051 \\ 0.036 & 0.056 & 0.072 & 0.061 & 0.079 & 0.057 & 0.018 \\ 0.024 & 0.037 & 0.199 & 0.215 & 0.071 & 0.020 & 0.004 \\ 0.014 & 0.023 & 0.121 & 0.413 & 0.513 & 0.197 & 0.045 \\ 0.007 & 0.012 & 0.062 & 0.212 & 0.622 & 0.586 & 0.141 \\ 0.003 & 0.004 & 0.023 & 0.078 & 0.229 & 0.497 & 0.292 \\ 0.000 & 0.001 & 0.003 & 0.011 & 0.033 & 0.071 & 0.129 \end{bmatrix} k*in \qquad \textbf{A.1}$$

The goal of the optimal load case algorithm is to find the load case combination that produces the largest amount of strain energy in the structure. Once the number of load cases to be used is defined, the matrix of possible load combinations is assembled. For the continuous beam structure of Chapter 3, it is determined that 4 load cases will be employed with a total of 7 possible load locations. The *PLC* matrix is created by assembling a system of binary column vectors of all combinations of 7 load locations taken 4 at a time. The *PLC* for this example is shown below.

$$PLC = \begin{bmatrix} 1\ 1\ 1\ 1\ 1\ 1\ 1\ 1\ 1\ 1\ 1\ 1\ 1\ 1\ 1\ 1\ 1\ 1\ 1\ 1\ 1\ 0\ 0\ 0\ 0\ 0\ 0\ 0\ 0\ 0\ 0\ 0\ 0\ 0\ 0\ 0 \\ 1\ 1\ 1\ 1\ 1\ 1\ 1\ 1\ 1\ 1\ 0\ 0\ 0\ 0\ 0\ 0\ 0\ 0\ 0\ 0\ 1\ 1\ 1\ 1\ 1\ 1\ 1\ 1\ 1\ 1\ 0\ 0\ 0\ 0\ 0 \\ 1\ 1\ 1\ 1\ 0\ 0\ 0\ 0\ 0\ 1\ 1\ 1\ 1\ 1\ 1\ 0\ 0\ 0\ 0\ 1\ 1\ 1\ 1\ 1\ 0\ 0\ 0\ 0\ 1\ 1\ 1\ 1\ 0 \\ 1\ 0\ 0\ 0\ 1\ 1\ 1\ 0\ 0\ 0\ 1\ 1\ 1\ 0\ 0\ 0\ 1\ 1\ 1\ 0\ 1\ 1\ 1\ 0\ 0\ 0\ 1\ 1\ 1\ 0\ 1\ 1\ 1\ 0\ 1 \\ 0\ 1\ 0\ 0\ 1\ 0\ 0\ 1\ 1\ 0\ 1\ 0\ 0\ 1\ 1\ 0\ 1\ 1\ 0\ 1\ 1\ 0\ 0\ 1\ 1\ 0\ 1\ 1\ 0\ 1\ 1\ 1\ 0\ 1\ 1 \\ 0\ 0\ 1\ 0\ 0\ 1\ 0\ 1\ 0\ 1\ 0\ 1\ 0\ 1\ 0\ 1\ 1\ 0\ 1\ 1\ 0\ 1\ 0\ 1\ 0\ 1\ 1\ 0\ 1\ 1\ 1\ 0\ 1\ 1\ 1 \\ 0\ 0\ 0\ 1\ 0\ 0\ 1\ 0\ 1\ 1\ 0\ 0\ 1\ 0\ 1\ 1\ 0\ 1\ 1\ 1\ 0\ 0\ 1\ 0\ 1\ 1\ 0\ 1\ 1\ 1\ 0\ 1\ 1\ 1\ 1 \end{bmatrix} \qquad \textbf{A.2}$$

Each column of *PLC* is used to form a diagonal matrix that will be multiplied by the *ESE* matrix of Eqn A.1 to form the strain energy contribution matrices (*SEC*) as described in Section 3.2.

After the optimal load cases are calculated and both the healthy and damaged response data have been collected, the damage detection problem of Eqn 2.3 can be defined. The OC algorithm can now solve the damage detection problem. The iteration results for damage detection are shown in Table A.1 on the following page.

The active variables for each iteration are shown in bold. From the T_i values of the first iteration it can be seen that the majority of the elements are near optimal, except for element 3. By the second iteration all elements nearly satisfy optimality. Variables that are shown to be inactive, were typically set inactive because they violated one of the side constraints.

Table A.1 Optimization Results for Damage Detection of the Continuous Beam Structure

Iter	I_1	I_2	I_3	I_4	I_5	I_6	I_7	I_8	I_9	λ_1	λ_2	λ_3	λ_4	λ_5	λ_6	λ_7	λ_8	T_1	T_2	T_3	T_4	T_5	T_6	T_7	T_8	T_9
1	540	540	540	1000	1000	1000	1000	1000	1000	0.36	0.35	-0.7	-0.7	4.32	-2.2	-2.2	3.28	1	1.013	0.663	1	1	1	1	1	1
2	545	543	449	1000	1000	1000	1000	1000	1000	0.23	0.32	0.06	0.06	0.39	0.32	0.32	0.88	0.965	0.998	1.041	1	1	1	1	1	1
3	536	543	458	1000	1000	1000	1000	1000	1000	0.24	0.44	-0.1	-0.1	0.83	0.14	0.14	1.05	1	1	1.001	1	1	1	1	1	1

Appendix B

After measuring the the healthy static deflection of the grid structure of Chapter 5, the analytical model must be updated to match the measurement data. After adjusting the moment of inertia and the torsion coefficients of the elements of the model, the following simulated response was found. The error between the measured and calculated response is also shown in the table. The load case and measurement locations are identical to those described in Table 5.2.

Table B.1 Healthy Deflection Measurements and Response of the Updated Grid Model

Load Case	Measured Node	Simulation Data (in)	Test Data (in)	Error (%)
1	2	-0.0290	-0.0291	-0.3254
	3	-0.0224	-0.0224	0.0197
	5	0.0105	0.0104	0.7243
	6	0.0084	0.0083	0.4193
2	2	-0.0224	-0.0224	0.0197
	3	-0.0243	-0.0244	-0.5679
	5	0.0132	0.0130	1.0336
	6	0.0105	0.0104	0.7243
3	2	0.0105	0.0104	0.7243
	3	0.0132	0.0130	1.0336
	5	-0.0243	-0.0244	-0.5679
	6	-0.0224	-0.0224	0.0197
4	2	0.0084	0.0083	0.4193
	3	0.0105	0.0104	0.7243
	5	-0.0224	-0.0224	0.0197
	6	-0.0290	-0.0291	-0.3254
5	9	-0.0290	-0.0291	-0.3254
	10	-0.0224	-0.0224	0.0197
	12	0.0105	0.0104	0.7243
	13	0.0084	0.0083	0.4193
6	9	-0.0224	-0.0224	0.0197
	10	-0.0243	-0.0244	-0.5679
	12	0.0132	0.0130	1.0336
	13	0.0105	0.0104	0.7243
7	9	0.0105	0.0104	0.7243
	10	0.0132	0.0130	1.0336
	12	-0.0243	-0.0244	-0.5679
	13	-0.0224	-0.0224	0.0197
8	9	0.0084	0.0083	0.4193
	10	0.0105	0.0104	0.7243
	12	-0.0224	-0.0224	0.0197
	13	-0.0290	-0.0291	-0.3254
9	15	-0.0165	-0.0165	0.0742
10	2	-0.0147	-0.0146	0.8375
	9	-0.0147	-0.0146	0.8375
	16	-0.0311	-0.0310	0.4764
11	3	-0.0123	-0.0123	0.4996
	10	-0.0123	-0.0123	0.4996
	17	-0.0287	-0.0286	0.3008
12	18	-0.0164	-0.0164	0.1300
13	5	-0.0123	-0.0123	0.4996
	12	-0.0123	-0.0123	0.4996
	19	-0.0287	-0.0286	0.3008
14	6	-0.0147	-0.0146	0.8375
	13	-0.0147	-0.0146	0.8375
	20	-0.0311	-0.0310	0.4764
15	21	-0.0165	-0.0165	0.0742

The induced damage case 1 of the structural grid system of Chapter 5 eliminates the moment capacity of one moment connection. The simulated measured healthy and damaged deflection data, with out error, is shown in Table B.2. The relative change in displacement from the healthy to the damaged case is also shown in the table. The load case and measurement locations are identical to those described in Table 5.2. Notice that the largest change in relative deflection was measured for load case 11.

Table B.2 Response Comparison of Structural Grid System for Damage Case 1 (no error)

Load Case	Measured Node	Healthy Data (in)	Damaged Data (in)	% Change
1	2	-0.0291	-0.0291	-0.0080
	3	-0.0224	-0.0224	-0.0176
	5	0.0104	0.0104	0.0225
	6	0.0083	0.0083	0.0224
2	2	-0.0224	-0.0224	-0.0176
	3	-0.0244	-0.0244	-0.0272
	5	0.0130	0.0130	0.0303
	6	0.0104	0.0104	0.0302
3	2	0.0104	0.0104	0.0225
	3	0.0130	0.0130	0.0303
	5	-0.0244	-0.0244	-0.0096
	6	-0.0224	-0.0224	-0.0084
4	2	0.0083	0.0083	0.0224
	3	0.0104	0.0104	0.0302
	5	-0.0224	-0.0224	-0.0084
	6	-0.0291	-0.0291	-0.0051
5	9	-0.0291	-0.0291	-0.0080
	10	-0.0224	-0.0224	-0.0176
	12	0.0104	0.0104	0.0225
	13	0.0083	0.0083	0.0224
6	9	-0.0224	-0.0224	-0.0176
	10	-0.0244	-0.0244	-0.0272
	12	0.0130	0.0130	0.0303
	13	0.0104	0.0104	0.0302
7	9	0.0104	0.0104	0.0225
	10	0.0130	0.0130	0.0303
	12	-0.0244	-0.0244	-0.0096
	13	-0.0224	-0.0224	-0.0084
8	9	0.0083	0.0083	0.0224
	10	0.0104	0.0104	0.0302
	12	-0.0224	-0.0224	-0.0084
	13	-0.0291	-0.0291	-0.0051
9	15	-0.0165	-0.0165	0.0000
10	2	-0.0146	-0.0146	-0.0479
	9	-0.0146	-0.0146	0.0479
	16	-0.0310	-0.0310	-0.0677
11	3	-0.0123	-0.0122	0.1939
	10	-0.0123	-0.0123	-0.1939
	17	-0.0286	-0.0287	-0.2974
12	18	-0.0164	-0.0164	-0.1282
13	5	-0.0123	-0.0123	0.0004
	12	-0.0123	-0.0123	-0.0004
	19	-0.0286	-0.0286	0.0000
14	6	-0.0146	-0.0146	0.0000
	13	-0.0146	-0.0146	0.0000
	20	-0.0310	-0.0310	0.0000
15	21	-0.0165	-0.0165	0.0000

The induced damage case 2 of the structural grid system of Chapter 5 removes the connection plates at one connection. Removal of the connection plates eliminates the moment resistance of one moment connection and also effectively reduces the moment of inertia of the girder in the vicinity of the same connection. The measured healthy and damaged deflection data is shown in Table B.3. The relative change in displacement from the healthy to the damaged case is also shown in the table. The load case and measurement locations are identical to those described in Table 5.2.

Table B.3 Response Comparison of Structural Grid System for Damage Case 2

Load Case	Measured Node	Healthy Data (in)	Damaged Data (in)	% Change
1	2	-0.0291	-0.0294	-1.0228
	3	-0.0224	-0.0232	-3.7491
	5	0.0104	0.0107	3.2479
	6	0.0083	0.0086	3.2056
2	2	-0.0223	-0.0233	-4.5359
	3	-0.0243	-0.0267	-9.5807
	5	0.0130	0.0140	7.3935
	6	0.0104	0.0112	7.3278
3	2	0.0104	0.0108	3.1485
	3	0.0130	0.0139	6.5627
	5	-0.0244	-0.0247	-1.1467
	6	-0.0224	-0.0226	-0.9417
4	2	0.0083	0.0086	3.6596
	3	0.0104	0.0111	7.0890
	5	-0.0223	-0.0227	-1.4976
	6	-0.0290	-0.0293	-0.9386
5	9	-0.0291	-0.0291	-0.2170
	10	-0.0224	-0.0224	-0.2209
	12	0.0104	0.0104	0.2072
	13	0.0083	0.0083	0.2729
6	9	-0.0223	-0.0224	-0.2018
	10	-0.0243	-0.0244	-0.2133
	12	0.0130	0.0130	0.2271
	13	0.0104	0.0104	0.1927
7	9	0.0104	0.0104	-0.2815
	10	0.0131	0.0130	-0.2404
	12	-0.0244	-0.0244	0.3508
	13	-0.0224	-0.0224	0.2728
8	9	0.0083	0.0083	0.1768
	10	0.0104	0.0104	0.1902
	12	-0.0224	-0.0224	-0.1919
	13	-0.0291	-0.0291	-0.1540
9	15	-0.0165	-0.0164	0.1771
10	2	-0.0146	-0.0149	-1.6333
	9	-0.0146	-0.0147	-0.2279
	16	-0.0310	-0.0312	-0.6384
11	3	-0.0123	-0.0133	-8.6953
	10	-0.0123	-0.0123	-0.0735
	17	-0.0286	-0.0293	-2.1428
12	18	-0.0164	-0.0164	0.2851
13	5	-0.0123	-0.0124	-1.4715
	12	-0.0123	-0.0122	0.0654
	19	-0.0286	-0.0287	-0.2909
14	6	-0.0146	-0.0147	-1.0103
	13	-0.0146	-0.0146	-0.2047
	20	-0.0309	-0.0310	-0.3528
15	21	-0.0165	-0.0165	-0.1591

Appendix C

As explained in Section 5.7.1, rotational displacement measurements were required in order to detect damage in connection elements. An alternative to measuring rotational displacements is to calculate the rotations directly from the deflection measurements and applied loads. To begin, consider the two simply supported beams with separate load cases shown below.
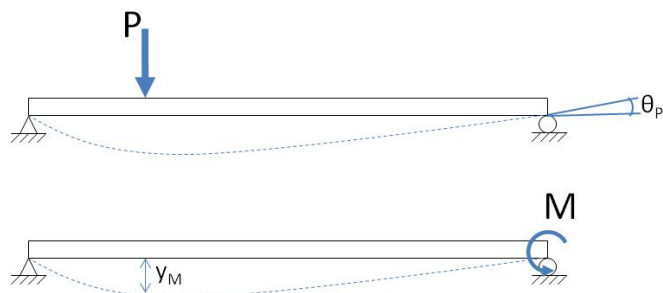

Figure C.1 Linear Elastic Beam with Two Unique Load Cases

Next, assuming linear elastic behavior, the Betti-Maxwell Reciprocal Theorem states [16]:

> If two sets of loads act on a linearly elastic structure, work done by the first set of loads in acting through the displacements produced by the second set of loads is equal to the work done by the second set of loads acting through the displacements produced by the first set.

Therefore, taking the two load cases shown in Figure C.1, a relation between the external work can be developed as:

$$P * y_M = M * \theta_P \qquad \text{C.1}$$

Solving for the rotational displacement at the support in terms of the vertical displacement along the beam, yields:

$$\theta_P = \frac{P y_M}{M} \qquad \text{C.2}$$

Thus Eqn C.2 provides a means of calculating rotational displacements in terms of the deflection measurements. It is recognized that there is an added difficulty in that a moment must now be applied to the structure, but the theory shows that there are alternate methods of determining rotational displacments without necessarily measuring them directly.

References

[1]   Back, T. and Schwefel, H. (1993). An overview of Evolutionary Algorithms for Parameter Optimization. *Evolutionary Computation*. Vol. 1, pp. 1-27.

[2]   Bakhtiari-Nejad, F. et al. (2005) A Structural Damage Detection Method Using Static Noisy Data. *Engineering Structures*. Vol. 27, pp.1784-1793.

[3]   Banan, M. R. et al. (1994). Parameter Estimation of Structures from Static Response: I. Computational Aspects. *Journal of Engineering Structures*. Vol. 120, No. 11, pp. 3243-3258.

[4]   Banan, M. R. et al. (1994). Parameter Estimation of Structures from Static Response: II. Numerical Simulation Studies. *Journal of Engineering Structures*. Vol. 120, No. 11, pp. 3259-3283.

[5]   Bernal, D. (2002). Load Vectors for Damage Localization. *Journal of Engineering Mechanics*. Vol. 128, No. 1, pp. 7-14.

[6]   Bertsekas, D. (1999). *Nonlinear Programming, 2nd edition*. Athena Scientific.

[7]   Bhatt, M. A. (2000). *Practical Optimization Methods*. New York, New York: Springer-Verlag.

[8]   Buda, G. and Caddemi, S. (2007). Identification of Concentrated Damages in Euler-Bernoulli Beams under Static Loads. *Journal of Engineering Mechanics*. Vol. 133, No. 8, Pp. 942-956.

[9]   Caddemi, S. and Morassi, A. (2005). Detecting Damage in a Beam by Static Tests. *Key Engineering Materials*. Vol. 293, pp. 493-500.

[10]   Caddemi, S. and Morassi, A. (2007). Crack Detection in Elastic Beams by Static Measurements. *International Journal of Solids and Structures*. Vol. 44, pp. 5301-5315.

[11]   Caicedo, J. M. et al. (2006). Benchmark Problem for Bridge Health Monitoring: Definition Paper. *Proceedings of the World Conference on Structural Control and Monitoring*, San Diego, CA, July 11-13.

[12]   Castaneda, N. E. (2008). In Situ Wireless Sensing for Distributed Structural Health Monitoring. *Master's Thesis. Department of Mechanical, Aerospace, and Structural Engineering at Washington University in St. Louis.*

[13]   Catbas, F. N. et al. (2008) Damage Assessment Using Flexibility and Flexibility-based Curvature for Structural Health Monitoring. *Smart Materials and Structures.* Vol. 17-015024, pp. 1-12.

[14]   Cheng, F. Y., and Truman, K. Z. Optimal Design of 3-D Reinforced Concrete and Steel Buildings Subjected to Static and Seismic Loads Including Code Provisions. *Civil Engineering Study Structural Series 85-20 Department of Civil Engineering University of Missouri-Rolla. Rolla, Missouri.* pp. 67-105.

[15]   Chou, J. and Ghaboussi, J. (2001). Genetic Algorithm in Structural Damage Detection. *Computers and Structures.* Vol. 79, pp. 1335-1353.

[16]   Cook, R. D. et al. (2002). *Concepts and Applications of Finite Element Analysis, 4th ed.* New York, New York: John Wiley & Sons, Inc.

[17]   Dhillon, B. S. et al. (1999). Interactive Design of Semi-rigid Steel Frames. *Journal of Structural Engineering.* Vol. 125, No. 5, pp. 556-564.

[18]   Doebling, S.W. et al. (1998). A Review of Damage Identification Methods that Examine Changes in Dynamic Properties. *Shock and Vibration Digest.* Vol. 30, No. 2, pp. 91-105.

[19]   Filho, M. S. et al. (2004). Wind Pressures in Framed Structures with Semi-rigid Connections. *Journal of the Brazilian Society of Mechanical Sciences and Engineering.* Vol. 26, No. 2, pp. 180-189.

[20]   Gao, Y. et al. (2004). Experimental Verification of the Damage Locating Vector Method. *Proceedings of the 1st International Workshop on Advanced Smart Materials and Smart Structures Technology,* Honolulu, Hawaii.

[21]   Gao, Y. et al. (2007). Experimental Verification of the Flexibility-based Damage Locating Vector Method. *Journal of Engineering Mechanics.* Vol. 133, No. 10, pp. 1043-1049.

[22]   Gill, P. E. (1981). *Practical Optimization.* New York: Academic Press.

[23]   Giraldo, D. F. (2006). A Structural Health Monitoring Framework for Civil Structures. *D.Sc. Dissertation. Department of Civil Engineering at Washington University in St. Louis.*

[24]   Gould, P. (1994). *Introduction to Linear Elasticity.* New York: Springer.

[25]   Haftka, R. T., and Kamat, M. P. (1985). *Mechanics of Structural Systems: Elements of Structural Optimization.* Boston, Massachusetts: Marinus Nijhoff Publishers.

[26]   Hajela, P. and Soeiro, F.J. (1990). Recent Developments in Damage Detection Based on System Identification Methods. *Structural Optimization. Vol. 2*, pp. 1-10

[27]   Hajela, P., Soeiro, F. J. (1990) Structural Damage Detection Based on Static and Modal Analysis. *AIAA Journal.* Vol. 26, No. 6, pp. 1110-1115.

[28]   Haug, E. J. and Arora, J. S. (1979). *Applied Optimal Design: Mechanical and Structural Systems.* New York, New York: Wiley-Interscience. pp. 319-328.

[29]   Haupt, R. L. and Haupt, S. E. (2004). *Practical Genetic Algorithms, second edition.* New Jersey: John Wiley & Sons, Inc.

[30]   Hjelmstad, K.D. and Shin, S. (1997). Damage Detection and Assessment of Structures from Static Response. *Journal of Engineering Mechanics.* Vol. 123, No. 6, pp. 568-576.

[31]   Hu, X. and Shenton, H. W. (2007). Dead Load Based Damage Identification Method for Long-term Structural Health Monitoring. *Journal of Intelligent Material Systems and Structures.* Vol. 18, pp. 923-938.

[32]   Joanna, J. S. and Knight, G. M. (2005). Dynamic Response of Steel Beams with Semi-rigid Connections. *The Institute of Engineers (India) Journal.* Vol. 86, pp. 123-126.

[33]   Johnson, L. and Truman, K. (2004). Damage Detection using Static Responses and Unconstrained, Nonlinear Optimization. *Master's Thesis. Department of Civil Engineering at Washington University in St. Louis.*

[34]   Kamat, M. et al. (1993) *Structural Optimization: Status and Promise.* Washington, DC: American Institute of Aeronautics and Astronautics. Vol. 150.

[35]   Khot, N. S. et al. (1979). Comparison of Optimality Criteria Algorithms for Minimum Weight Design of Structures. *AIAA Journal.* Vol. 17, No.2, pp.182-190.

[36]   Kirsch, U. (1993). *Structural Optimization: Fundamentals and Applications.* Berlin, Germany: Springer-Verlag.

[37]   Kouchmeshky, B. et al. (2006). Co-evolutionary Algorithm for Structural Damage Identification using Minimal Physical Testing. *International Journal for Numerical Methods in Engineering.* Vol. 65, No. 5, pp. 1085-1107.

[38]   Lanata F. and Del Grosso, A. (2006). Damage Detection and Localization for Continuous Static Monitoring of Structures using a Proper Orthogonal Decomposition of Signals. *Smart Materials and Structures.* Vol. 15, pp. 1811-1829.

[39]   Ma, J. and Asundi, A. (2001). Structural Health Monitoring using a Fiber Optic Polarmetric Sensor and a Fiber Optic Curvature Sensor-static and Dynamic Test. *Smart Materials and Structures.* Vol.10, No.2, pp.181-188.

[40]   Makris, P. A. et al. (2006). Discrete Variable Optimization of Frames Using a Strain Energy Criterion. *Structural and Multidisciplinary Optimization.* Vol. 31, pp. 410-417.

[41]   Messina, A. et al. (1998). Structural Damage Detection by a Sensitivity and Statistical-based Method. *Journal of Sound and Vibration.* Vol. 216, No. 5, pp.791-808.

[42]   Michalewicz, Z. et al. (1996). Evolutionary Algorithms for Constrained Engineering Problems. *International Symposium on Methodologies for Intelligent Systems.*

[43]   Oh, B. H. et al. (1999). Damage Assessment of Structures using Static and Dynamic Test Data. *Transactions of the 15th International Conference on Structural Mechanics and Reactor Technology.* pp. 179-186.

[44]   Ozturk, A. U. and Catal, H. H. (2005). Dynamic Analysis of Semi-rigid Frames. *Mathematical and Computational Applications.* Vol. 10, No. 1, pp.1-8.

[45]   Paige, C. C. and Saunders, M. A. (1982). LSQR: An Algorithm for Sparse Linear Equations and Sparse Least Squares. *ACM Transactions on Mathematical Software.* Vol. 8, No. 1, pp.43-71.

[46]   Park, P. et al. (2006). Crack Detection by Static Measurements in Steel Beams. *Key Engineering Materials.* Vol. 321, pp.394-399.

[47]   Press, W. H. et al. (2002). *Numerical Recipes in C: The Art of Scientific Computing, second edition.* Cambridge University Press.

148

[48]   Salawu, O.S. (1997). Detection of Structural Damage through Change in Frequency: A Review. *Engineering Structures*. Vol. 19, No. 9, pp. 718–723.

[49]   Salawu, O.S. and Williams, C. (1995). Review of Full-scale Dynamic Testing of Bridge Structures. *Engineering Structures*. Vol. 17, No. 2, pp. 113-121.

[50]   Sanayei, M. and Onipede, O. (1991). Damage Assessment of Structures using Static Test Data. *AIAA Journal*. Vol. 29, No. 7, pp. 1174-1179.

[51]   Sanayei, M. and Saletnik, M. J. (1996). Parameter Estimation of Structures from Static Strain Measurements. I: Formulation. *Journal of Structural Engineering*. Vol. 122, No. 5, pp. 555-562.

[52]   Sanayei, M. and Saletnik, M. J. (1996). Parameter Estimation of Structures from Static Strain Measurements. II: Error Sensitivity Analysis. *Journal of Structural Engineering*. Vol. 122, No. 5, pp. 563-572.

[53]   Sanayei, M. and Scampoli, S. (1991). Structural Element Stiffness Identification from Static Test Data. *Journal of Engineering Mechanics*. Vol. 117, No. 5, pp. 1021-1036.

[54]   Sanayei, M., et al. (1997) Structural Model Updating using Experimental Static Measurements. *Journal of Structural Engineering*. Vol. 123, No. 6, pp. 792-798.

[55]   Seaburg, P. A. and Carter, C. J. (1997). *Steel Design Guide Series: Torsional Analysis of Structural Steel Members*. American Institute of Steel Construction, Inc.

[56]   Skrinar, M. and Plibersek, T. (2005). New Finite Element for Transversely Cracked Slender Beams Subjected to Transverse Loads. *Computational Materials Science*. Vol. 39, pp. 250-260.

[57]   Terlaje, A. (2006). Damage Detection in 2-D Steel Moment Frames using Static Response Data and Optimality Criterion. *Master's Thesis. Department of Civil Engineering at Washington University in St. Louis.*

[58]   Terlaje, A. and Truman, K. (2006). Damage Detection of 2-D Frames using Static Response Data and Optimality Criterion. *Proceedings of the Tenth East Asia-Pacific Conference on Structural Engineering and Construction,* Bangkok, Thailand, August 3-5.

[59]   Terlaje, A. and Truman, K. (2006). Damage Detection using Static Response Data and Optimality Criterion. *Proceedings of the SMCD 2006 International Conference on Advances in Engineering Structures, Mechanics & Construction*, University of Waterloo, Waterloo, Ontario, Canada, May 14-17.

[60]   Terlaje, A. and Truman, K. (2006). Earthquake Damage Detection using Static Response Data and Optimality Criterion. *Proceedings of the 8th National Conference on Earthquake Engineering*, San Francisco, CA, April 18-22.

[61]   Terlaje, A. and Truman, K. (2007). A Static Response Based Parameter Identification Algorithm using OC Optimization. *Proceedings of the 11th International Conference on Civil, Structural, and Environmental Engineering Computing*, St. Julians, Malta, September 18-21.

[62]   Terlaje, A. and Truman, K. (2008). Detection of Reduced Stiffness in Lateral Load Resisting Systems due to Seismic Damage. *Proceedings of the 14th World Conference on Earthquake Engineering*, Beijing, China, October 12-17.

[63]   Terlaje, A. S. and Truman, K. Z. (2007). Parameter Identification and Damage Detection using Structural Optimization and Static Response Data. *Advances in Structural Engineering, An International Journal.* Vol. 10, No.6, pp. 607-621.

[64]   Vanderplaats, G. N. (1984). *Numerical Optimization Techniques for Engineering Design: With Applications.* McGraw-Hill, Inc.

[65]   Venkayya, V. B. (1989). Optimality Criteria: A Basis for Multidisciplinary Design Optimization. *Computational Mechanics.* Vol. 5, No. 1, pp.1-21.

[66]   Wang, X. et al. (2001). Structural Damage Identification using Static Test Data and Changes in Frequencies. *Engineering Structures.* Vol. 23, No. 6, pp. 610-621.

Curriculum Vitae

Augusto S. Terlaje III

Date of Birth	June 12, 1981	
Place of Birth	Agana, Guam	

Education	**Ph. D Structural Engineering**	May 2010
	M.S. Structural Engineering	2006
	B.S. Civil Engineering	2004
	Washington University in St. Louis – St. Louis, MO	
	B.S. Mathematics	2002
	University of Puget Sound – Tacoma, WA	

Teaching Experience	Engineering Mechanics I - Course Instructor	2004-2006
	Structural Dynamics Laboratory - Course Instructor	2008
	Fluid Mechanics, Design of Steel Structures, and Analysis and Design of Aerospace Structures - Teaching Assistant	2005-2009
	Research Experience for Undergraduates (REU) – Graduate Mentor	2005-2007
	Mechanical, Aerospace, and Structural Engineering Department – Washington University in St. Louis	

Honors	Department of Education, Graduate Assistance in Areas of National Need (GAANN) research fellow
	2006 AISC Fred R. Havens Fellowship winner
	King T. & Adele M. Coffey Memorial Scholar
	Recipient of President's Scholarship (UPS)

Activities/ Memberships	Peer reviewer for the journal Engineering Structures
	Tau Beta Pi, Engineering Honor Society
	Chi Epsilon, Civil Engineering Honor Society
	American Society of Civil Engineers (ASCE) student member

Publications

A. S. Terlaje III and K. Z. Truman. "Parameter Identification and Damage Detection Using Structural Optimization and Static Response Data." *Advances in Structural Engineering, An International Journal.* March 2007.

A. Terlaje and K. Truman. "Detection of Reduced Stiffness in Lateral Load Resisting Systems due to Seismic Damage." *Proceedings, 14th World Conference on Earthquake Engineering,* Beijing, China, October 12-17, 2008.

A. Terlaje and K. Truman. "A Static Response Based Parameter Identification Algorithm Using OC Optimization." *Proceedings, 11th International Conference on Civil, Structural, and Environmental Engineering Computing,* St. Julians, Malta, September 18-21, 2007.

A. Terlaje and K. Truman. "Damage Detection of 2-D Frames Using Static Response Data and Optimality Criterion." *Proceedings, Tenth East Asia-Pacific Conference on Structural Engineering and Construction,* Bangkok, Thailand, August 3-5, 2006.

A. Terlaje and K. Truman. "Damage Detection Using Static Response Data and Optimality Criterion." *Proceedings, SMCD 2006 International Conference on Advances in Engineering Structures, Mechanics & Construction,* University of Waterloo, Waterloo, Ontario, Canada, May 14-17, 2006.

A. Terlaje and K. Truman. "Earthquake Damage Detection Using Static Response Data and Optimality Criterion." *Proceedings, 8th National Conference on Earthquake Engineering,* San Francisco, CA, April 18-22, 2006.